ETHYLBENZENE DEHYDROGENATION INTO STYRENE:

KINETIC MODELING AND REACTOR SIMULATION

A Dissertation

by

WON JAE LEE

Submitted to the Office of Graduate Studies of
Texas A&M University
in partial fulfillment of the requirements for the degree of

DOCTOR OF PHILOSOPHY

December 2005

Major Subject: Chemical Engineering

ETHYLBENZENE DEHYDROGENATION INTO STYRENE:

KINETIC MODELING AND REACTOR SIMULATION

A Dissertation

by

WON JAE LEE

Submitted to the Office of Graduate Studies of
Texas A&M University
in partial fulfillment of the requirements for the degree of

DOCTOR OF PHILOSOPHY

Approved by:

Co-Chairs of Committee,	Rayford G. Anthony
	Gilbert F. Froment
Committee Members,	Daniel F. Shantz
	Michael P. Rosynek
Head of Department,	Kenneth R. Hall

December 2005

Major Subject: Chemical Engineering

ABSTRACT

Ethylbenzene Dehydrogenation into Styrene:

Kinetic Modeling and Reactor Simulation. (December 2005)

Won Jae Lee, B.S., SungKyunKwan University;

M.S., Pohang University of Science and Technology

Co-Chairs of Advisory Committee: Dr. Rayford G. Anthony
Dr. Gilbert F. Froment

A fundamental kinetic model based upon the Hougen-Watson formalism was derived as a basis not only for a better understanding of the reaction behavior but also for the design and simulation of industrial reactors.

Kinetic experiments were carried out using a commercial potassium-promoted iron catalyst in a tubular reactor under atmospheric pressure. Typical reaction conditions were temperature = 620°C, steam to ethylbenzene mole ratio = 11, and partial pressure of N_2 diluent = 0.432 bar. Experimental data were obtained for different operating conditions, i.e., temperature, feed molar ratio of steam to ethylbenzene, styrene to ethylbenzene, and hydrogen to ethylbenzene and space time. The effluent of the reactor was analyzed on-line using two GCs.

Kinetic experiments for the formation of minor by-products, i.e. phenylacetylene, α-methylstyrene, β-methylstyrene, etc, were conducted as well. The reaction conditions were: temperature = 600°C ~ 640°C, a molar ratio of steam to ethylbenzene = 6.5, and

partial pressure of N_2 diluent = 0.43 bar and 0.64 bar. The products were analyzed by off-line GC.

The mathematical model developed for the ethylbenzene dehydrogenation consists of nonlinear simultaneous differential equations in multiple dependent variables. The parameters were estimated from the minimization of the multiresponse objective function which was performed by means of the Marquardt algorithm. All the estimated parameters satisfied the statistical tests and physicochemical criteria. The kinetic model yielded an excellent fit of the experimental data.

The intrinsic kinetic parameters were used with the heterogeneous fixed bed reactor model which is explicitly accounting for the diffusional limitations inside the porous catalyst. Multi-bed industrial adiabatic reactors with axial flow and radial flow were simulated and the effect of the operating conditions on the reactor performance was investigated.

The dynamic equilibrium coke content was calculated using detailed kinetic model for coke formation and gasification, which was coupled to the kinetic model for the main reactions. The calculation of the dynamic equilibrium coke content provided a crucial guideline for the selection of the steam to ethylbenzene ratio leading to optimum operating conditions.

To my late grandfather

To my parents

To my wife

ACKNOWLEDGEMENTS

TABLE OF CONTENTS

Page

LIST OF FIGURES

FIGURE   Page

FIGURE   Page

FIGURE   Page

FIGURE   Page

LIST OF TABLES

TABLE   Page

CHAPTER I

INTRODUCTION

The styrene process was developed in the 1930s by BASF (Germany) and Dow Chemical (USA). Over 25×10^6 tons/year of styrene monomer is produced worldwide.[1] The annual production of styrene in the U.S.A. exceeds 6×10^6 tons.[2] The major commercial process for the production of styrene is the dehydrogenation of ethylbenzene, which accounts for 85% of the commercial production.[3] The potassium-promoted iron oxide catalyst has been extensively used for styrene production.[4]

The average capacity of ethylbenzene dehydrogenation plants is over 100,000 metric tons per year and plants which have a capacity of 400,000 metric ton per year is not uncommon.[5] Obviously, a small improvement in the plant operation will lead to a substantial increase of returns. Nevertheless, the research towards the fundamental kinetic modeling based upon the Hougen-Watson approach has not been pursued by most styrene producers and researchers. They rely on the empirical polynomial correlations for the unit optimization.[6-8] Furthermore, the reaction rates published in the most of papers are not intrinsic but effective.[9, 10] An intrinsic kinetic model based upon the fundamental principles is essentially required for the optimization of the various reactor configurations with different operating conditions. The objectives of this research

_____

This dissertation follows the style and format of *Industrial and Engineering Chemistry Research*.

are to develop the mathematical kinetic model for the ethylbenzene dehydrogenation and to investigate the effect of operating conditions on the fixed bed industrial reactor.

In addition to the major reactions in ethylbenzene dehydrogenation, i.e., formation of styrene, benzene, and toluene, the understanding of the kinetic behavior of the minor by-products, such as phenylacetylene, α-methylstyrene, β-methylstyrene, cumene, n-propylbenzene, divinylbenzene, and stilbene, is also important in terms of the styrene monomer quality and separation cost of the final products. The formation of these minor by-products is not taken into account for the fundamental kinetic model.

Chapter II covers the literature review. The general features of ethylbenzene dehydrogenation are briefly discussed. The theoretical and literature backgrounds are presented in each chapter. Chapter III explains the experimental methods of ethylbenzene dehydrogenation. The experimental set-up and quantitative product analysis using GC are discussed. Chapter IV describes the results of kinetic experiments for the formation of major products and minor by-products. The kinetic data for the formation of major products were obtained for the estimation of intrinsic kinetic parameters. In chapter V the fundamental kinetic model and the results of the parameter estimations are presented. Chapter VI deals with the simulation of a multi-bed adiabatic reactor with *axial* flow using the pseudohomogeneous model. Since this model does not explicitly account for the diffusional limitations inside the porous catalyst pellet, the heterogeneous model is used for the reactor simulation in chapter VII. In chapter VIII, the concept of dynamic equilibrium coke content is presented and the effect of the operating conditions on the dynamic equilibrium coke content along the fixed bed

adiabatic reactor is discussed. Chapter IX illustrates the simulation of a multi-bed adiabatic reactor with *radial* flow. The effect of the feed conditions on the reactor performance is examined.

CHAPTER II

LITERATURE REVIEW

2.1 Chemistry of Ethylbenzene Dehydrogenation

The main reaction produces styrene and hydrogen.

$$\text{Ethylbenzene} \leftrightarrow \text{styrene} + H_2, \qquad \Delta H_r\,(620^oC) = 124.83 \text{ kJ/mol}$$

The dehydrogenation reaction is usually conducted at temperatures above 600^oC with an excess of steam. The ethylbenzene dehydrogenation is an endothermic and reversible reaction with an increase in the number of mole due to reaction. High equilibrium conversion can be achieved by a high temperature and a low ethylbenzene partial pressure. The main byproducts are benzene and toluene.[11]

$$\text{Ethylbenzene} \rightarrow \text{benzene} + C_2H_4, \qquad \Delta H_r\,(620^oC) = 101.50 \text{ kJ/mol}$$

$$\text{Ethylbenzene} + H_2 \rightarrow \text{toluene} + CH_4, \qquad \Delta H_r\,(620^oC) = -65.06\text{kJ/mol}$$
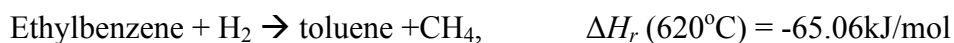
2.2 Role of Promoter in Ethylbenzene Dehydrogenation

Potassium is the main promoter of Fe_2O_3. It increases the activity by more than one order of magnitude, and also slightly increases the selectivity to styrene and the stability of the catalyst. The effect of the potassium promotion on the activation energy has been reported in numerous publications. According to Shibata and Kiyoura[12], on *unpromoted* iron oxide catalyst (Fe_2O_3) the apparent activation energy was found to be 117.6 kJ/mol and on promoted catalyst (0.5 wt% K_2O-Fe_2O_3, 3.0 wt% K_2O-Fe_2O_3 and 10.0 wt% K_2O-Fe_2O_3) it was 180.6 kJ/mol. They concluded that the high activity of the

potassium-promoted catalyst is caused by a high preexponential factor, which can be explained in terms of a higher concentrations of active sites. The difference in specific surfaces between unpromoted and promoted catalyst was found to be very small.

Coulter et al.[13] studied the kinetics using unpomoted and K-promoted polycrystalline catalysts. The unpromoted catalyst yielded an apparent activation energy of 155.4 kJ/mol. As found in Addiego et al.[14], the increase of potassium loading intially decreases the apparent activation energy to 88.2 kJ/mol and the further addition of potassim leads to an increase of the apparent activation energy to 142.8 kJ/mol. Addiego et al.[14] showed that the addition of potassium did not alter the adsorption geometry and the nature of active sites, although there was a decrease in the formation of byproducts. Coulter et al.[13] and Shekhah et al.[15] reached the same conclusion that the active sites of unpromoted and promoted catalysts are identical.

It has been well established in the last decades that the promotional role of potassium consists of the formation of an active phase, $KFeO_2$.[13, 16-18] Hirano[18-20] was the first to investigate the nature of the active sites with XRD and XPS. $KFeO_2$ (potassium ferrite) was assumed to take part in the formation of the active sites of the catalyst. Muhler et al.[21] demonstrated that the active state is equilibrium between $KFeO_2$ and $K_2Fe_{22}O_{34}$. The active phase can be reduced by hydrogen to KOH and Fe_3O_4 (magnetite). The schematic life cycle of a potassium-promoted catalyst is shown in Figure 2.1. Coulter et al.[13] also identified the surface active sites which consist of Fe^{3+}, specifically in
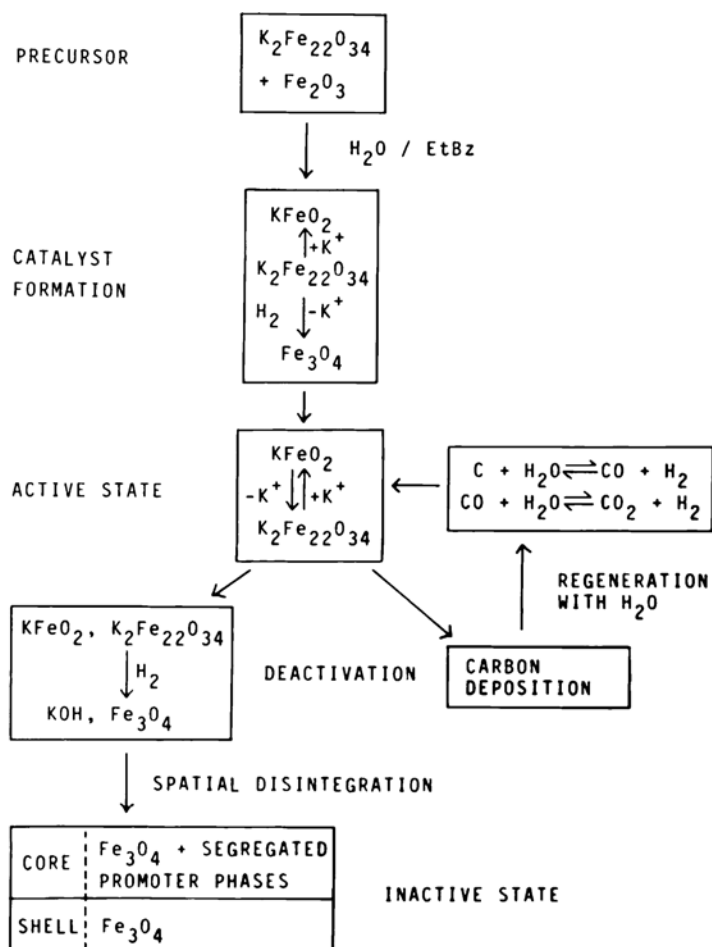
Figure 2.1. Schematic life cycle of a prototype catalyst without any promoter additives.[21] With permission from Elsevier B. V.

the form of $KFeO_2$. The sequence of catalytic activity (KFe_xO_y > Fe_2O_3 > Fe_3O_4) was confirmed by Kuhrs.[22]

Shaikhutdinov et al.[23] studied the surface structures and adsorption behavior of water, ethylbenzene, and styrene on the well-defined oxide films, such as $Fe_3O_4(111)$, α-$Fe_2O_3(0001)$, and $KFe_xO_y(111)$. Competitive adsorption of ethylbenzene and styrene on the film revealed that 17% of the chemisorption sites on KFe_xO_y was occupied by styrene, whereas 43% of these sites are occupied by styrene on α-Fe_2O_3. Since the sites are covered by less product molecule styrene, they concluded that KFe_xO_y is more active than unpromoted α-Fe_2O_3.

Kuhrs et al.[22, 24] performed a combined surface science and reactivity study on epitaxial iron oxide model catalyst films with $Fe_3O_4(111)$, α-$Fe_2O_3(0001)$, and $KFe_xO_y(111)$. They showed that a longer activation period was required for $KFe_xO_y(111)$. After activation, the activity was enhanced and the surface was covered completely with carbon. This carbon was considered not to inhibit the reaction but to be active in the reaction as observed on other metal oxide catalyst.[25, 26] However, the investigation of IR studies by Addiego et al.[14] and Auger studies by Coulter et al.[13] showed a different conclusion. The addition of potassium not only significantly decreased the surface carbon concentration, but helped the catalyst to reach a steady-state more quickly by decreasing the induction period to steady-state activity.

The potassium compound gives the catalyst a self-regenerative property that maintains the catalyst activity for a long time without significant loss of activity at lower steam to oil ratios, e.g., ratios of < 2:1 by weight. Stobbe and coworkers[16] indicated

although $KFeO_2$ showed high activity and selectivity, but it was not sufficiently active in catalyzing carbon gasification to entirely suppress the coking. They concluded that complete suppression of coking required the additional presence of highly dispersed potassium carbonate. According to Addiego et al.,[14] potassium suppresses the amount of carbonaceous deposits. Shekhah et al.[15] concluded that the increase of potassium loading leads to the decrease in initial conversion rate due to the coverage of active sites by excess potassium. High loadings of potassium, however, resulted in lowering the deactivation rate by coke. Potassium was continuously removed as a form of volatile KOH during the reaction. The removal rate was faster if only steam and no EB was fed than with a mixed feed.

A recent improvement to the manufacture of the catalysts is to incorporate small amounts of vanadium and other modifiers, which can beneficially affect the pore structure of the catalysts. Cr and Al are considered to be structural promoters, as they can enter in the Fe^{3+} compounds. Ce oxide increases the activity and Mo the selectivity. The addition of both Ce and Mo was suggested by Hirano[20] to improve the catalyst composition. The catalyst stability during the reaction can perhaps be enhanced by the addition of other oxides. Hirano[26] also studied the effect of addition of a series of alkaline earth oxides to the potassium-promoted iron oxide catalyst on dehydrogenation activity. He found that MgO-containing catalyst exhibited the best activity and stability even at low steam to ethylbenzene ratio. Ndlela and Shanks[27] demonstrated that the potassium played a vital role in stabilizing Fe_2O_3 against its reduction and the addition of Cr and V appeared to retard the effect of potassium on the reduction resistance of Fe_2O_3.

Miyakoshi et al.[28, 29] reported that among Mn, Co, Ni, Cu, and Zn, Mn-substituted Fe-K catalysts prepared by a sol-gel method enhanced the catalytic activity and suppressed coke formation. The activation energies determined from the Arrhenius plot are 93.7 kJ/mol and 91.6 kJ/mol for 20% Mn-substituted Fe-K oxide and Fe-K oxide, respectively. Since the difference in the activation energies was not appreciable, the increased catalytic activity resulted from the increased number of active sites. The active phase, $KFeO_2$, is found to be stabilized by the substitution of Mn, while unsubstituted catalyst is readily pyrolyzed to KOH and iron oxides, which is consistent with the studies by Muhler et al.[17, 21, 30] The stabilization effect of Mn on the potassium loss from the active phase was elucidated by means of thermal alkali desorption method by Kotarba et al.[31]

2.3 Role of Steam in Ethylbenzene Dehydrogenation

Steam is present in excess in the ethylbenzene dehydrogenation process. In the last decades, great efforts were invested to decrease the steam/hydrocarbon ratio to molar values lower than 6, essentially through modifications in catalyst compositions. The overall effects of the increase of the steam/hydrocarbon ratio are to increase the selectivity for styrene at the same level of conversion and the lifetime and stability of the catalyst. Advantages of using steam are: (1) steam can provide the heat to maintain the reaction temperature, (2) steam acts as a diluent to shift the equilibrium conversion to higher value through a decrease of the partial pressures of ethylbenzene and hydrogen, and (3) steam removes the carbonaceous deposition by the gasification reaction. The

investigation of the effect of steam on the catalyst activity was studied by Coulter et al.[13] They showed that surface carbon level decreased with increasing H_2O/EB molar ratio and that a H_2O/EB molar ratio of three is optimum to minimize the carbon content on the surface while maximizing the activity of the catalyst.

2.4　　　Kinetics of Ethylbenzene Dehydrogenation

Wenner and Dybdal[32] were the first to conduct an experimental investigation by using a commercial catalyst in a integral reactor to develop the rate equations for the formation of styrene, benzene, and toluene (reaction 1, 2, and 3, respectively in section 2.1). The following equations were developed

$$r_1 = k_1 \left(P_{EB} - P_{ST} P_{H_2} / K_{eq} \right)$$
$$r_2 = k_2 P_{EB} \qquad (2.1)$$
$$r_3 = k_3 P_{EB} P_{H_2}$$

where k_i is the rate coefficient of reaction i, P_j is the partial pressure of components j, and K_{eq} is the equilibrium constant. Apparent kinetic parameters were evaluated using the pseudohomogeneous model.

Carra and Forni[33] performed kinetic studies in the temperature range of 770K-900K over the industrial catalyst, Shell 105. The intrinsic rate of styrene formation was developed, based upon Langmuir-Hinshelwood kinetics.

$$\frac{dX}{d(W/F)} = \frac{k_1 \left(P_{EB} - P_{H_2} P_{ST} / K_{eq} \right)}{P_{EB} + z P_{ST}} \qquad (2.2)$$

where $z = K_{ST}/K_{EB}$. The activation energy of k_1 was 191.7 kJ/mol.

Sheel and Crowe[9] obtained the kinetic parameters of the rate equations of Eq. (2.1) using a pseudohomogeneous model. Since they collected experimental data from a single bed adiabatic industrial reactor, the kinetic parameters are effective, not intrinsic.

Czerny and Katerla[3] developed rate equations by fitting the experimental data which were measured in an integral reactor.

$$(F/V)\ln\left(\frac{1}{1-X}\right) = \alpha + \beta\left(\frac{F}{V}\right)x \qquad (2.3)$$

where F/V is the ratio of feed molar flow rates of ethylbenzene to the volume of the catalyst, α and β are parameters which include the rate constants and adsorption coefficients, respectively. Activation energy in the range 820 K-860K was 167.6 kJ/mol.

Hirano[18-20] investigated the kinetics over various iron oxide catalysts in a differential reactor. The rate of styrene formation was independent of the partial pressure of steam and of ethylbenzene. However, styrene addition to the ethylbenzene feed decreased the rate of styrene formation. The rate equations were reported:

$$r_{ST} = \frac{k_1 K_{EB} P_{EB}}{K_{EB} P_{EB} + K_{ST} P_{ST}}$$

$$r_{BZ} = \frac{k_2 \left(K_{EB}\right)_{BZ} P_{EB}}{1 + \left(K_{EB}\right)_{BZ} P_{EB}} \qquad (2.4)$$

$$r_{TO} = \frac{k_3 \left(K_{EB}\right)_{TO} P_{EB}}{1 + \left(K_{EB}\right)_{TO} P_{EB}}$$

where $(K_{EB})_{BZ}$ and $(K_{EB})_{TO}$ are the equilibrium constant of ethylbenzene adsorption on the benzene formation sites and that on the toluene formation sites, respectively.

Lee[11] studied the effect of the internal diffusion on the apparent activation energy. The apparent activation energy for the particle size of 0.6-0.7mm was 96 kJ/mol and that for the large particle size of 3.2 mm or 4.8mm diameter was 63 kJ/mol, which indicates the internal diffusion limitation.

Abdalla et al.[34] extracted intrinsic kinetic parameters from industrial reactor data with commercial catalyst by using a heterogeneous model based on the dusty gas model. The rate equations in Eq. (2.1) were used together with the steam reforming of CH_4 and C_2H_4 and the water-gas shift reaction.

More recently Dittmeyer et al.[35] developed kinetics for a commercial catalyst (Süd-Chemie AG) using a BERTY-type gradientless recycle reactor. They showed that the controlled addition of CO_2 suppressed the formation of styrene and toluene. The production of CO_2 was attributed to the steam reforming of ethylbenzene and CH_4. The rate equations were based on the Hougen-Watson type formula for the main reaction and the power law for the steam reforming reactions.

$$r_1 = \frac{k_1 \left(P_{EB} - P_{ST} P_{H_2}/K_{eq} \right)}{\left(1 + K_{ST} P_{ST}\right)\left(1 + K_{CO2} P_{CO_2}\right)}$$

$$r_2 = \frac{k_2 P_{EB}}{\left(1 + K_{CO2} P_{CO_2}\right)}$$

$$r_2' = k_2' P_{EB} \tag{2.5}$$

$$r_3 = \frac{k_3 P_{EB}}{\left(1 + K_{CO2} P_{CO_2}\right)}$$

where r_2 is for the reaction $EB + 2H_2 \rightarrow BZ + 2CH_4$ and r_2' is for the reaction of $EB \rightarrow BZ + C_2H_4$.

Table 2.1 shows the summary of the activation energies for the formation of styrene, benzene, and toluene given in the literature.

Table 2.1. Summary of the activation energies for the formation of styrene, benzene, and toluene

Catalyst	Activation energy, kJ/mol			Reference
	Styrene	Benzene	Toluene	
Fe-K	126.0	152.0	213.8	Hirano[20]
Fe-K-Cr-Mg	111.7	132.72	215.5	Hirano[26]
Commercial iron catalyst	90.9	207.9	91.5	Sheel and Crowe[9]
Commercial iron catalyst (Süd-Chemie)	158.6	114.2	208.6	Dittmeyer et al.[35]
Commercial iron catalyst	101.2	139.4	131.5	Wenner and Dybdal[32]
Commercial iron catalyst (Shell 105)	191.7	212.7	91.2	Carra and Forni[33]; Majumdar and Mitra[36]
Commercial iron-chromium catalyst (KMS-1)	193.6	205.4	252.0	Lebedev et al.[37]
Commercial iron catalyst (Shell 105)	276.8	314.6	167.6	Sheppard et al.[38]
-	160.3	118.9	181.5	Kolios and Eigenberger[6]

2.5   Kinetics of Coke Formation

2.5.1   Introduction

Coke is hydrogen-deficient carbonaceous residues deposited on the surface. It is considered to be formed by a condensation polymerization which eventually leads to the formation of such a large polymer structure as to block the active sites on the catalyst surfaces.[39] For instance, in catalytic cracking the analysis of a coke deposit on a used cracking catalyst indicated a mixture of solid and semiliquid mixture of polynuclear aromatics, such as dimmers and trimers of naphthalene, phenanthrene, etc.[40] Besides the form of hydrogen-deficient polymers or aromatics, in some reactions the element carbon can form coke, which includes the metal carbide phase of Fisher-Tropsch synthesis on iron-based catalysts and the filamentous phase for steam reforming of methane on nickel-based catalysts.[39]

Coke formation is a complicate process that oversimplified empirical correlation obtained by Voorhies[41] from the cracking of gas oil feedstock has been widely accepted.

$$C_C = At^n \quad \text{with } 0.5 < n < 1 \tag{2.6}$$

where t is the process time and A and n are constants. The values of n were determined for different reactions. Voorhies postulated that the rate of coke formation was controlled by diffusion mechanism and not dependent on the space time; the diffusion rate could be expressed as inversely proportional to the weight percent of carbon deposited. Ozawa and Bischoff[42] used the thermogravimetric method to measure the weight of coke formed on catalyst for the cracking of ethylene over a silica-alumina catalyst for various process times. They found that a simple empirical correlation was

not completely adequate in relating the weight of coke deposited on the catalyst to the process time. Also Eberly et al.[43] showed that the production of coke in fixed beds over wide space velocities was not completely independent of space velocity. In general, the correlation, Eq. (2.6), has been used in many systems over the years for its simplicity. However, the origin of coke was totally neglected.

A theoretical and mechanistic approach of kinetic modeling of coke formation was first investigated by Froment and Bischoff.[44, 45] Froment and Bischoff[44] pointed out that the rate of coke formation can not be established without taking into account the rate of main reaction, since coke is formed, definitely, from the reaction mixture. Two activity functions, i.e., an exponential dependence of the catalyst activity on the coke content and a hyperbolic dependence on the coke content, were introduced to show the effect of the coke on the catalyst activity.

Deactivation functions are defined as the ratio of rates of a chemical reaction for the main reaction:

$$\frac{r_{Ai}}{r_{Ai}^o} = \Phi_{Ai} \tag{2.7}$$

where r_{Ai}^o is the initial reaction rate in absence of coke.

Deactivation function for the coke formation is

$$\frac{r_C}{r_C^o} = \Phi_C \tag{2.8}$$

where r_C^o is the initial coking rate. Therefore, the rate equation of coke formation is given by

$$\frac{dC_C}{dt} = r_C^o \Phi_C \qquad (2.9)$$

The initial coking rate, r_C^o, is a function of operating conditions, i.e., temperature and partial pressures. The following deactivation functions were suggested by Dumez and Froment.[46]

$$\begin{aligned}
\Phi &= 1 - \alpha C_C \\
\Phi &= \left(1 - \alpha C_C\right)^2 \\
\Phi &= \exp\left(-\alpha C_C\right) \qquad (2.10) \\
\Phi &= \frac{1}{1 + \alpha C_C} \\
\Phi &= \left(1 + \alpha C_C\right)^{-2}
\end{aligned}$$

Numerous investigations for the kinetic modeling of coke have been conducted by Froment and co-workers. Examples are: isomerization of pentane on the reforming catalyst,[47] steam/CO_2 reforming of methane,[48, 49] steam cracking,[50] dehydrogenation of 1-butene into butadiene,[46, 51] and dehydrogenation of ethylbenzene into styrene.[52] Reviews for a rigorous formulation of a kinetic model of coke formation were presented by Froment.[53, 54]

2.5.2   Deactivation by Site Coverage

For the main reaction $A \rightarrow B$, the rate is written

$$r_A = r_A^o \varphi_A \qquad 0 \leq \varphi_A \leq 1 \tag{2.11}$$

where r_A^o is given by

$$r_A^o = kC_t^{n_A} f\left(C_j, K_j, ...\right) \tag{2.12}$$

and $\varphi_A = \left(C_t - C_{Cl}\right)/C_t$ is the deactivation function for this reaction when a single site is involved. Generally, if the main reaction involves n_A sites in the rate determining step, then the deactivation function φ_A is formulated as

$$\varphi_A = \left(\frac{C_t - C_{Cl}}{C_t}\right)^{n_A} \tag{2.13}$$

Since a coking reaction itself is also deactivated by the coke, the rate of coke formation can be described by

$$r_C = r_C^o \varphi_C \qquad 0 \leq \varphi_C \leq 1 \tag{2.14}$$

where

$$r_C^o = k_C C_t^{n_C} g\left(C_j, K_j, ...\right) \tag{2.15}$$

In the same way as Eq. (2.13) the deactivation function is given by

$$\varphi_C = \left(\frac{C_t - C_{Cl}}{C_t}\right)^{n_C} \tag{2.16}$$

The approach explained here relates the deactivation function φ to the coke content C_C, namely $\varphi = f(C_c)$. De Pauw and Froment[55] and Dumez and Froment[46] derived an

exponential relationship between deactivation function and coke content, which was determined by means of an electrobalance. An electrobalance is the primary equipment for the kinetic analysis of coke formation. The literature regarding this can be found in Ozawa and Bischoff for ethylene cracking,[42] Wagner and Froment for methane steam reforming,[56] Beirnaert et al. for catalytic cracking of n-hexane,[57] and Snoeck et al. for methane cracking.[58]

2.5.3   Deactivation by Site Coverage and Pore Blockage

If coke growth and pore blockage are involved in the coking mechanism, Eqs. (2.13) and (2.16) are no longer valid with respect to the definition of the deactivation functions in Eqs. (2.11) and (2.14), respectively. Beeckman and Froment[59, 60] investigated this situation. They treated the deactivation by site coverage and pore blockage using probability functions. The internal structure of the particle was first assumed to be a single pore. The deactivation function depended on the textural properties of catalyst and physical properties of coke. Marin et al.[51] explained the deactivation by coke deposition in butene dehydrogenation on Cr_2O_3/Al_2O_3 in terms of site coverage and pore blockage.

Beeckman and Froment[61] extended the deactivation study to a stochastic pore network model and considered diffusion, reaction, and deactivation by site coverage only. The pore network was represented by a Bethe-tree in which the pores of catalyst are represented by the bonds of a tree and their intersections are represented by the nodes. Since the percolation theory, which is a more reliable model to describe the pore

structure, was introduced by Sahimi and Tsotsis[62] to model the catalyst deactivation, a number of studies were made in this area.[63-66] The percolation theory was intensively reviewed by Sahimi et al.[67]

2.6   Deactivation Phenomena in Ethylbenzene Dehydrogenation

Both the catalyst and the process have been improved during the last 70 years. However, the migration of potassium promoter and its loss from the catalyst still remain as major problems.[11, 68] For adiabatic operation the potassium compounds are slightly volatile, so potassium migrates in the direction of the fluid flow in the catalyst bed. On the microscale, it moves from the exterior to the core of each catalyst pellet due to the temperature gradient resulting from the endothermicity of the reaction.[69] This migration and loss of potassium result in a serious loss of activity, selectivity to styrene, and mechanical strength. Muhler et al.[21] indicated that hydrogen formed as product of the reaction can reduce the active catalysts to magnetite, Fe_3O_4. Once these phases are formed, segregation of the phases occurs, leading to a potassium-rich core and a potassium-depleted shell in the catalyst.

Another problem associated with loss of potassium from the catalyst surface is the increase in the acidity of the iron oxide. This leads to an increase of cracking reactions especially to benzene and toluene and results in a decreased selectivity.[11]

The problem with using high concentrations of potassium is the vulnerability of the iron oxide catalyst to moisture increases with increasing potassium concentration.[70] The catalysts can undergo substantial changes under process conditions which decrease

their physical integrity. An increase in pressure drop across the reactor typically results from the physical degradation of the catalyst. The reduction of Fe_2O_3 to Fe_3O_4 causes a transformation in the lattice structure of the catalyst, resulting in the poor physical strength and a susceptibility to degradation by contact with water at temperatures below 100^oC. Dellinger et al.[70] claim that the addition of sodium and calcium compounds to iron catalysts improves the stability of the dehydrogenation catalyst.

2.7   Industrial Processes

2.7.1   Adiabatic Reactor

Over 75% of the styrene plants use adiabatic dehydrogenation in multiple reactors or single reactor with separate beds. The reheating of the reaction mixture can be accomplished either by injection of superheated steam or indirect superheated steam heat exchangers. Fresh ethylbenzene is mixed with recycled ethylbenzene and vaporized with addition of steam to prevent ethylbenzene from undergoing cracking reactions, which reduces the yields of styrene. The stream is further heated in a heat exchanger. Superheated steam is mixed to increase the feed temperature up to ca. 640^oC. The effluent from the first reactor is reheated prior to passage through the second reactor. Most adiabatic reactors are of the radial type, which are essential for low pressure-drop operation.[3, 71] The diagram of the radial reactor is shown in Figure 2.2.
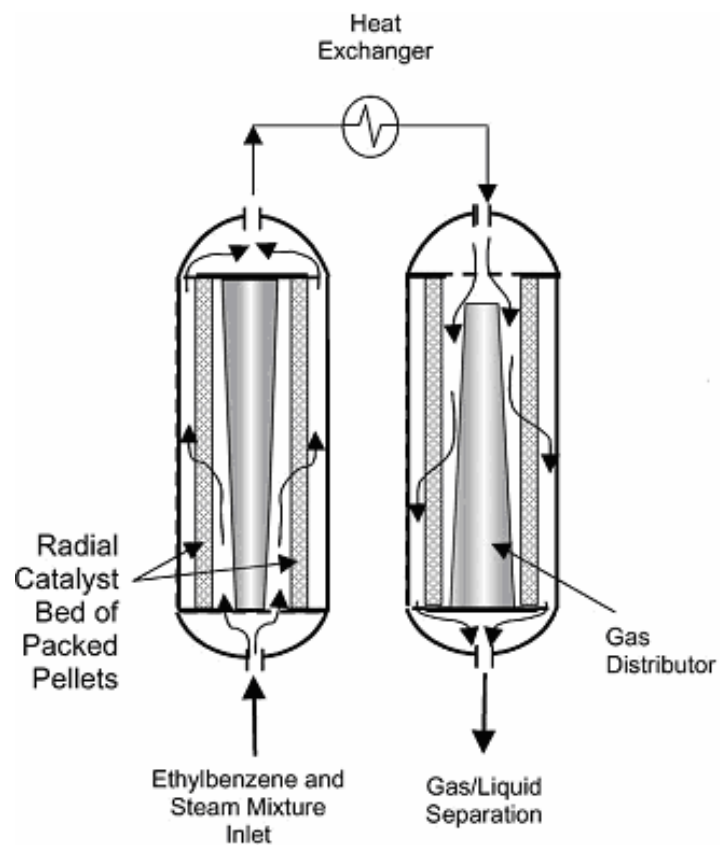
Figure 2.2. Diagram of radial-flow reactor.[72] With permission from Elsevier B. V.

2.7.2   Isothermal Reactor

Two major types of isothermal reactors have been used for ethylbenzene dehydrogenation reaction. The Lurgi reactor employs 20,000 to 30,000 tubes, 1 to 2-1/2 inch diameter and 8 to 10 ft length packed with catalyst and uses a molten salt mixture of sodium, lithium, and potassium carbonates as the heating medium.[73] The molten salt is circulated through an external heater to maintain its temperature at about 630°C. This system is typically operated under vacuum and a steam to ethylbenzene ratio of 0.6-0.9 by weights.

The other major process is used by BASF.[73] The heat of reaction is supplied by hot flue gas from a fired heater at 760°C. The steam to ethylbenzene weight ratio can be about 1 and steam temperatures are lower than in the adiabatic process. The packed tubes are fewer in number and larger; 4-8 in diameter and 8-13 ft length. Both isothermal processes have advantages in yield and savings in steam cost. However, the maximum practical size of a single isothermal reactor limits the total capacity to less than a single adiabatic reactor. Furthermore, construction of multitubular reactor is expensive.

2.8   Alternative Processes

One of the commercial routes to produce styrene involves coproduction of propylene oxide. Direct air oxidation of ethylbenzene gives ethylbenzene hydroperoxide (EBHP) and other byproducts with ~13 % of conversion and ~90 % selectivity to EBHP.[3] EBHP reacts then with propylene over metallic catalyst and gives α-methylbenzyl alcohol. Finally, α-methylbenzyl alcohol is dehydrated to styrene. This

process is commercialized by ARCO Chemical (formerly Oxirane) and by Shell. Approximately 1.2×10^6 tons/year is produced with this technology.[74]

The SMART process licensed by ABB Lummus oxidizes the H_2 formed by ethylbenzene dehydrogenation over noble metal catalyst place between single iron catalyst beds. The removal of H_2 increases the ethylbenzene conversion up to 80% per pass, maintaining the same styrene selectivity as for the conventional process.[74]

2.9 Minor by-products in Ethylbenzene Dehydrogenation

2.9.1 Impurities in Styrene Monomer

The process operating variables determine the variation of minor by-products in styrene monomer during ethylbenzene dehydrogenation. Table 2.2 shows the typical concentration of impurities in styrene. The separation of ethylbenzene and styrene requires 70-100 trays depending on the desired ethylbenzene content. Other minor products, such as *α*-methylstyrene, *i*-propylbenzene (cumene), *n*-propylbenzene, ethyltoluene, and vinyltoluene are removed in the final styrene distillation. The purity of the feed ethylbenzene affects the xylene content in styrene product.[3] Diethylbenzene in the feedstock ethylbenzene may be partially converted to divinylbenzene. Since divinylbenzene can polymerize very fast to make insoluble material in the purification process, the content of diethylbenzene must be below 0.04%.[75]

In modern styrene processes the content of diethylbenzene is minimized to around 8 ppm wt.[76] Traces of stilbene, diphenyl, naphthalene, and anthracene have been

found in high-boiling tar products.[73] Table 2.3 presents physical properties of the minor compounds in the reaction products.

Table 2.2. Typical concentration of styrene and minor by-products[77]

Component	Concentration, wt %
styrene	99.74
ethylbenzene	0.043
α-methylstyrene	0.028
isopropylbenzene	0.008
n-propylbenzene	0.004
m- and p-ethyltoluene	0.014
m- and p-xylene	0.125
o-xylene	0.030

2.9.2   Specification of Styrene Monomer

For quality control almost all styrene manufacturers use ASTM D2827-00 as a standard specification for styrene monomer. It requires minimum styrene purity of 99.7 wt%, but many styrene manufacturers produce higher purity styrene. For instance, minimum 99.85 wt% styrene is claimed by Lummus/UOP SM process.[76] The purity of styrene was determined by freezing point method (ASTM D3799-95), but this standard test method was withdrawn in 2000. Instead, a gas chromatography method is used to determine the overall purity of styrene.[77] Table 2.4 shows the ASTM specifications and test methods. ASTM for the styrene analysis using GC is shown in Appendix A.

Table 2.3. Physical properties of the minor products[78]
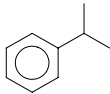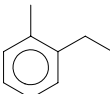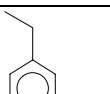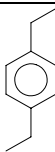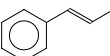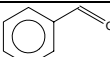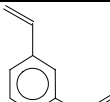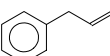
			FW	bp (°C)	d
cumene (isopropylbenzene)		$C_6H_5CH(CH_3)_2$	120.20	152-154	0.864
2-ethyltoluene		$C_2H_5C_6H_4CH_3$	120.20	164-165	0.887
m-diethylbenzene (1,3-diethylbenzene)		$C_6H_4(C_2H_5)_2$	134.22	181.7	0.860
p-diethylbenzene (1,4-diethylbenzene)		$C_6H_4(C_2H_5)_2$	134.22	184	0.862
α-methylstyrene		$C_6H_5(CCH_3)=CH_2$	118.18	165-169	0.909
phenylacetylene (ethynylbenzene)		$C_6H_5C{\equiv}CH$	102.14	142-144	0.930
β-methylstyrene (1-propenylbenzene)		$C_6H_5CH=CHCH_3$	118.18	175	0.911
benzaldehyde		C_6H_5CHO	106.12	178-179	1.044
m-divinylbenzene (1,3-diethenylbenzene)		$C_6H_4(CH=CH_2)_2$	130.19	195-197	0.914
indene		C_9H_8	116.16	181.6	0.996
naphthalene		$C_{10}H_8$	128.17	217.7	0.963
allybenzene (2-propenylbenzene)		$C_6H_5CH_2CH=CH_2$	118.18	156-157	0.892

Table 2.4. ASTM specification for styrene monomer[3, 79]

	ASTM D2827-00	Typical analysis	ASTM test method
Purity, min., wt %	99.7	99.8	D5135 *
Aldehydes, max., wt% as benzaldehyde	0.02	0.003	D2119
Peroxides, max., mg/kg as H_2O_2	100	5	D2340
Polymer, max., mg/kg	10	0	D2121, test method A
Inhibitor, mg/kg	10 to 15	12	D4590
Color, max., Pt/Co scale	10	7	D1209
Impurities			D5135 **

* Purity was determined by freezing point using ASTM 3799-95. This method was discontinued in 2000.

** Prior to 2000, impurities were determined by gas chromatography using D5135. Now, this method is being used to determine overall purity of styrene monomer

CHAPTER III

EXPERIMENTAL METHODS

3.1   Introduction

Kinetic experiments of ethylbenzene dehydrogenation into styrene were performed using a commercial potassium-promoted iron catalyst in a tubular reactor. The details of the experimental fixed-bed set-up consisting of feed-, reactor-, and analysis- section are shown in Figure 3.1. The analysis section is divided into two subsections: On-line analysis for major components and off-line analysis for minor products. As a method of textural characterization of the catalyst N_2 adsorption is described.

3.2   Feed and Reactor Section

Nitrogen served as a diluent for the reaction and as an internal standard for the GC analysis. The mass flow rate of nitrogen was controlled by a mass flow controller (OMEGA). The liquid feeds, i.e. ethylbenzene/styrene and water, were pumped and controlled by means of two precise syringe pumps (HARVARD). Before starting the reaction the calibration of the mass flow controller and syringe pumps was carried out.

Great attention was paid to have liquids and gases well mixed through the two preheaters before they were fed to the reactor. The detailed schematic of preheaters is shown in Figure 3.2. Water was pumped through a feed tube extending to the middle section of the first preheater, which was filled with α-Al_2O_3 beads (Saint-Gobain NorPro,

D-99). The temperature of the preheater was kept at 200$^{\mathrm{o}}$C. Nitrogen was fed to the bottom of the preheater. The two streams of water and nitrogen traveled through the preheater separately and were heated up to vaporize the water before the two gaseous streams met at the middle section. The gaseous mixture of steam and nitrogen left the first preheater and was then fed to the second preheater where the temperature was kept at 200$^{\mathrm{o}}$C. In the second preheater the gaseous mixture of steam, nitrogen, and ethylbenzene/styrene was fed in the same manner. The effluent from the second evaporator was fed to the top of the reactor.

The reactor was a stainless steel tube and had a dimension of 1 inch of inner diameter and 18 inch of length. The inner surface of the reactor was plated with chromium to suppress coke formation on the surface of the reactor. The reactor was heated by a furnace surrounding the reactor tube. Three OMEGA type-K thermocouples were located on the inside wall of the furnace. They transmitted the temperature signal to digital OMEGA temperature controllers to control the temperature of the furnace. The temperature inside the reactor was monitored by an OMEGA type-K thermocouple. A movable thermocouple was placed inside the thermowell, which was located inside the reactor, to measure the axial temperature profile along the reactor. The thermowell was made of a stainless steel.

The reactor was packed with the catalyst as shown in Figure 3.3. For the catalyst bed dilution iron catalyst with the particle size of 0.25 – 0.42 mm was mixed with the same particle size of inert α-Al_2O_3 in the weight ratio of 1 to 6. The upper and lower
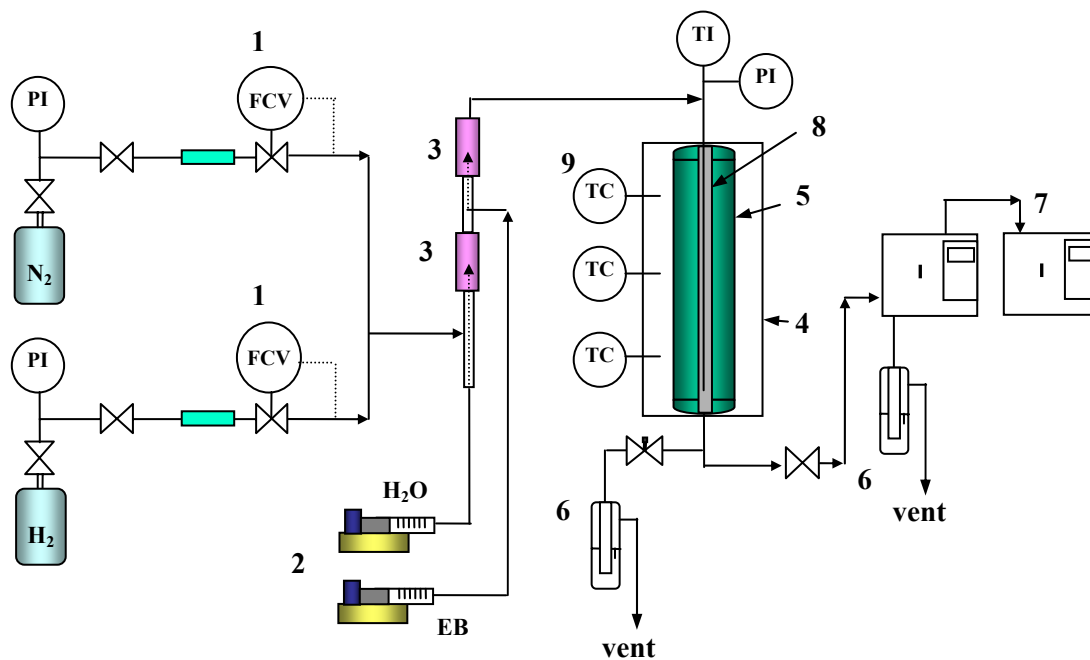
Figure 3.1. Experimental fixed-bed set-up for the kinetic study of ethylbenzene dehydrogenation: (1) mass flow control valve; (2) liquid syringe pump; (3) mixer & preheater; (4) furnace; (5) fixed-bed reactor; (6) scrubber; (7) gas chromatographs (TCD & FID); (8)thermowell; (9) temperature controller.
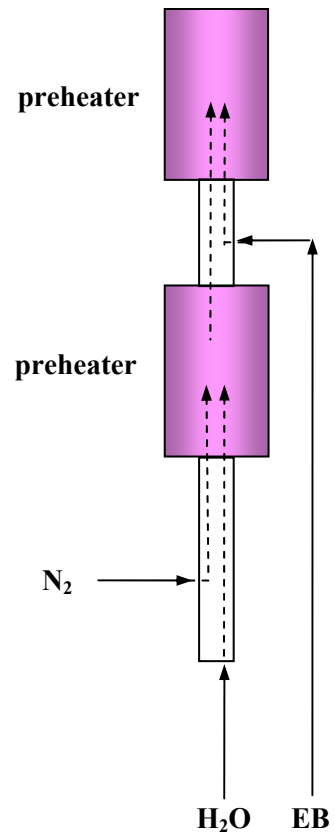
Figure 3.2. Schematic of preheaters

Flow in   Thermocouple

Thermowell

23cm   **Pre-Section** (α-alumina only)

44cm   3cm   **Catalyst bed** (catalyst + α-alumina)

28cm   **Post-Section** (α-alumina only)

2.54cm

Flow out
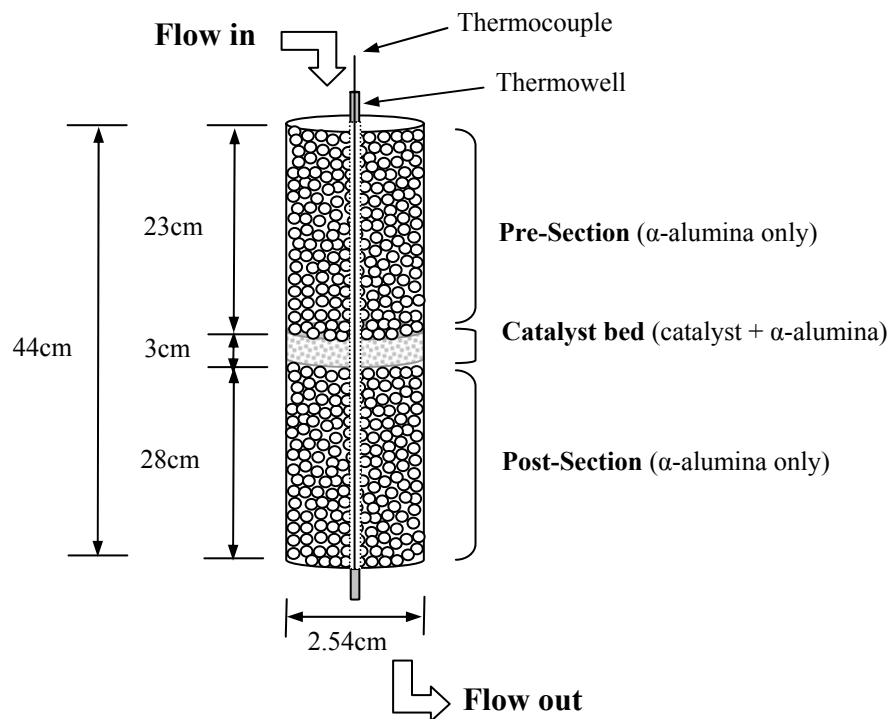
Figure 3.3. Schematic diagram of reactor packing and dimension.

sections of the reactor were filled with α-Al_2O_3 beads which serves two functions: preheating and mixing of reactants and reduction of the free volume of the reactor.

Before the experiments were conducted, the pelletized commercial potassium-promoted iron catalyst was crushed and sieved to have an appropriate particle size of 0.25 – 0.42 mm to avoid internal diffusion resistance. The diagnostic test for the possible external mass transfer limitation was done in the way guided by Froment and Bischoff.[80] The gases passed through the catalyst bed, reacted, and then left the reactor at the bottom. In order to prevent the condensation of the liquid products all the tube lines were wrapped with heating tape and the temperature was maintained around 145°C.

The exit stream of the reactor was divided into two streams. One stream was the main amount of gas. It was sent to the heat exchanger, where water was used as a cooling medium, to condense the liquid products. These were sampled for *off-line analysis* of the minor by-products. The detailed *off-line analysis* procedure will be explained in section 3.3.2. The other stream was a smaller amount of gas which was sent to the gas chromatograph (GC), a Shimadzu GC-17A equipped with a thermal conductivity detector (TCD) followed by a Hewlett Packard (HP) 5890 with a flame ionization detector (FID) for the *on-line analysis*. The detailed *on-line analysis* procedure will be presented in section 3.3.1.

3.3   GC Analysis Section

3.3.1   On-line GC Analysis for Major Reactions

The effluent of the reactor was analyzed on-line using the two GCs connected in series: Shimadzu GC-17A with TCD followed by HP 5890 with FID. Helium gas was used as a carried gas for the GC analysis. The transfer line between GCs was heated at $145^{o}C$. The Shimadzu GC-17A was equipped with the valve system to inject the product gases and switch the valves in a programmable manner, which enables to separate all the chemical species through the columns. A timing program for switching the valves was stored in the Shimadzu GC-17A and ran during the analysis. The oven temperature programs of Shimadzu 17-A and Hewlett Packard 5890 and valve switching timing program should be matched in order to accomplish the desired separation. The list of timing programs is shown in Table 3.1.

The configuration of switching valves and columns is depicted in Figure 3.4. The three capillary columns used for the separation of mixture compounds are as follows:

- MolSieve: HP PLOT Molecular Sieve 5A, 0.53 mm ID $\times$ 25 μm $\times$ 15 m (Separation of H_2 and N_2)

- P-Q: J&W GS-Q capillary column, 0.53 mm ID $\times$ 30 m (Separation of N_2, CO, CO_2, CH_4, C_2H_4, and H_2O)

- HP-5: Agilent HP-5 capillary column, 0.53 mm ID $\times$ 1.5 μm $\times$ 30 m (Separation of aromatic compounds)

Table 3.1. Operating conditions for the GC analysis

Time schedule for	Time	Function	Value	
Switching valves	0.01	Event	-91	(6 port valve OFF)
	0.02	Event	-92	(sampling valve OFF)
	0.05	Event	92	(sampling valve ON)
	0.08	Event	91	(6 port valve ON)
	4.20	Event	-92	(sampling valve OFF)
	7.90	Event	-91	(6 port valve OFF)
HP GC (FID) conditions	Initial: 30°C			
Oven temperature	Rate 1: 15°C/min			
	Final 1: 95°C			
	Rate 2: 6°C/min			
	Final 2: 120°C for 5.5min			
Detector temperature	280°C			
Carrier gas	He			
Shimadzu GC (TCD) conditions				
Oven temperature	Initial: 60°C			
	Rate 1: 15°C/min			
	Final 1: 30°C for 10min			
	Rate 2: 15°C/min			
	Final 2: 60°C for 4min			
Injector temperature	170°C			
Detector temperature	165°C			
Carrier gas	He			

The eluting compounds were detected by two detectors in series: TCD followed by FID. On the TCD, N_2, H_2, CO, CO_2, H_2O, benzene, toluene, ethylbenzene, and styrene were analyzed. On the FID, CH_4, C_2H_4, benzene, toluene, ethylbenzene, and styrene were analyzed. An example of retention times of the eluting compounds is listed in Table 3.2. N_2 was used as an internal standard for the TCD analysis. Ethylbenzene was chosen as a secondary internal standard because it showed on the TCD and on the FID as one of the major compounds, so that it could be used to 'tie' TCD analysis and FID analysis.

To calibrate liquid standard mixtures with known concentrations were fed to the experimental unit as described in section 3.2 using precision syringe pumps. For the preparation of gas standard mixtures, pure gases were fed by means of mass flow controllers and then mixed in the preheaters and reactor. Mass flow controllers were calibrated using a soap bubble flowmeter. During the calibration, preheaters, reactor, and tube lines were heated between $140^{o}C$ and $200^{o}C$. Samples were injected to the GCs five to ten times. At least three different concentration levels were used, which resulted in the GC data with retention times and peak areas of the standard mixture. The calibration was completed by plotting the weight ratios of component j to EB (and weight ratio of EB to N_2) against the corresponding peak area ratios.

By using the measured feed rates and the GC analysis, EB conversion, conversions into product i, and selectivities of product i were calculated using the definitions below.

- EB conversion (%) $= 100 \times \dfrac{F_{EB}^0 - F_{EB}}{F_{EB}^0}$

- Conversion of EB into product j (%) $= 100 \times \dfrac{F_j - F_j^0}{F_{EB}^0}$

- Selectivity of product j (%) $= 100 \times \dfrac{F_j - F_j^0}{F_{EB}^0 - F_{EB}}$

where $F_{EB}{}^0$ is the feed molar flow rate of ethylbenzene, $F_j{}^o$ is the feed molar flow rate of product j, F_{EB} is the molar flow rate of ethylbenzene, and F_j is the molar flow rate of product j.
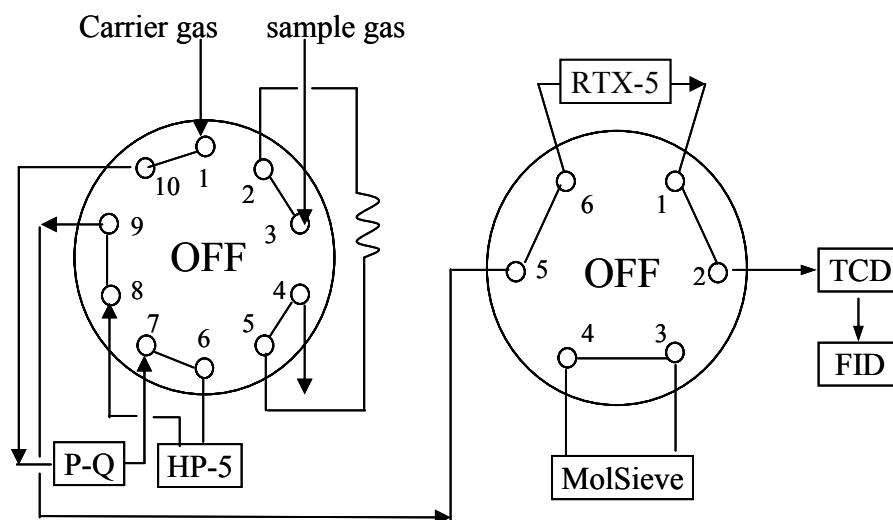
Note) P-Q: Porapak Q column; MolSieve: Molecular Sieve 5A column

Figure 3.4. Configuration of switching valves and GC columns.

Table 3.2. Example of GC retention times of the effluent components

Components	Retention time, min (TCD)	Retention time, min (FID)
H_2	4.816	-
N_2	5.183	-
CH_4	5.733	5.833
CO	7.566	-
CO_2	9.55	-
C_2H_4	9.916	10.000
Benzene	10.550	10.650
Toluene	13.683	13.783
Ethylbenzene	15.683	15.833
Styrene	16.333	16.566

3.3.2 Off-line GC Analysis for Minor Side Reactions

As described in section 3.2, the liquid products were condensed and collected in the sample container. The liquid was separated into two phases, i.e., a water phase and a hydrocarbon phase, at the ambient temperature, approximately $22^{\circ}C$. Since the temperature dependence of the solubility of aromatics in the water is not significant between $0^{\circ}C$ and $25^{\circ}C$, no further chilling of the condensed sample was performed. The detailed data of solubility and mole fraction of aromatics in the saturated water solution are shown in Tables 3.3 and 3.4.[81]

The standard samples with two concentration levels were injected into the injection port of GC using a microsyringe. The GC used for *off-line analysis* is second

HP 5890, which is different from that utilized for *on-line analysis*. The operating conditions of the GC are as follows:

- GC: HP 5890 (FID)

- Column: DB-WAXETR (Agilent) - 0.25 μm × 60m × 0.25mm

  – polar-fused silica capillary column internally coated with crosslinked polyethylene glycol

  – temperature range: 30^oC to 260^oC

- Injector temperature: 200^oC

- Detector temperature: 250^oC

- Carrier gas & flow rate: He, 3.5ml/min

- Column head pressure: 120 kPa

Figure 3.5 shows the oven temperature program for the off-line analysis.

A typical amount injected into the GC was 1.0 μl. Repeated injections of standard samples, normally 5~8 times, were performed to ensure reproducibility of the analysis. Figure 3.6 shows the FID chromatogram of a standard mixture sample. It shows the peaks of minor by-products, such as cumene, phenylacetylene, *n*-propylbenzene, α-methylstyrene, β-methylstyrene, divinylbenzene, and stilbene. The GC data processing was the same as that for *on-line analysis*. For the standard test method for analysis of styrene by capillary gas chromatography, refer to the ASTM D5135-95.[77]
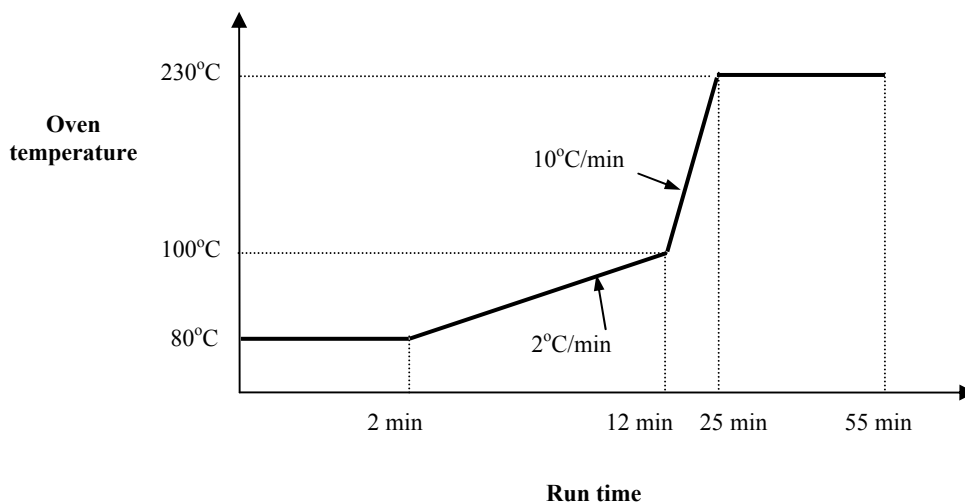
Figure 3.5. Oven temperature program for the off-line analysis.

Table 3.3. Solubility of aromatics in the saturated water solution (g aromatic/100g saturated solution)[81]

aromatics	Temp. (K)				
	273	283	293	298	303
styrene	-	0.029	0.030	0.025±0.006	0.034
ethylbenzene	0.020	0.018	0.0181±0.0004	0.0169±0.0009	0.0190
benzene	0.169 ± 0.013	0.178 ± 0.003	0.176±0.003	0.177± 0.004	0.181 ± 0.004
toluene	0.069 ± 0.003	0.059 ± 0.004	0.057±0.003	0.053 ± 0.002	0.059 ± 0.004
cumene	-	0.006 [§]	0.0056±0.0007 [¶]	0.0056±0.0007	0.0074±0.0009

[§] Measured at 288K.

[¶] Measured at 298K.

Table 3.4. Mole fraction of aromatics in the saturated water solution[81]

aromatics	Temp. (K)				
	273	283	293	298	303
styrene	-	5.00×10^{-5}	5.20×10^{-5}	4.30×10^{-5}	5.90×10^{-5}
ethylbenzene	3.40×10^{-5}	3.10×10^{-5}	3.07×10^{-5}	2.87×10^{-5}	3.20×10^{-5}
benzene	3.90×10^{-4}	4.11×10^{-4}	4.06×10^{-4}	4.09×10^{-4}	4.18×10^{-4}
toluene	1.35×10^{-4}	1.15×10^{-4}	1.11×10^{-4}	1.04×10^{-4}	1.15×10^{-4}
cumene	-	0.90×10^{-5} *	0.84×10^{-5} §	0.84×10^{-5}	1.11×10^{-5}

* Measured at 288K.

§ Measured at 298K.
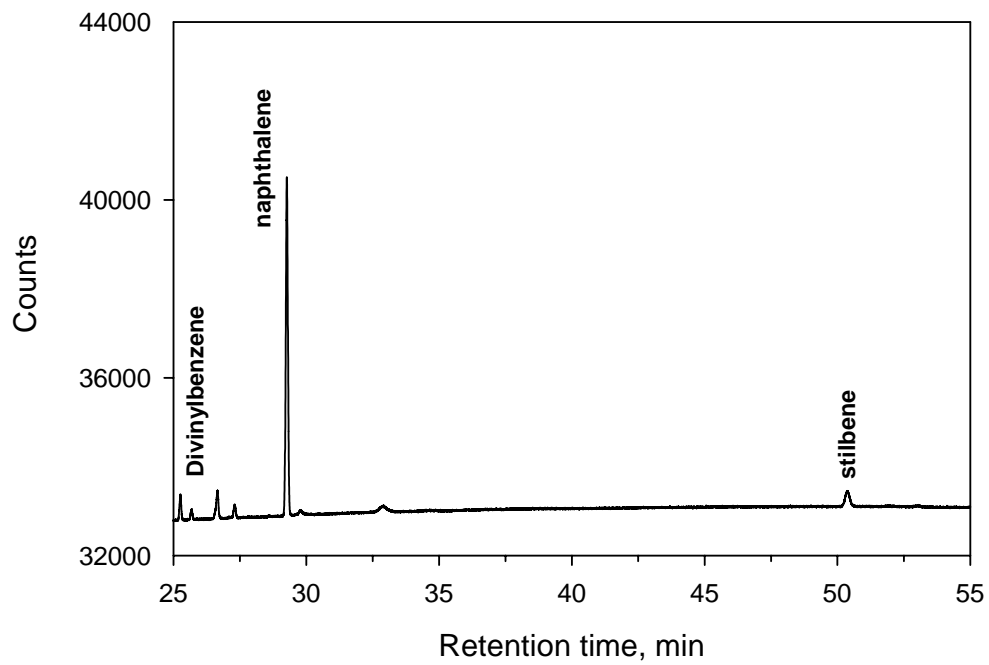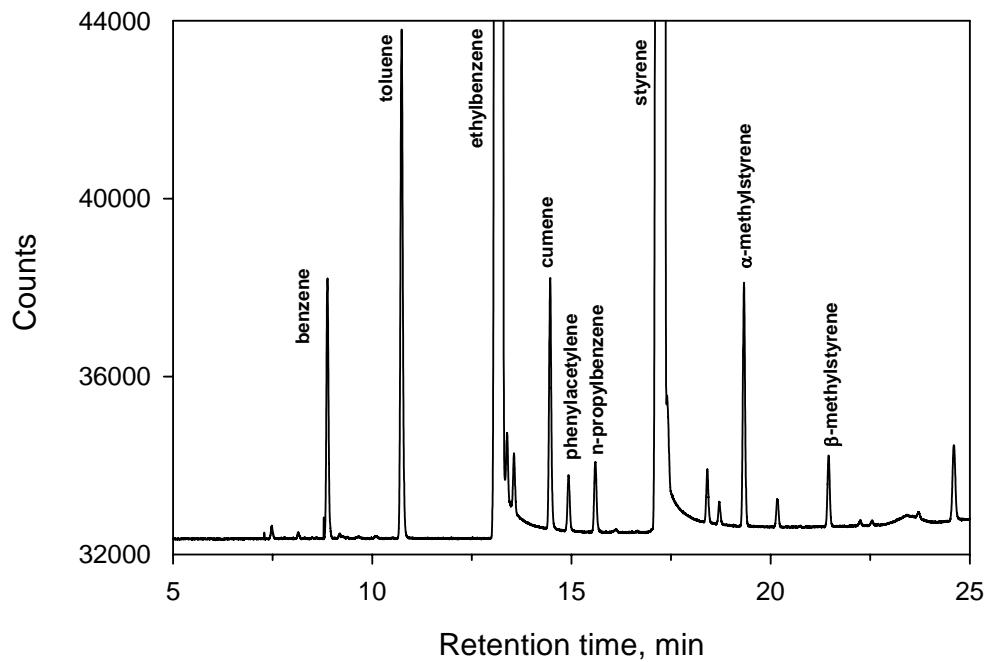
Figure 3.6. FID chromatogram of standard mixture sample.

3.4 **Catalyst Characterization: Nitrogen Adsorption**

The catalyst surface area, isotherms, and pore size distribution were measured using an ASAP 2000 (Micromeritics). Nitrogen was used as an adsorbent at the liquid nitrogen boiling point, i.e., 77.35 K. The adsorption and desorption data were processed by ASAP 2010 software. Surface area is determined when the BET equation,[82]

$$\frac{P}{V(P_0 - P)} = \frac{1}{V_m C} + \frac{(C-1)}{V_m C} \frac{P}{P_0}$$

is applied by plotting $P/V(P_0-P)$ against P/P_0 (where P_0 is the vapor pressure of the adsorbate at the adsorption temperature, P is the pressure of gas, V is the volume of gas adsorbed, V_m is the monolayer volume, and C is a constant.

The slope and intercept of the plot yield the monolayer volume capacity in the adsorption and the constant, C. The number of moles adsorbed in the monolayer is $V_m/0.0224$ when the monolayer volume is examined at standard temperature and pressure, i.e., 0^oC and1 bar. The specific surface area in m^2/g is calculated by the following equation.

$$S_g = \frac{V_m}{0.0224} \times 6.023 \times 10^{23} \times A$$

where A is the area occupied by each adsorbed molecule.

The pore size distribution is generated by ASAP 2010 software based on the BJH method proposed by Barrett, Joyner, and Halenda.[83]

CHAPTER IV

EXPERIMENTAL RESULTS

4.1 Experimental Results for the Major Reactions

4.1.1 Experimental Procedure

The fresh iron catalyst should be activated before the kinetic experiments are performed. Great attention must be paid to the activation procedure. The standard condition used for the catalyst activation is:

- Temperature: $620^{o}C$

- H_2O/EB feed ratio: 11 mol/mol

- Space time: 80 gcat hr/mol EB

- Partial pressure of N_2: 0.432 bar

The temperature was raised to $620^{o}C$ under a N_2 flow through the reactor. The temperature was kept at $620^{o}C$ for 12 hours. Water started to be pumped first to the preheater in order to prevent the catalyst deactivation which may occur when only ethylbenzene is pumped. Ethylbenzene began to be injected to the preheater 1 or 2 minutes after the injection of water. During the night the feed of ethylbenzene and water were always shut off and the temperature was maintained at $620^{o}C$ under N_2 flow. It took 3 or 4 days to fully activate the fresh catalyst on the basis of the 12 to 14 hours' operation a day.

The kinetic data were collected at various reaction conditions: temperature, space time, feed molar ratios of H_2O/EB, feed molar ratios of ST/EB, and feed molar ratios of H_2/EB. Experiments were carried out at 3 different temperatures: $600^{o}C$, $620^{o}C$, $640^{o}C$. Space times were in the range between 6 gcat hr/mol of EB and 70 gcat hr/mol of EB, depending on the temperature. Kinetic experiments were always performed at the reaction conditions where the low 'approach to equilibrium' could be achieved. The total absolute pressure inside the reactor was 1.04 bar for all the experiments. The calculation of total absolute pressure inside the reactor was based upon 0.99 bar (14.56 psi) of the averaged barometric pressure of College Station area. Daily barometric pressures have been measured at Easterwood Airport in College Station which is elevated at 305 feet above sea level by the Office of the Texas State Climatologist of Department of Atmospheric Science at Texas A&M University in College Station. The collected data were used to calculate the averaged barometric pressure.

The partial pressure drop between bulk fluid and surface of a catalyst particle was calculated according the procedure given in Froment and Bischoff.[84] Calculation proved that external mass transfer resistance was negligible. Internal mass transfer resistance was also insignificant because of the small particle size of the catalyst.

Steady state was usually attained 3 – 4 hours after the reaction conditions were changed. At the standard condition mentioned above the catalyst remained active for several weeks, depending on the amount of catalyst. Whenever the kinetic experiments were carried out, the activity of the catalyst was first checked to confirm that the catalyst was not deactivated.

4.1.2   Nitrogen Adsorption

The surface area determined by BET was 2.16 ± 0.07 m²/g. The particle size of the catalyst sample for BET analysis was the same as that used in the kinetic experiments. The surface area of the commercial potassium-promoted iron catalyst for ethylbenzene dehydrogenation is quite low because of the large pore size required for a high styrene selectivity.[71, 85, 86] The high calcination temperature is the main cause of the reduction of the BET surface area. Courty[86] showed when the calcination temperatures were 920°C, 940°C, and 970°C, the BET surface areas were 3.2 m²/g, 2.5 m²/g, and 2.2 m²/g, respectively. The corresponding average pore diameters were 270nm, 320nm, and 480nm. Rossetti el al.[86] measured BET surface area and pore size distribution for the commercial catalyst (Süd Chemie AG) and reported BET surface area is 2.8 m²/g and the pore size distribution is narrow and centered around 0.35μm (350nm) determined by mercury porosimetry.

The macro-porosity of the commercial catalyst was observed from the adsorption-desorption isotherms. Note that pores greater than 50nm are termed macropores; those smaller than 2 nm, micropores by the IUPAC classification.[87] Figure 4.1 shows the adsorption-desorption isotherms for the commercial catalyst. No appreciable hysteresis was observed. The shape of the isotherm is the *Type II* isotherm, called *sigmoid* and *S-shaped isotherm,* according to the five types isotherms proposed by Brunauer and coworkers.[88] *Type II* isotherm is frequently encountered on nonporous materials or macroporous materials. The inflection point or 'knee' of the isotherm occurs

when the monolayer adsorption is complete. As the relative pressure increases, a multilayer adsorption proceeds.[82]
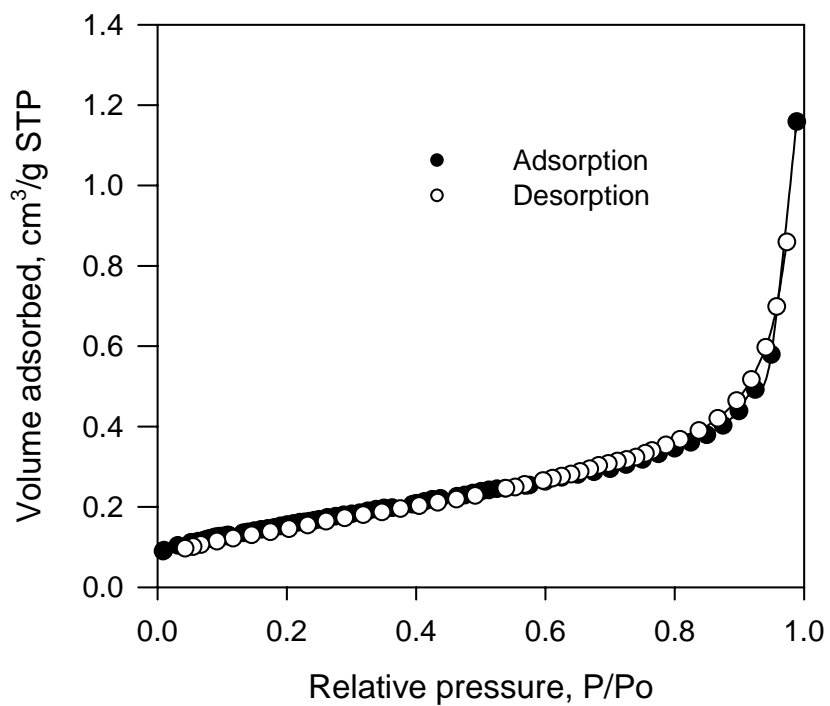
Figure 4.1. Adsorption and desorption isotherms for the commercial catalyst.

4.1.3   Long Run Test

The catalytic ethylbenzene dehydrogenation was carried out for 14 days to observe the variation of the catalyst activity under standard condition. For kinetic studies the catalyst bed should be isothermal. An axial temperature inside the reactor was measured by a movable thermocouple located inside the thermowell. The catalyst bed, which is the mixture of catalyst and α–alumina diluent, was placed between 23cm and 26cm from the entrance of reactor. Temperature was well controlled to be isothermal at the catalyst bed.

Figure 4.2 shows the ethylbenzene conversion as a function of run length. Ethylbenzene conversion data were scattered before 50 hours run length, which means the catalyst does not reach the fully activated state yet. After 50 hours run length, the catalyst activity was finally stable and was maintained until 150 hours run length. No more experiments were conducted after the 150 hours run length. The ethylbenzene conversion averaged between 50 hours and 150 hours was (75.81 ± 1.03) %, where the number following the ± sign indicates one standard deviation.

Figure 4.3 shows the ethylbenzene conversion into styrene as a function of run length. The equilibrium conversion of ethylbenzene into styrene calculated from thermodynamics at the reaction conditions was 85%. The calculation procedure will be discussed in section 6.3.1. The experimental conversions into styrene are far below the thermodynamic equilibrium conversion. The variation of the styrene selectivity is given in Figure 4.4. The averaged styrene selectivity was (92.25 ± 1.43) %.

The selectivity of benzene and C_2H_4 and the selectivity of toluene and CH_4 are plotted as a function of run length in Figures 4.5 and 4.6, respectively. A closer investigation of these figures reveals the non-stoichiometric evolution of CH_4 and C_2H_4 during the reaction. This is the reason that numerous papers include in the reactor simulation the additional steam reforming reaction of CH_4 and C_2H_4 along with water-gas shift reaction, which are assumed to be irreversible.[9, 10, 35, 38, 89]

$$CH_4 + H_2O \rightarrow CO + 3H_2$$

$$C_2H_4 + 2H_2O \rightarrow 2CO + 4H_2$$

$$CO + H_2O \rightarrow CO_2 + H_2$$
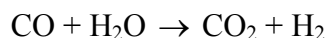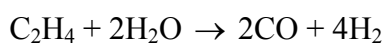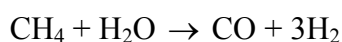
But this is the global way of describing the formation of CO and CO_2. The detailed reaction scheme of the coke deposition on the catalyst surface formed from CH_4 and C_2H_4 followed by the coke gasification with steam was not taken into account.

The complete set of reactions of steam reforming of CH_4 was presented by Xu and Froment.[90] Furthermore, according to the kinetic models for the carbon formation and gasification on the Ni catalyst studied by Snoeck and Froment,[49, 58] coke is formed by methane cracking and Boudouard reaction and then is gasified by H_2, CO_2, and steam. On the same line with this can it be postulated that CH_4 and C_2H_4 may form coke on the surface of the catalyst and the coke undergo gasification reaction with steam to give CO and CO_2.

The conversions into CH_4 and C_2H_4 collected from the experiments at different sets of reaction conditions were found to range between 1% and 2%. Since the low concentrations of CH_4 and C_2H_4 in the reaction mixture do not allow a reliable kinetic

modeling, no steam reforming reactions are taken into account in the present investigation.
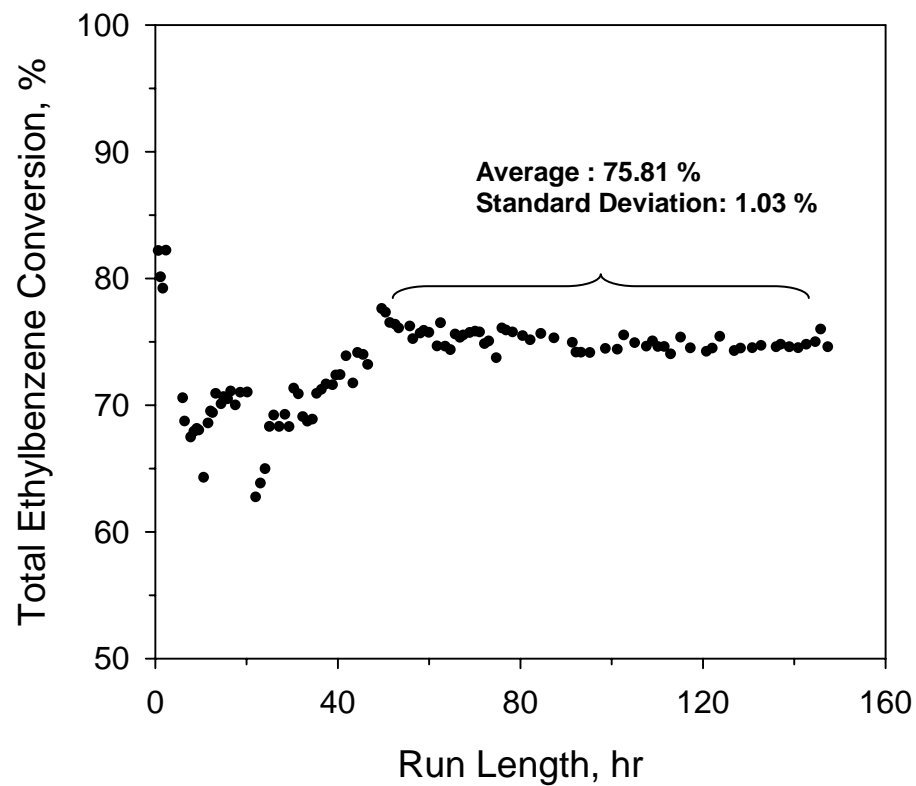
Figure 4.2. Total ethylbenzene conversion as a function of run length for $T = 620^{\circ}C$; Space time = 80 gcat hr/mol EB; $H_2O/EB = 11$ mol/mol; $P_{N2} = 0.432$ bar.
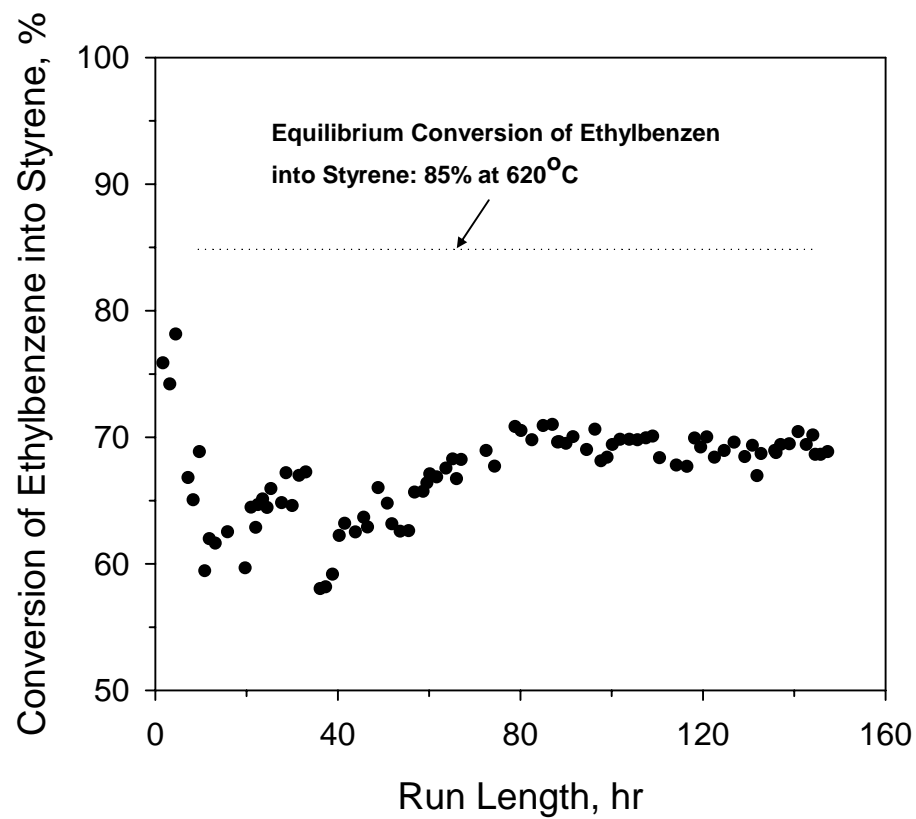
Figure 4.3. Ethylbenzene conversion into styrene as a function of run length for $T =$ 620°C; Space time = 80 gcat hr/mol EB; H_2O/EB = 11 mol/mol; P_{N2} = 0.432 bar.
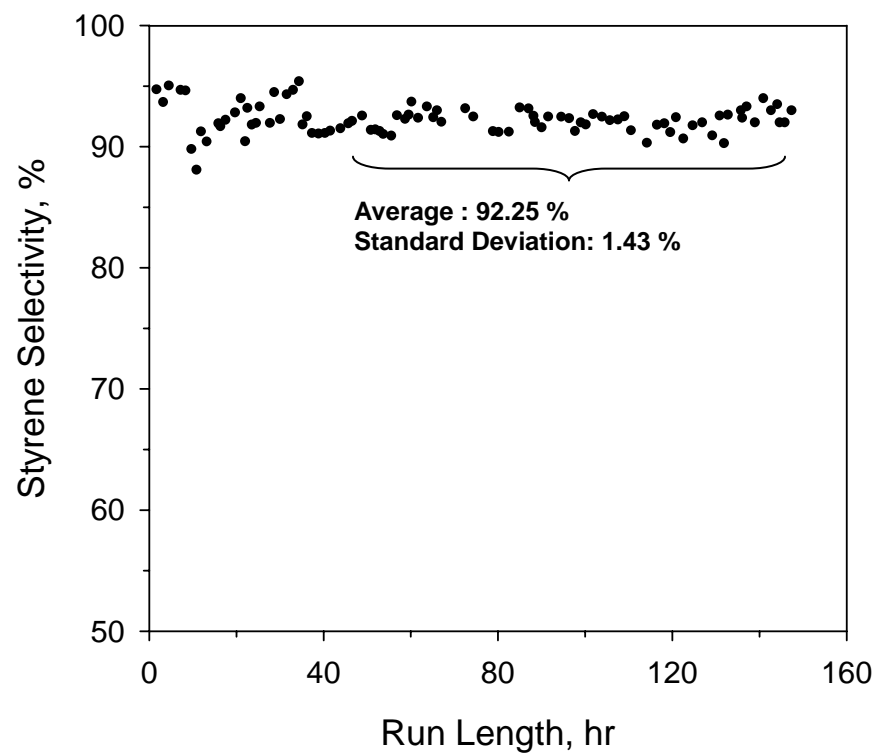
Figure 4.4. Styrene selectivity as a function of run length for $T = 620^{\circ}C$; Space time = 80 gcat hr/mol EB; H_2O/EB = 11 mol/mol; P_{N2} = 0.432 bar.
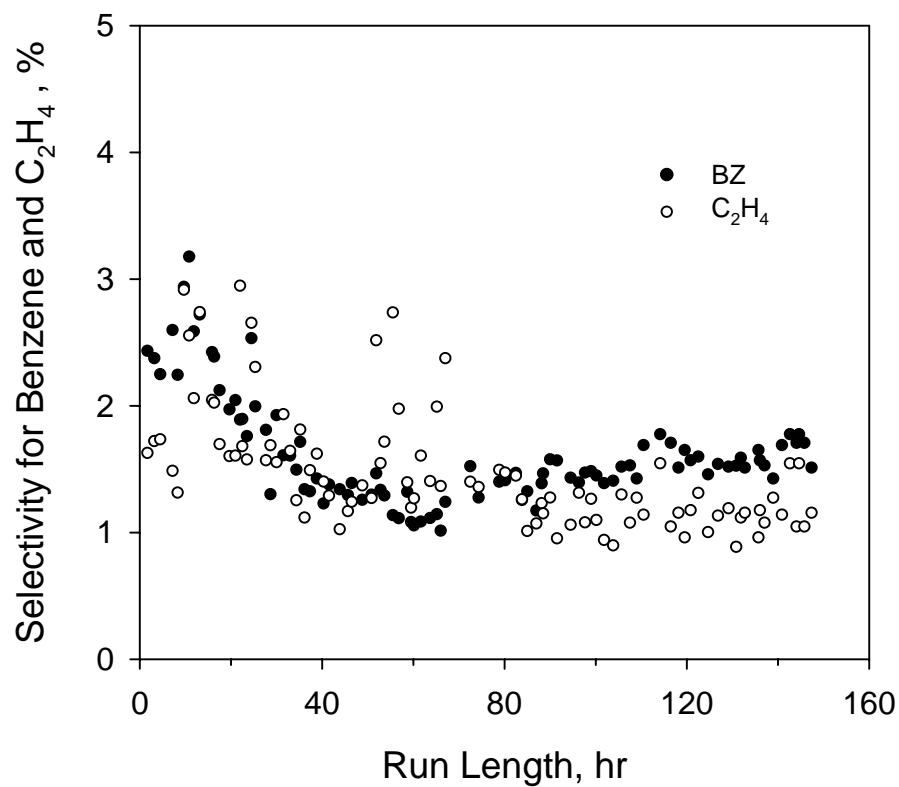
Figure 4.5. Selectivity for benzene and C_2H_4 formation as a function of run length for T = 620°C; Space time = 80 gcat hr/mol EB; H_2O/EB = 11 mol/mol; P_{N2} = 0.432 bar.
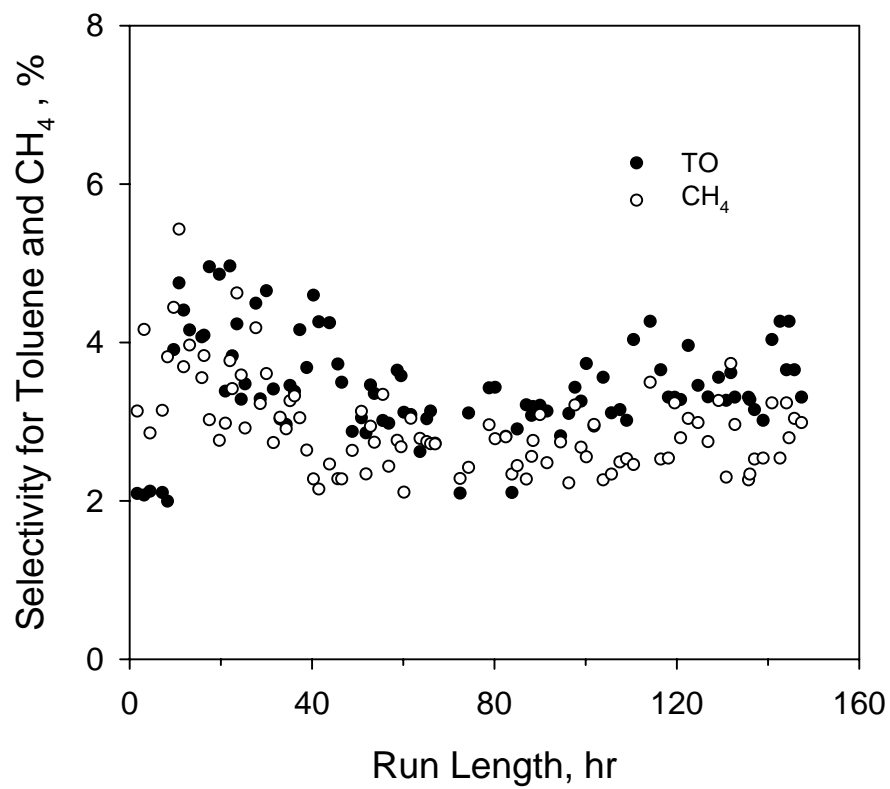
Figure 4.6. Selectivity for toluene and CH_4 formation as a function of run length for $T =$ 620°C; Space time = 80 gcat hr/mol EB; H_2O/EB = 11 mol/mol; P_{N2} = 0.432 bar.

4.1.4   Effect of Temperature

Experimental data were collected by injecting the sample 6-10 times into on-line GC set-up at the same reaction conditions. The averaged values are plotted in the following figures. The standard deviations at each point are very small (about 1% of the averaged value), so that the no error bars are shown in the figures.

Figure 4.7 shows the effect of temperature and space time on the total ethylbenzene conversions. The total ethylbenzene conversion did not increase appreciably when the space times were greater than around 70 gcat hr/mol at all the temperatures because the reactions approach the equilibrium at these high space times. For the reactions to be controlled by kinetics, experiments were usually conducted at the low space time region, i.e., 10 gcat hr/mol EB to 70 gcat hr/mol EB. These experiments data for kinetic studies are appropriate for the kinetic modeling, which will be discussed in chapter V. The experimental results are shown in Figure 4.8. The solid lines in the figure are drawn to fit the data.

Figure 4.9 shows the effect of temperature and space time on the conversion into styrene for all the temperatures. The calculated equilibrium conversions of ethylbenzene into styrene are 80.4%, 85.0%, 88.8% at $600^{o}C$, $620^{o}C$, and $640^{o}C$, respectively. The corresponding experimental conversions into styrene were 60.0%, 71.6%, and 79.1% at 62 gcat hr/mol. Figure 4.10 shows the styrene selectivity as a function of total ethylbenzene conversion for all the temperatures. The styrene selectivity evolved in an opposite way to the total ethylbenzene conversion. The styrene selectivity tended to be

low as the temperature decreased because the competitive reactions producing by-products become pronounced as the temperature increases.

A plot of the benzene selectivity against the total ethylbenzene conversion for all the temperatures is shown in Figure 4.11. The benzene selectivity was almost constant around 1% at $600^{o}C$, even though total ethylbenzene conversion increased. At $640^{o}C$, the benzene selectivity increased from 2.4% to 3.4% as the total ethylbenzene conversion increased from 50 %to 86 %. The increase of toluene selectivity with total ethylbenzene conversion was more significant than benzene selectivity as shown in Figure 4.12. The toluene selectivity was far below 1% at the total ethylbenzene conversion of 22%. It reached 6% as the total ethylbenzene conversion increased up to 86%. Since the selectivity can be expressed by the ratio of the rate of product formation to the rate of ethylbenzene consumption, one can conclude that the rate of benzene formation is not affected very much by the total ethylbenzene conversion (or space time). The rate of toluene formation, however, is enhanced as the total ethylbenzene conversion (or space times) increases.
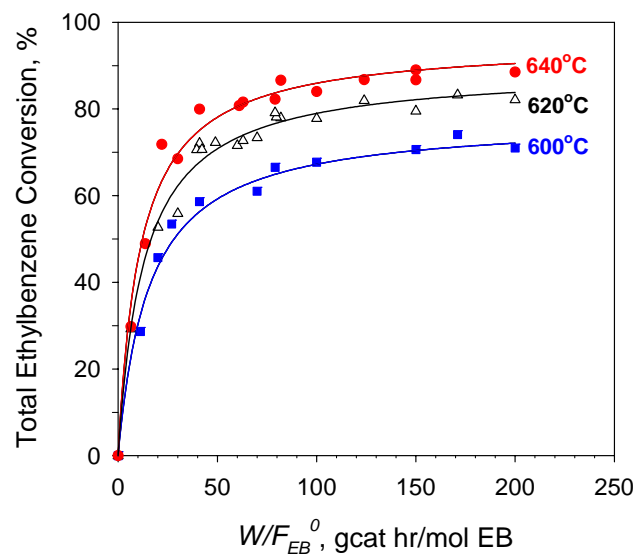
Figure 4.7. Effect of temperature and space time on total ethylbenzene conversion over a wide range of space times for P_T = 1.04 bar; P_{N2} = 0.432 bar; H_2O/EB = 11 mol/mol; ST/EB = 0; H_2/EB = 0.
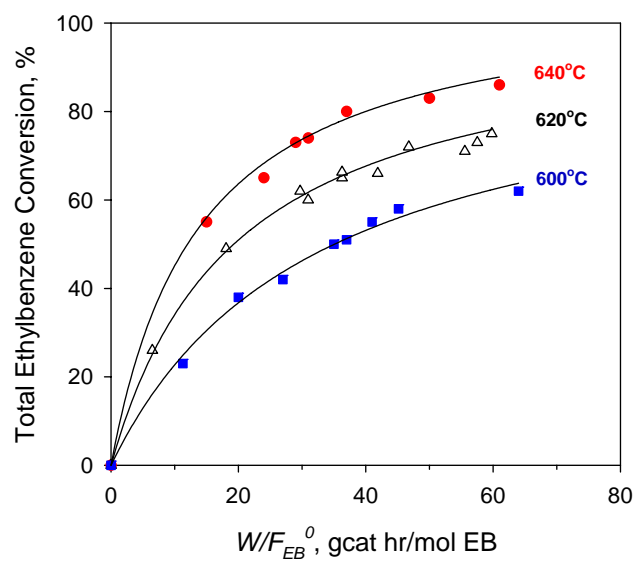
Figure 4.8. Effect of temperature and space time on total ethylbenzene conversion over a narrow range of space times for P_T = 1.04 bar; P_{N2} = 0.432 bar; H_2O/EB = 11 mol/mol; ST/EB = 0; H_2/EB = 0.
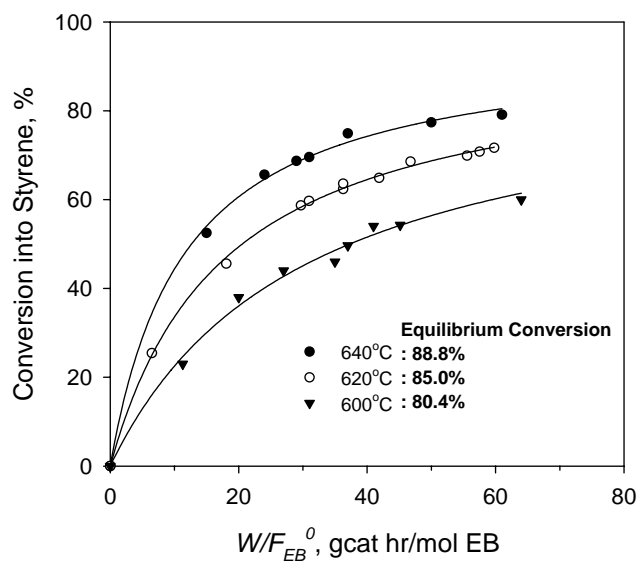
Figure 4.9. Effect of temperature and space time on ethylbenzene conversion into styrene for T = 600°C, 620°C, and 640°C; P_T = 1.04 bar; P_{N2} = 0.432 bar; H_2O/EB = 11 mol/mol; ST/EB = 0; H_2/EB = 0.
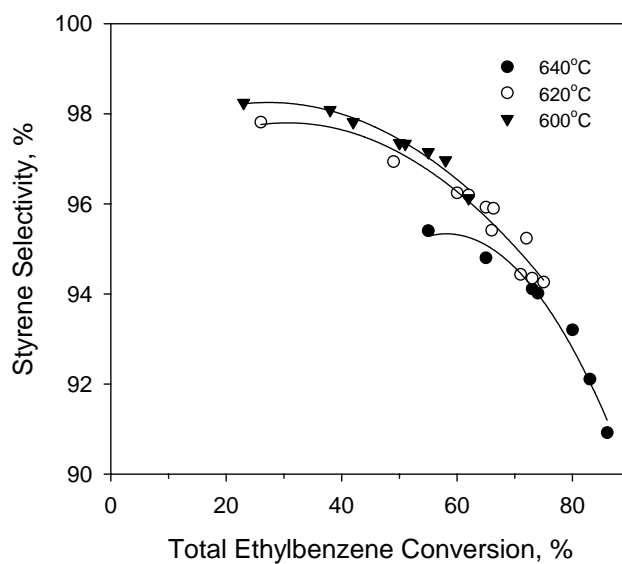
Figure 4.10. Styrene selectivity as a function of total ethylbenzene conversion for T = 600°C, 620°C, and 640°C, P_T = 1.04 bar; P_{N2} = 0.432 bar; H_2O/EB = 11 mol/mol; ST/EB = 0; H_2/EB = 0.
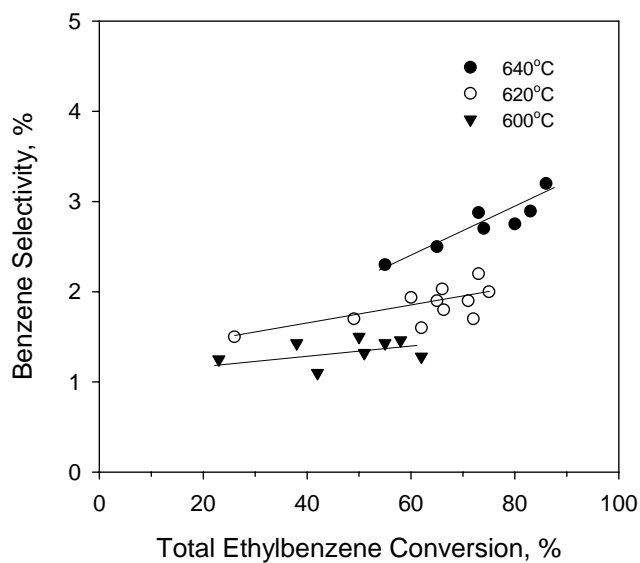
Figure 4.11. Benzene selectivity as a function of total ethylbenzene conversion for $T =$ 600°C, 620°C, and 640°C, P_T = 1.04 bar; P_{N2} = 0.432 bar; H_2O/EB = 11 mol/mol; ST/EB = 0; H_2/EB = 0.
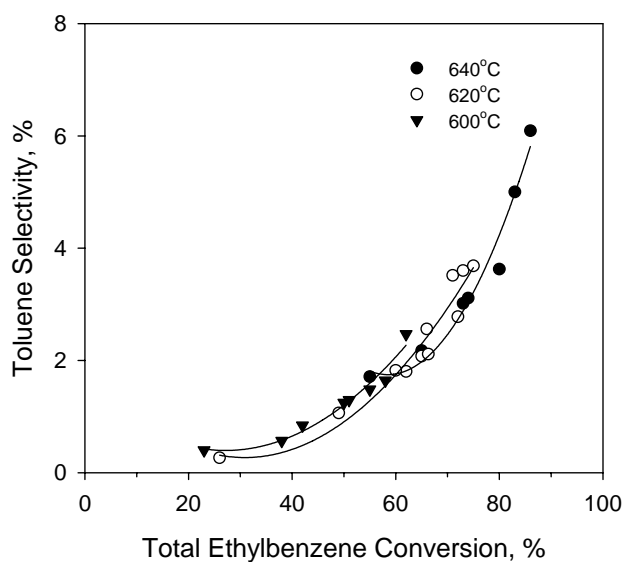
Figure 4.12. Toluene selectivity as a function of total ethylbenzene conversion for $T =$ 600°C, 620°C, and 640°C, P_T = 1.04 bar; P_{N2} = 0.432 bar; H_2O/EB = 11 mol/mol; ST/EB = 0; H_2/EB = 0.

4.1.5   Effect of Feed Composition

4.1.5.1   Effect of Steam to Ethylbenzene Feed Ratio

Figures 4.13, 4.14, and 4.15 show the influence of H_2O/EB feed ratios of 11mol/mol and 7mol/mol on the total ethylbenzene conversion and the styrene selectivity at 600^oC, 620^oC, and 640^oC, respectively. The increase of H_2O/EB feed ratio did not lead to an increase of the total ethylbenzene conversion and the styrene selectivity over the low range of space time, i.e., lower than 30 gcat hr/mol. Even at the high space time of 62 gcat hr/mol the effect of increasing H_2O/EB feed ratio on the total ethylbenzene conversion was insignificant. However, the effect of the H_2O/EB feed ratio on the styrene selectivity tended to be more important as the total ethylbenzene conversion increased. This is mainly due to the increased reaction rate of the by-product formation. To achieve the maximum styrene selectivity one may prefer to increase the H_2O/EB feed ratio, reduce the temperature, and lower the total ethylbenzene conversion. But process economics will determine the optimal operating conditions to maximize the profit.

4.1.5.2   Effect of Styrene to Ethylbenzene Feed Ratio

Figures 4.16, 4.17, and 4.18 show the effect of ST/EB feed ratios of 0 mol/mol, 0.2 mol/mol, and 0.3 mol/mol on the total ethylbenzene conversion and the styrene selectivity at 600^oC, 620^oC, and 640^oC, respectively.
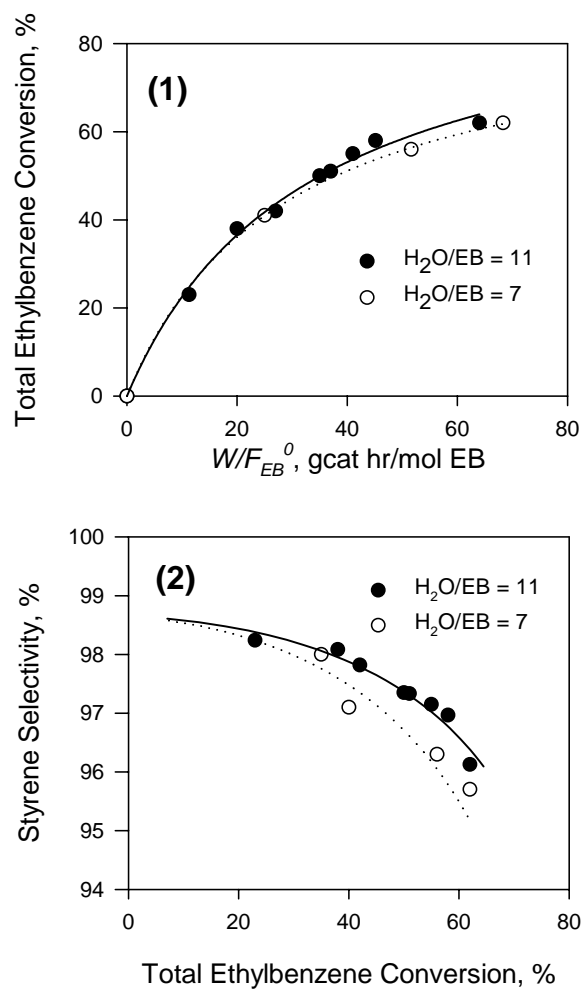
Figure 4.13. Effect of H_2O/EB ratios of 11 and 7 on the total ethylbenzene conversion (1) and styrene selectivity (2) for $T = 600^{\circ}C$; $P_T = 1.04$bar; ST/EB = 0; $H_2/EB = 0$.
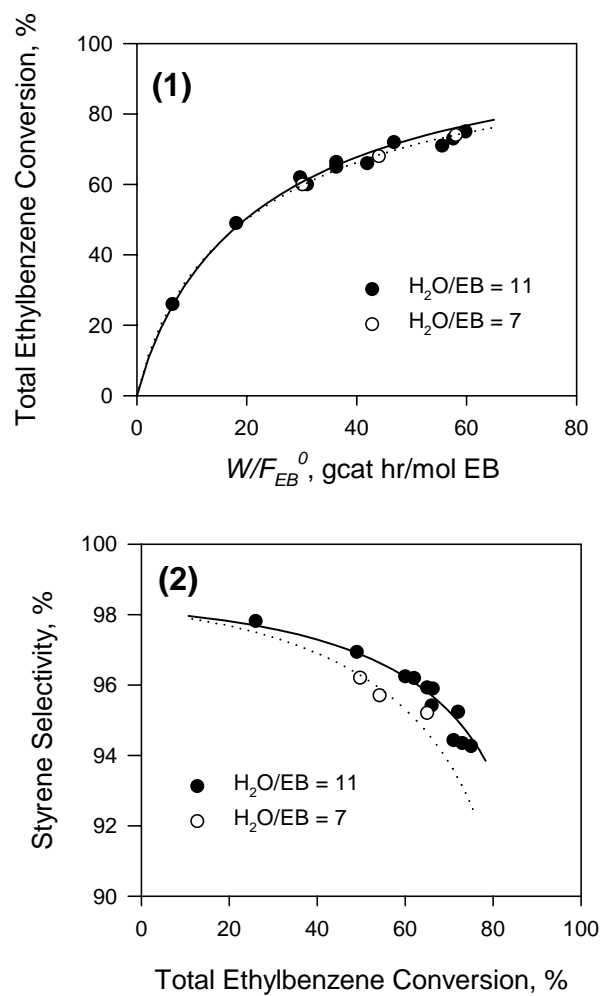
Figure 4.14. Effect of H_2O/EB ratios of 11 and 7 on the total ethylbenzene conversion (1) and styrene selectivity (2) for $T = 620^{\circ}C$; $P_T = 1.04bar$; $ST/EB = 0$; $H_2/EB = 0$.
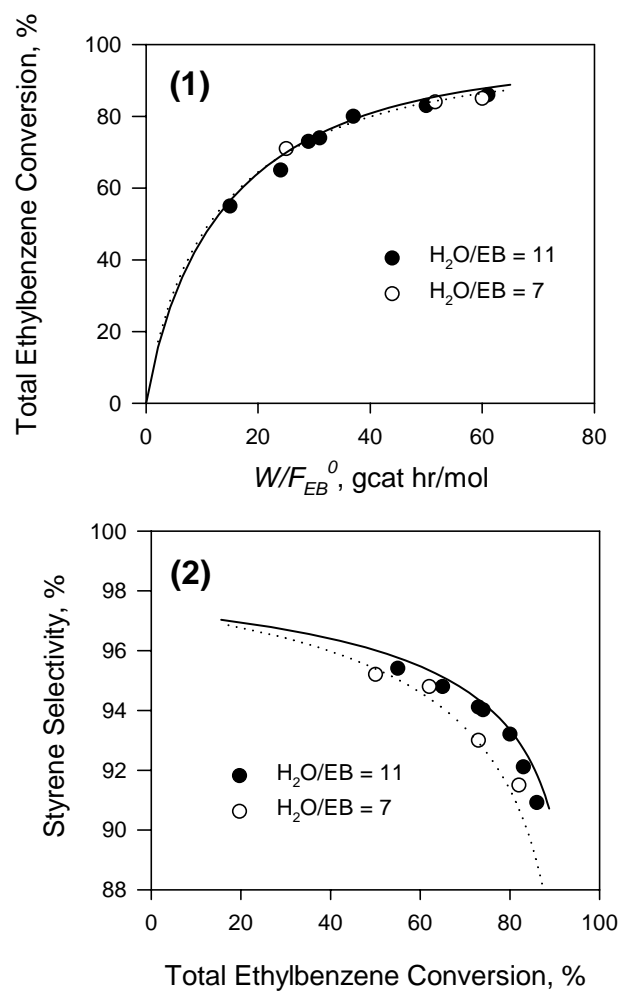
Figure 4.15. Effect of H_2O/EB ratios of 11 and 7 on the total ethylbenzene conversion (1) and styrene selectivity (2) for $T = 640^{\circ}C$; $P_T = 1.04$bar; ST/EB = 0; H_2/EB = 0.

As the feed ratio increased the total ethylbenzene conversion decreased. Since the styrene added in the feed adsorbs competitively on the active sites of the catalyst, the rate of ethylbenzene consumption decreased. Furthermore, the adsorbed styrene on the surface turned into the carbonaceous deposit, which causes the catalyst deactivation. The styrene selectivities were highly affected by the addition of styrene. As the ST/EB feed ratio increased, the styrene selectivity decreased.

4.1.5.3   Effect of Hydrogen to Ethylbenzene Feed Ratio

Figure 4.19 shows the experimental results to illustrate the kinetic behavior of the catalyst when hydrogen was added to the feed. Since hydrogen is involved in the formation of toluene from styrene, the toluene selectivity increased while styrene suffers from the side reaction. The addition of hydrogen further reduces the iron catalyst, which leads to the fast catalyst deactivation.
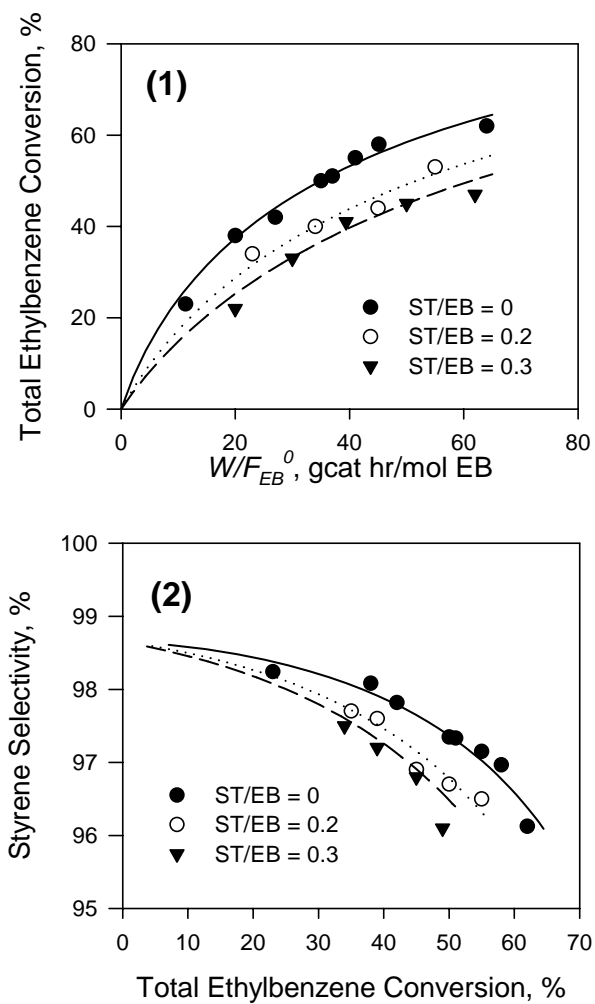
Figure 4.16. Effect of ST/EB ratios of 0, 0.2, and 0.3 on the total ethylbenzene conversion (1) and styrene selectivity (2) for $T = 600^{\mathrm{o}}$C; $P_T = 1.04$bar; $H_2O/EB = 11$; $H_2/EB = 0$.

Figure 4.17. Effect of ST/EB ratios of 0, 0.2, and 0.3 on the total ethylbenzene conversion (1) and styrene selectivity (2) for $T = 620^{\circ}C$; $P_T = 1.04$bar; $H_2O/EB = 11$; $H_2/EB = 0$.
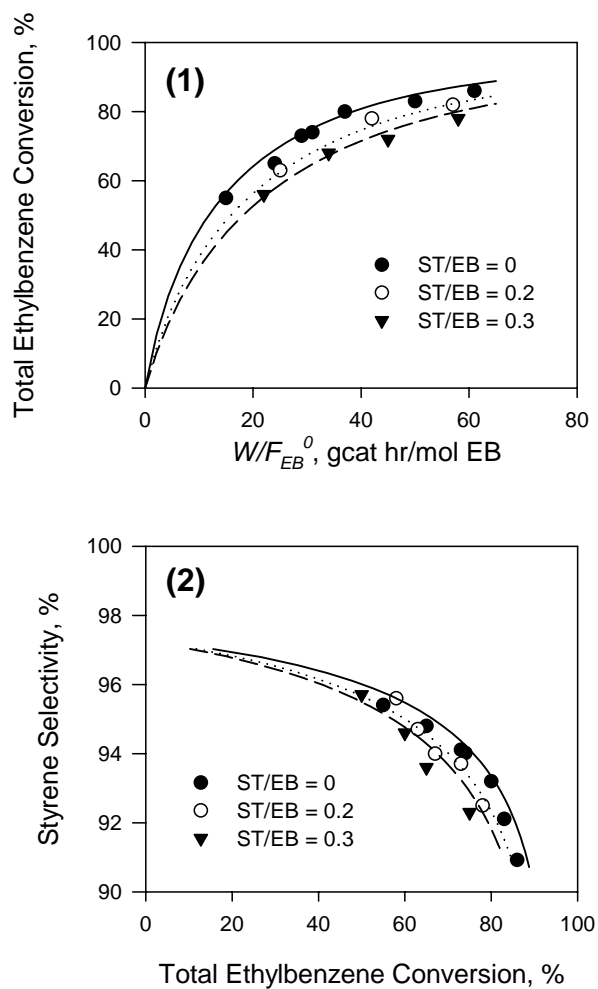
Figure 4.18. Effect of ST/EB ratios of 0, 0.2, and 0.3 on the total ethylbenzene conversion (1) and styrene selectivity (2) for $T = 640^{\circ}C$; $P_T = 1.04bar$; $H_2O/EB = 11$; $H_2/EB = 0$.
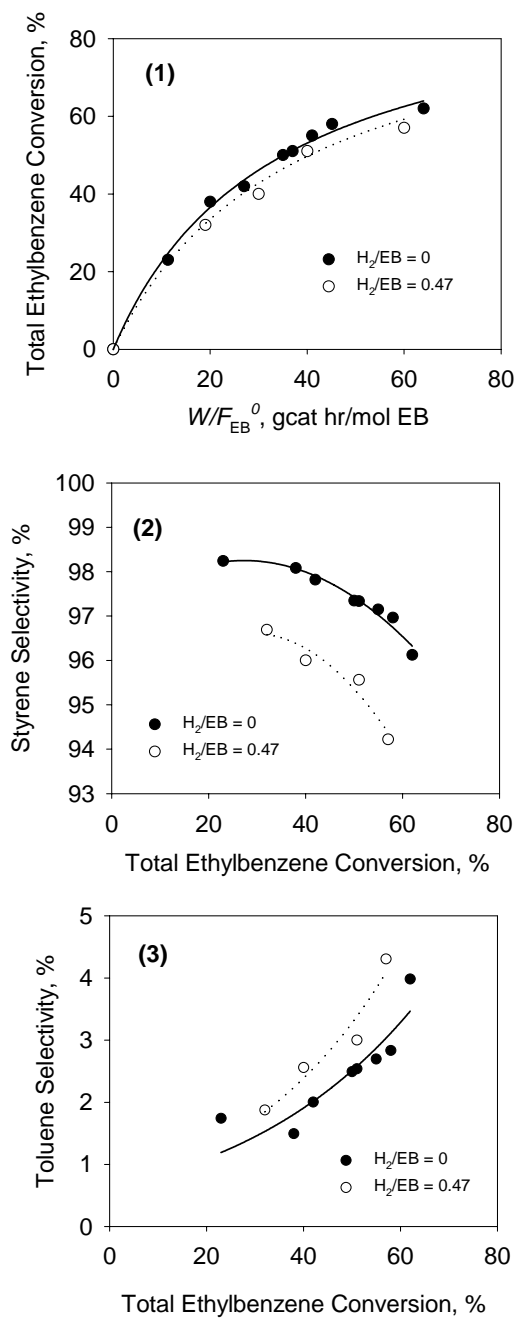
Figure 4.19. Effect of H_2/EB ratios of 0, and 0.47 on the total ethylbenzene conversion (1), styrene selectivity (2), and toluene selectivity (3) for $T = 600^{\circ}$C; $P_T = 1.04$bar; H_2O/EB = 11; ST/EB = 0.

4.2   Experimental Results for the Minor Side Products

4.2.1   Experimental Procedure

Kinetic experiments for the formation of minor by-products were performed at the reaction condition shown in Table 4.1. The minor by-products include phenylacetylene, α-methylstyrene, β-methylstyrene, cumene, *n*-propylbenzene, divinylbenzene, and stilbene. A feed molar ratio of H_2O/EB of 6.5 was used because the preliminary experiments showed that the lower molar ratio of H_2O/EB enhanced the formation of minor by-products. The concentrations of minor by-products were so low that the quantitative analysis using on line GC analysis was impossible.

The experimental procedure was the same as that described in section 4.1.1. The quantitative analysis of the minor by-products was conducted using off-line GC presented in section 3.3.2. Experimental data shown in the following figures are the averaged values obtained from 5-10 times of sample injections into the GC. The standard deviations around the averages were appreciable, due to the low concentration in the liquid mixture.

Table 4.1. Catalytic reaction conditions used for the minor by-products analysis

Temperature, $^{\circ}$C	600, 620, 640
H_2O/EB, mol/mol (wt/wt)	6.5
Total pressure, bar	1.04
Partial pressure of steam and EB, bar	0.43, 0.64

4.2.2   **Effect of Temperature and Partial Pressure of Ethylbenzene and Steam**

The selectivities of by-products are plotted against the total ethylbenzene conversion in the following figures. Figures 4.20, 4.21, and 4.22 refer to $P_{EB+H2O} = 0.43$ bar. Figures 4.23, 4.24, and 4.25 refer to $P_{EB+H2O} = 0.64$ bar.

The phenylacetylene selectivity profiles (Figures 4.20 and 4.23) did not depend upon the total ethylbenzene conversions for all the reaction conditions. There was an exception: the phenylacetylene selectivity increased as the total ethylbenzene conversion increased at $600^{o}C$ and $P_{EB+H2O} = 0.43$ bar (Figure 4.20). It might be due to the experimental error. A close investigation of figures indicates that phenylacetylene seems to be formed via a primary reaction, i.e. dehydrogenation of ethylbenzene. Furthermore, one can conclude from the constant phenylacetylene selectivity with total ethylbenzene conversion that the phenylacetylene selectivity has the same dependency on the partial pressure of ethylbenzene as total ethylbenzene conversion. However, this hypothesis holds if both the phenylacetylene formation and ethylbenzene consumption are catalytically. The production of phenylacetylene from dehydrogenation of styrene in pyrolysis was observed by Bruinsma and Moulijn.[91, 92] The investigation of the reaction mechanism forming the by-products will be excluded because it is beyond the scope of the present research.

The selectivities of β-methylstyrene, α-methylstyrene, and cumene tended to decrease as the total ethylbenzene conversion increases. Divinylbenzene, which includes both *m*- divinylbenzene and *p*-divinylbenzene, showed very low concentration which

made the quantitative analysis unreliable. No correlation with reaction conditions or the total ethylbenzene conversion was found.

The selectivity of stilbene (Figures 4.22 and 4.25) was highly increased as the temperature increased. The selectivity profiles of stilbene were inconsistent at all reaction conditions. It indicates that the formation of stilbene involves a complex reaction scheme. Bruinsma and Moulijn[91, 92] reported that stilbene was produced from the pyrolysis of toluene, ethylbenzene, styrene, and phenylacetylene. At temperature around 900K stilbene was believed to be formed from styrene rather than ethylbenzene. Toluene pyrolysis gives stilbene through the dimerization of radical intermediates and a subsequent dehydrogenation, which occurs at low temperature around 900K.
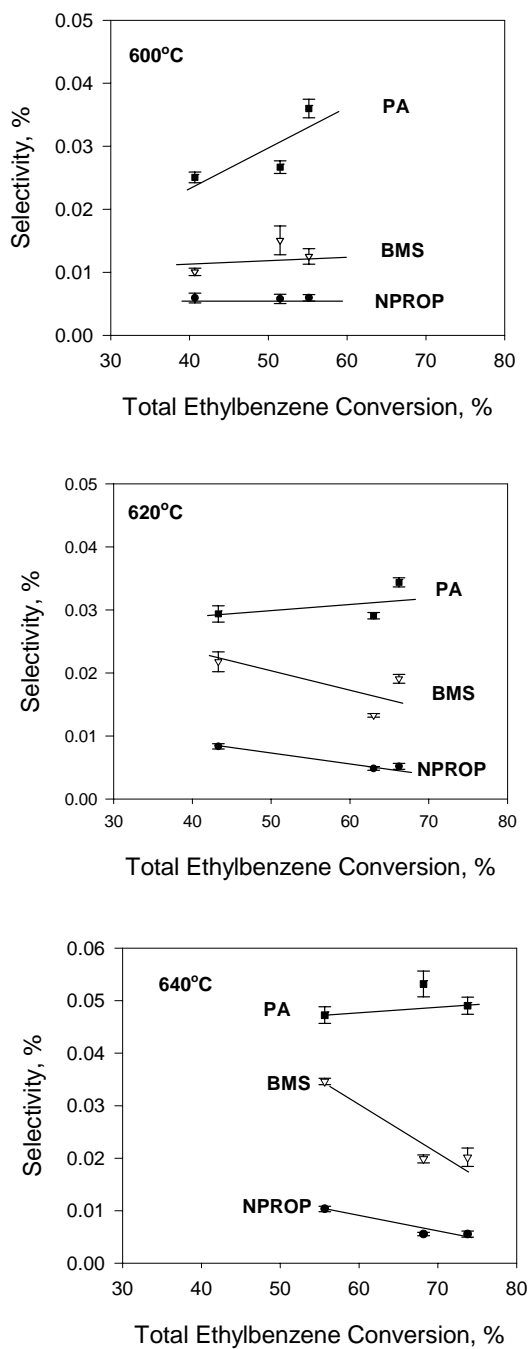
Figure 4.20. Selectivities of phenylacetylene (PA), β-methylstyrene (BMS), and *n*-propylbenzene (NPROP) as a function of EB conversion at 600°C, 620°C, and 640°C for $P_{EB+H2O} = 0.43$ bar; $H_2O/EB = 6.5$ mol/mol.
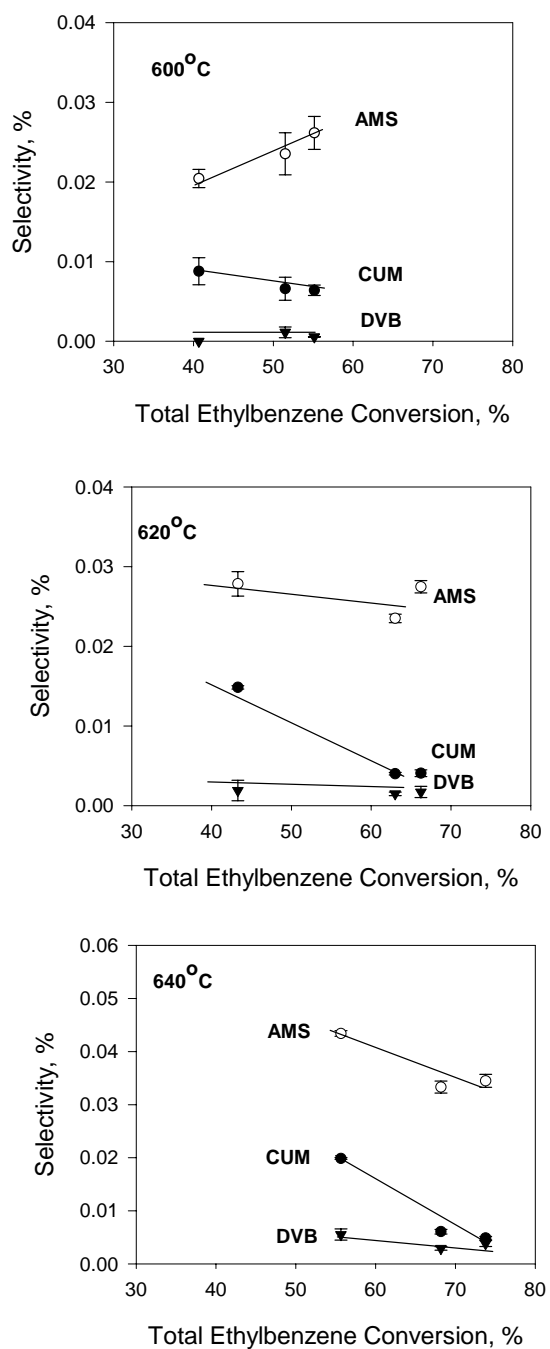
Figure 4.21. Selectivities of α-methylstyrene (AMS), cumene (CUM), and divinylbenzene (DVB) as a function of EB conversions at 600°C, 620°C, and 640°C for P_{EB+H2O} = 0.43 bar; H_2O/EB = 6.5 mol/mol.
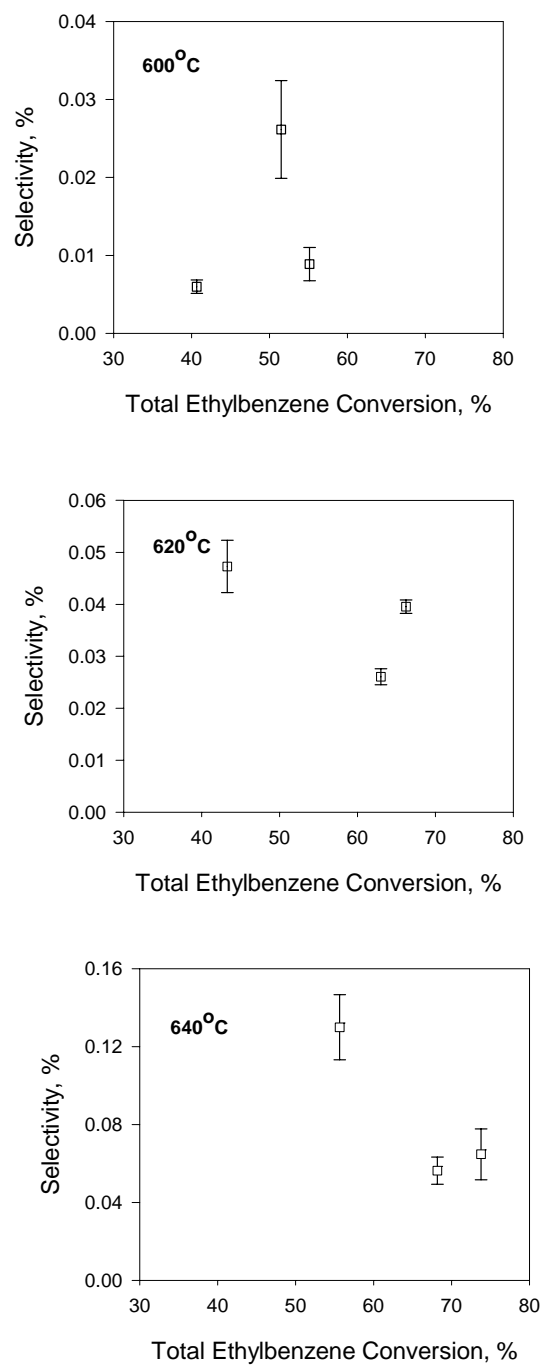
Figure 4.22. Selectivities of stilbene as a function of EB conversion at 600°C, 620°C, and 640°C for P_{EB+H2O} = 0.43 bar; H_2O/EB = 6.5 mol/mol.
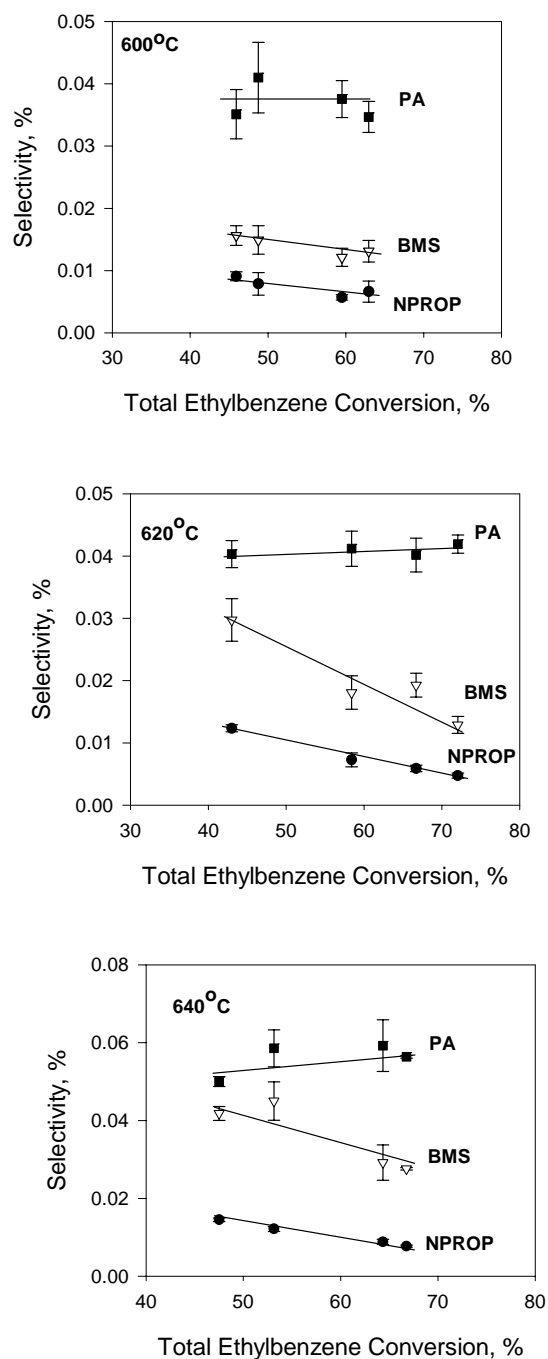
Figure 4.23. Selectivities of phenylacetylene (PA), β-methylstyrene (BMS), and *n*-propylbenzene (NPROP) as a function of EB conversion at 600°C, 620°C, and 640°C for $P_{EB+H2O} = 0.64$ bar; $H_2O/EB = 6.5$ mol/mol.
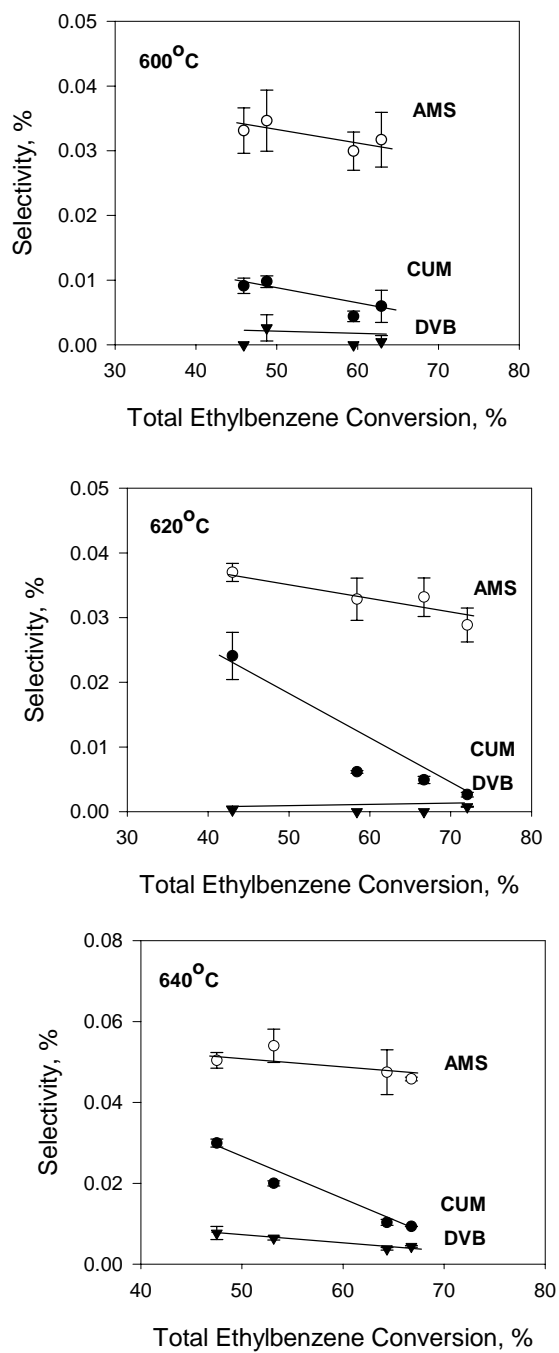
Figure 4.24. Selectivities of α-methylstyrene (AMS), cumene (CUM), and divinylbenzene (DVB) as a function of EB conversion at 600°C, 620°C, and 640°C for $P_{EB+H2O} = 0.64$ bar; $H_2O/EB = 6.5$ mol/mol.
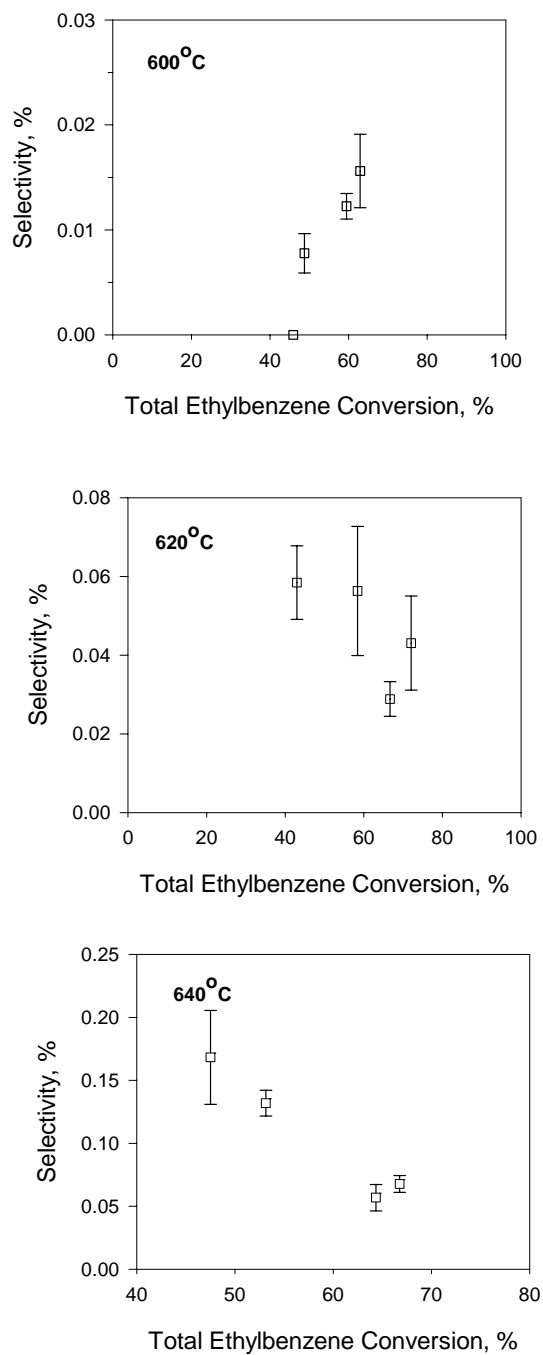
Figure 4.25. Selectivities of stilbene as a function of EB conversion at 600°C, 620°C, and 640°C for $P_{EB+H2O} = 0.64$ bar; $H_2O/EB = 6.5$ mol/mol.

CHAPTER V

KINETIC MODELING OF ETHYLBENZENE

DEHYDROGENATION

5.1   Introduction

The intrinsic kinetics of heterogeneous catalysis refer to the rate expressions for the processes of adsorption, surface reaction, and desorption on the active sites of catalyst. This means the intrinsic rate equations are expressed in terms of concentrations and temperatures at the surface of the catalyst. If the transport processes are taken into account, then intrinsic kinetics reduce to the effective rates, which are expressed in terms of concentrations and temperature in the bulk fluid. This concept was first treated by Hougen and Watson[93], who applied the work of Langmuir and Hinshelwood to derive intrinsic kinetics of fluid-solid catalytic reactions.[94, 95] For a bimolecular reaction the Langmuir-Hinshelwood mechanism involves the surface reaction between two adsorbed species, while the Rideal-Eley mechanism deals with the surface reaction between a surface species and a gaseous species.[96] It is noteworthy to review the key assumptions behind the Langmuir theory:[95, 97] (1) Gas molecules adsorb on a finite number of equivalent sites on a uniform surface. (2) The adsorbed species do not interact, and their energies are independent whether the absorbed species on neighborhood sites are present or not. (3) Each site can adsorb only one gas molecule and form monolayer coverage.

In reality, however, many studies have reported nonuniform catalyst surfaces. Even in this case, Boudart[98] recommended the use of classical kinetics (Hougen-Watson

kinetics) in that " in spite of their approximate nature, they hinted at a kinetic mechanism that might be verifiable or improvable, as contrasted with empirical power rate laws that are solely designed to fit data." Froment and Bischoff[95] concluded that "operating conditions lead to a surface which is almost completely covered by species, so that the nonuniformities are no longer felt. In such a case the use of Hougen-Watson rate equations, based on the Langmuir isotherm, is not only useful, but it is also correct."

The empirical first- and second-order polynomial kinetic models are very common modeling approach for ethylbenzene dehydrogenation. To predict the reactor performance precisely beyond the operating range of the production unit, the detailed Hougen-Watson kinetic model needs to be developed. The Hougen-Watson formalism provides not only a better understanding of the reaction behavior but also the essential elements for the design and simulation of the industrial reactor. In this work, we propose the fundamental kinetic model and present the result of estimating parameters, i.e., rate coefficients and adsorption equilibrium coefficients by nonlinear regression method.

The data analysis is based on the integral method of kinetic analysis, as described by Froment and Bischoff[95] and Froment.[99] The calculated conversions are obtained through the integration of the continuity equations for the reaction components in a tubular reactor with plug flow, which leads to

$$\frac{W}{F_A^0} = f\left(x, k, K_A, \ldots\right) \tag{5.1}$$

where W is the amount of the catalyst, F_A^0 is the feed molar flow rate of component A, x_A is its conversion, and k and K_A, ... are parameters to be determined.

The Mathematical model developed for the ethylbenzene dehydrogenation consists of nonlinear simultaneous equations in multiple dependent variables. The parameters are estimated from the minimization of the multiresponse objective function which is performed by means of the Marquardt algorithm.

The significance of the individual model parameters is tested by comparing the estimate b_j with its standard deviation. If its ratio exceeds the tabulated $\alpha/2$-percentage point of the t-distribution, the assumption $b_j = 0$ is rejected. The estimate is then significantly different from zero and effectively contributes to the model. The validity of the final estimated parameter values are tested using the criteria proposed by Boudart and co-authors.[100, 101]

5.2   Formulation of Rate Equations

5.2.1   Thermal Reactions

Since thermal reactions take place in the void sections of the catalyst bed and in the zones without catalyst these reaction rates should be incorporated into the kinetic model. Thermal reactions involve free radical mechanisms. However, simplified molecular reaction schemes will be a good approximation for the simulation or design purpose, given the low thermal conversions.[5, 102] The equivalent molecular scheme is represented by

$$\text{EB} \underset{k_{t1}^{-1}}{\overset{k_{t1}}{\rightleftharpoons}} \text{ST} + \text{H}_2 \qquad\qquad r_{t1} = k_{t1}\left(P_{EB} - P_{ST}P_{H_2}/K_{eq}\right)$$

$$\text{EB} \xrightarrow{k_{t2}} \text{BZ} + \text{C}_2\text{H}_4 \qquad\qquad r_{t2} = k_{t2}P_{EB} \qquad\qquad (5.2)$$

$$\text{EB} + \text{H}_2 \xrightarrow{k_{t3}} \text{TO} + \text{CH}_4 \qquad\qquad r_{t3} = k_{t3}P_{EB}$$
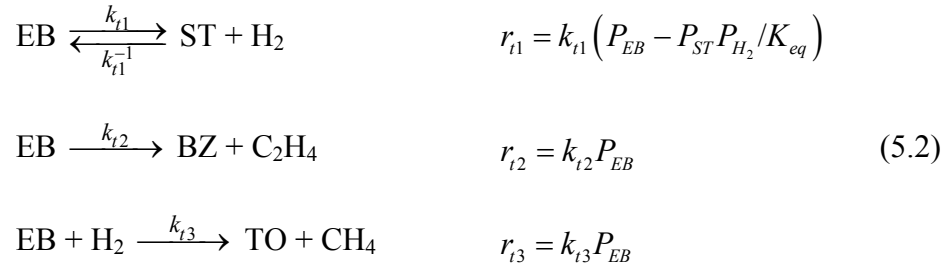
where k_{ti} is the rate constant of reaction i, r_{ti} is the rate of the thermal reaction i in kmol/$\left(m_f^3 \cdot hr\right)$, P_j is the partial pressure of component j in bar, and K_{eq} is the equilibrium constant in bar.

The kinetic parameters for these reactions are shown in Table 5.1. A_{ti} and E_{ti} represent the true preexponential factors and activation energies for the thermal reaction i, respectively.

Table 5.1. Preexponential factors and activation energies for the thermal reactions

i	A_{ti} [kmol/(m_f^3 hr bar)]	E_{ti} [kJ/mol]
1	2.2215×10^{16}	272.23
2	2.4217×10^{20}	352.79
3	3.8224×10^{17}	313.06

5.2.2   Catalytic Reactions

Let us consider the main and side reactions of ethylbenzene dehydrogenation which are taking place on the surface of the catalyst.

$$
\begin{aligned}
&\text{Reaction 1:}\quad \text{EB} \rightleftharpoons \text{ST} + \text{H}_2 && r_{c1}\\[6pt]
&\text{Reaction 2:}\quad \text{EB} \rightarrow \text{BZ} + \text{C}_2\text{H}_4 && r_{c2}\\[6pt]
&\text{Reaction 3:}\quad \text{EB} + \text{H}_2 \rightarrow \text{TO} + \text{CH}_4 && r_{c3}\\[6pt]
&\text{Reaction 4:}\quad \text{ST} + 2\text{H}_2 \rightarrow \text{TO} + \text{CH}_4 && r_{c4}
\end{aligned}
\tag{5.3}
$$
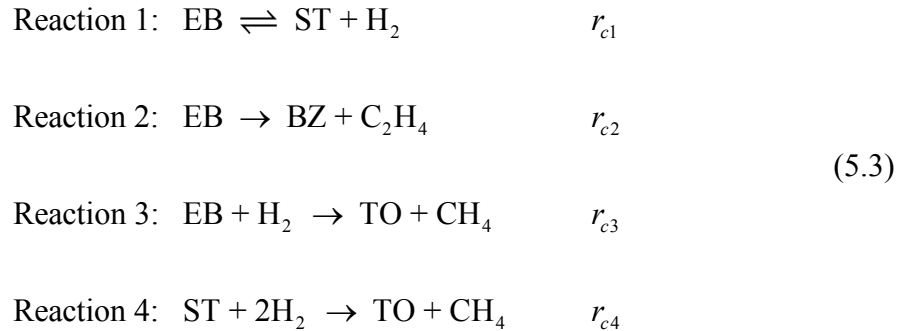
where r_{ci} is the rate of *catalytic* reaction i in kmol/(kg cat. hr).

For the derivation of the rate equations, H_2 is assumed to adsorb *molecularly* on the surface of the catalyst to react with adsorbed ethylbenzene. The chemisorption of ethylbenzene and H_2 will be written as

$$
\begin{aligned}
&\text{EB} + l \rightleftharpoons \text{EB-}l && K_{EB}\\[6pt]
&\text{H}_2 + l \rightleftharpoons \text{H}_2\text{-}l && K_{H_2}
\end{aligned}
\tag{5.4}
$$
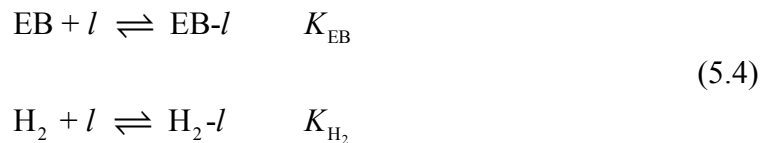
where l is the adsorption site on the surface of the catalyst, K_j is the adsorption equilibrium constant of component j.

Devoldere and Froment[103] performed parameter estimation using an extensive set of experimental data and showed by rigorous parameter estimation and model

discrimination that the surface reactions are the rate-determining step. These surface reactions can be written

$$\text{Reaction 1:} \quad \text{EB-}l + l \underset{k_{sr,1}^{-1}}{\overset{k_{sr,1}}{\rightleftarrows}} \text{ST-}l + \text{H}_2\text{-}l \qquad \text{rds1}$$

$$\text{Reaction 2:} \quad \text{EB-}l + l \xrightarrow{k_{sr,2}} \text{BZ-}l + \text{C}_2\text{H}_4\text{-}l \qquad \text{rds2}$$

$$\text{Reaction 3:} \quad \text{EB-}l + \text{H}_2\text{-}l \xrightarrow{k_{sr,3}} \text{TO-}l + \text{CH}_4\text{-}l \quad \text{rds3} \qquad (5.5)$$

$$\text{Reaction 4:} \quad \text{ST-}l + \text{H}_2\text{-}l \xrightarrow{k_{sr,4}} \text{Z-}l + l \qquad \text{rds4}$$

$$\text{Z-}l + \text{H}_2\text{-}l \rightleftharpoons \text{TO-}l + \text{CH}_4\text{-}l \qquad K_Z$$
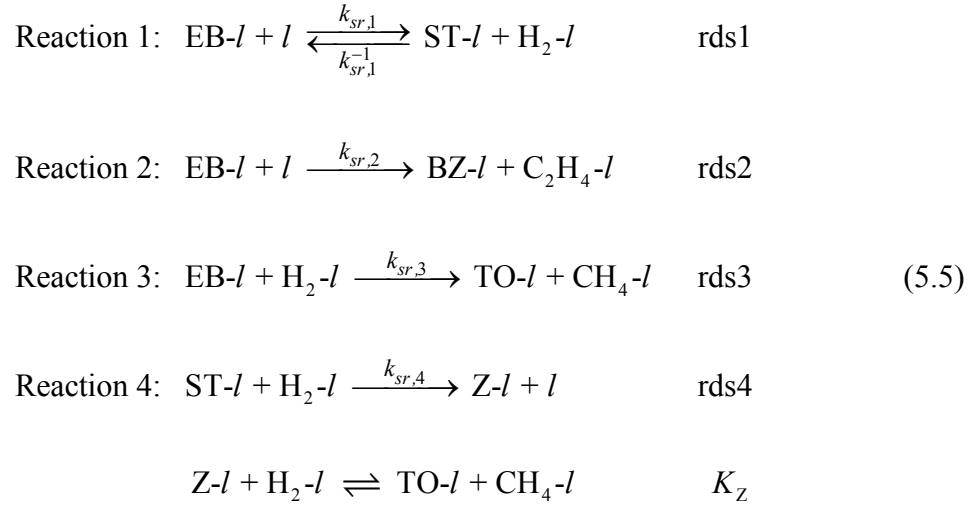
where rds$i$ stands for the rate-determining step of reaction i.

For the desorption step,

$$\text{ST-}l \rightleftharpoons \text{ST} + l \qquad 1/K_{ST}$$

$$\text{H}_2\text{-}l \rightleftharpoons \text{H}_2 + l \qquad 1/K_{H_2}$$

$$\text{BZ-}l \rightleftharpoons \text{BZ} + l \qquad 1/K_{BZ}$$

$$\qquad\qquad\qquad\qquad\qquad\qquad\qquad\qquad (5.6)$$

$$\text{TO-}l \rightleftharpoons \text{TO} + l \qquad 1/K_{TO}$$

$$\text{C}_2\text{H}_4\text{-}l \rightleftharpoons \text{C}_2\text{H}_4 + l \qquad 1/K_{C_2H_4}$$

$$\text{CH}_4\text{-}l \rightleftharpoons \text{CH}_4 + l \qquad 1/K_{CH_4}$$
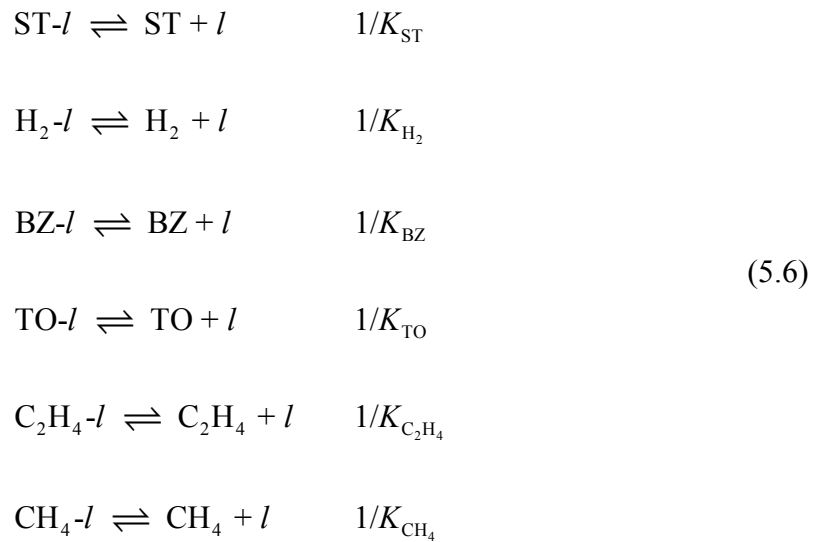
From Eq. (5.4), the concentrations of adsorbed ethylbenzene and adsorbed hydrogen can be expressed by means of the Langmuir isotherm

$$C_{EBl} = K_{EB}P_{EB}C_l$$

$$C_{H_2l} = K_{H_2}P_{H_2}C_l$$

(5.7)

where C_l is the concentration of vacant site and C_{jl} is the concentration of chemisorbed j. From Eq. (5.5), the product of concentrations between adsorbed toluene and adsorbed methane is given by

$$C_{TOl}C_{CH_4l} = K_Z C_{Zl}C_{H_2l} \qquad (5.8)$$

The concentrations of other adsorbed species are obtained from Eq. (5.6).

$$C_{STl} = K_{ST}P_{ST}C_l$$

$$C_{BZl} = K_{BZ}P_{BZ}C_l$$

$$C_{C_2H_4l} = K_{C_2H_4}P_{C_2H_4}C_l \qquad (5.9)$$

$$C_{TOl} = K_{TO}P_{TO}C_l$$

$$C_{CH_4l} = K_{CH_4}P_{CH_4}C_l$$

Since the total concentration of active site, C_t, is assumed to be constant, the site balance can be written

$$C_t = C_l + C_{EBl} + C_{H_2l} + C_{STl} + C_{BZl} + C_{TOl} + C_{C_2H_4l} + C_{CH_4l} + C_{Zl}$$

$$= C_l \left(1 + K_{EB}P_{EB} + K_{H_2}P_{H_2} + K_{ST}P_{ST} + K_{BZ}P_{BZ} + K_{TO}P_{TO} + K_{C_2H_4}P_{C_2H_4} \right. \tag{5.10}$$

$$\left. + K_{CH_4}P_{CH_4} + \frac{K_{TO}P_{TO}K_{CH_4}P_{CH_4}}{K_Z K_{H_2}P_{H_2}} \right)$$

Anticipating on the results of the parameter estimation that revealed that the adsorption equilibrium constants of benzene, toluene, C_2H_4, and CH_4 can not be estimated significantly due to the low concentrations in the reactions,[103] the site balance equation reduces to

$$C_t \cong C_l \left(1 + K_{EB}P_{EB} + K_{H_2}P_{H_2} + K_{ST}P_{ST} \right) \tag{5.11}$$

The concentration of vacant sites, C_l, can be expressed in terms of C_t, kinetic parameters and operating variables.

$$C_l = \frac{C_t}{\left(1 + K_{EB}P_{EB} + K_{H_2}P_{H_2} + K_{ST}P_{ST} \right)} \tag{5.12}$$

From rds1 of Eq. (5.5) and Eqs. (5.7) and (5.9), the rate equation for the ethylbenzene dehydrogenation can be developed into

$$r_{c1} = k_{sr,1}C_{EBl}C_l - k_{sr,1}^{-1}C_{STl}C_{H_2l} = \frac{k_1 K_{EB} \left(P_{EB} - P_{ST}P_{H_2}/K_{eq} \right)}{\left(1 + K_{EB}P_{EB} + K_{H_2}P_{H_2} + K_{ST}P_{ST} \right)^2} \tag{5.13}$$

Similarly, from rds2 of Eq. (5.5) and Eq. (5.7) the rate equation for the formation of benzene from ethylbenzene is

$$r_{c2} = k_{sr,2} C_{EBl} C_l = \frac{k_2 K_{EB} P_{EB}}{\left(1 + K_{EB} P_{EB} + K_{H_2} P_{H_2} + K_{ST} P_{ST}\right)^2} \tag{5.14}$$

From rds3 of Eq. (5.5) and Eq. (5.7), the rate equation for the formation of toluene from ethylbenzene is

$$r_{c3} = k_{sr,3} C_{EBl} C_{H_2 l} = \frac{k_3 K_{EB} P_{EB} K_{H_2} P_{H_2}}{\left(1 + K_{EB} P_{EB} + K_{H_2} P_{H_2} + K_{ST} P_{ST}\right)^2} \tag{5.15}$$

From rds4 of Eq. (5.5) and Eqs. (5.7) and (5.9), the rate equation for the formation of toluene from styrene is

$$r_{c4} = k_{sr,4} C_{STl} C_{H_2 l} = \frac{k_4 K_{ST} P_{ST} K_{H_2} P_{H_2}}{\left(1 + K_{EB} P_{EB} + K_{H_2} P_{H_2} + K_{ST} P_{ST}\right)^2} \tag{5.16}$$

5.3   Formulation of Continuity Equations for the Reacting Species

The steady state continuity equations for the reacting species are derived for a plug flow reactor in which four independent chemical reactions occur. Plug flow is a perfectly ordered flow in which all the fluid elements move with a uniform velocity along parallel streamlines.[104] The mass balance over a differential cross-section of the reactor bed for a reactant, i.e., ethylbenzene, gives

$$F_{EB} - \left(F_{EB} + dF_{EB}\right) = r_{EB} dW \tag{5.17}$$

where r_{EB} is the rate of disappearance of ethylbenzene in kmol/kgcat. hr and F_{EB} is the molar flow rate of ethylbenzene in kmol/hr, and W is the weight of catalyst in kgcat. Since the conversion of EB is defined by

$$F_{EB} = F_{EB}^0 \left(1 - X_{EB}\right) \tag{5.18}$$

where F_{EB}^0 is the feed molar flow rate of ethylbenzene in kmol/hr and X_{EB} is the conversion of ethylbenzene, the steady state continuity equations for ethylbenzene becomes

$$\frac{dX_{EB}}{d\left(W/F_{EB}^0\right)} = r_{EB} \tag{5.19}$$

where W/F_{EB}^0 is the space time in $\left(\text{kgcat} \cdot \text{hr}\right)/\text{kmol}$.

From the reaction scheme of Eq. (5.3), the rate of disappearance of ethylbenzene can be written by summing the rates of reaction 1, 2, and 3.

$$r_{EB} = r_{c1} + r_{c2} + r_{c3} \tag{5.20}$$

Substituting Eq. (5.20) into Eq. (5.19) gives

$$\frac{dX_{EB}}{d\left(W/F_{Eb}^0\right)} = r_{c1} + r_{c2} + r_{c3} \tag{5.21}$$

Similarly, the steady state continuity equations for benzene, toluene, and hydrogen can be derived as follows:

$$\frac{dX_{BZ}}{d\left(W/F_{EB}^o\right)} = r_{c2}$$

$$\frac{dX_{TO}}{d\left(W/F_{EB}^o\right)} = r_{c3} + r_{c4} \tag{5.22}$$

$$\frac{dX_{H_2}}{d\left(W/F_{EB}^o\right)} = r_{c1} - r_{c3} - 2r_{c4}$$

The complete set of continuity equations for the reacting species accounting for both catalytic and thermal reactions in the catalyst bed and voids are given by

$$\frac{dX_{EB}}{d\left(W/F_{EB}^o\right)} = r_{c1} + r_{c2} + r_{c3} + \left(r_{t1} + r_{t2} + r_{t3}\right)\frac{\varepsilon_B}{\rho_B}$$

$$\frac{dX_{BZ}}{d\left(W/F_{EB}^o\right)} = r_{c2} + r_{t2}\frac{\varepsilon_B}{\rho_B}$$

$$\frac{dX_{TO}}{d\left(W/F_{EB}^o\right)} = r_{c3} + r_{c4} + r_{t3}\frac{\varepsilon_B}{\rho_B}$$

$$\frac{dX_{H_2}}{d\left(W/F_{EB}^o\right)} = r_{c1} - r_{c3} - 2r_{c4} + \left(r_{t1} - r_{t3}\right)\frac{\varepsilon_B}{\rho_B}$$

(5.23)

where ε_B is the void fraction of bed in m_f^3/m_r^3 and ρ_B is the catalyst bulk density in kgcat./m_r^3. The rate expressions of the thermal reactions are given in Eq. (5.2). Note that thermal reactions inside the voids of the catalyst itself are not taken into account.

The value of the catalyst bulk density, ρ_B, and bed porosity, ε_B, shown in Eq. (5.23) are calculated by the following procedure: The measured ρ_B is 1422 kgcat./m_r^3. ε_B is calculated by

$$1 - \varepsilon_B = \frac{\rho_B}{\rho_s}$$

where ρ_s is the density of catalyst particle, 2500 kgcat./m_p^3, which is given by the catalyst manufacturer. Then ε_B becomes:

$$\varepsilon_B = 1 - \frac{\rho_B}{\rho_s} = 1 - \frac{1422 \text{ kgcat/}m_r^3}{2500 \text{ kgcat/}m_p^3} = 0.4312 \text{ } m_f^3/m_r^3$$

Now, ε_B / ρ_B is given by

$$\frac{\varepsilon_B}{\rho_B} = \frac{0.4312}{1422} = 0.000303 \ \text{m}_f^3/\text{kgcat}$$

Since in Eqs. (5.13) through (5.16) the rate equations are expressed in terms of partial pressure of ethylbenzene, styrene, and hydrogen, the partial pressures should be converted to the conversions in order to integrate the coupled differential equations, Eq. (5.23), numerically with respect to space time.

The conversions of ethylbenzene into styrene, benzene, toluene, and hydrogen are defined by

$$
\begin{aligned}
X_{ST} &= \frac{F_{ST} - F_{ST}^o}{F_{EB}^o} \\[6pt]
X_{TO} &= \frac{F_{TO} - F_{TO}^o}{F_{EB}^o} \\[6pt]
X_{BZ} &= \frac{F_{BZ} - F_{BZ}^o}{F_{EB}^o} \\[6pt]
X_{H_2} &= \frac{F_{H_2} - F_{H_2}^o}{F_{EB}^o}
\end{aligned}
\qquad (5.24)
$$

The molar flow rate of the components can be calculated from:

$$\text{ethylbenzene: } F_{EB} = F_{EB}^o \left(1 - X_{ST} - X_{BZ} - X_{TO}\right)$$

$$\text{styrene: } F_{ST} = F_{ST}^o + F_{EB}^o X_{ST}$$

$$\text{benzene: } F_{BZ} = F_{BZ}^o + F_{EB}^o X_{BZ}$$

$$\text{toluene: } F_{TO} = F_{TO}^o + F_{EB}^o X_{TO}$$

$$\text{hydrogen: } F_{H_2} = F_{H_2}^o + F_{EB}^o X_{H_2} \tag{5.25}$$

$$\text{methane: } F_{CH_4} = F_{CH_4}^o + F_{EB}^o X_{TO}$$

$$\text{ethylene: } F_{C_2H_4} = F_{C_2H_4}^o + F_{EB}^o X_{BZ}$$

$$\text{nitrogen: } F_{N_2} = F_{N_2}^o$$

$$\text{steam: } F_{H_2O} = F_{H_2O}^o$$

The total molar flow rate is then given by the summation of the molar flow rates of each component

$$F_T = \sum_i^9 F_i \tag{5.26}$$
$$= F_T^o + F_{EB}^0 \left(X_{TO} + X_{BZ} + X_{H_2}\right)$$

The partial pressures of component i is obtained from

$$P_i = P_T \frac{F_i}{F_T} \tag{5.27}$$

where P_i is the partial pressure of component i, P_T is the total pressure, F_i is the molar flow rate of component i, and F_T is the total molar flow rate.

Finally, the expression of the partial pressure of ethylbenzene, styrene, benzene, toluene, ethylene, methane, and hydrogen in terms of feed mole fractions and conversions are shown below.

$$P_{EB} = \frac{y_{EB}^0 \left(1 - X_{ST} - X_{BZ} - X_{TO}\right)}{1 + y_{EB}^0 \left(X_{TO} + X_{BZ} + X_{H_2}\right)} P_T$$

$$P_{ST} = \frac{y_{ST}^0 + y_{EB}^0 X_{ST}}{1 + y_{EB}^0 \left(X_{TO} + X_{BZ} + X_{H_2}\right)} P_T \qquad (5.28)$$

$$P_{H_2} = \frac{y_{H_2}^0 + y_{EB}^0 X_{H_2}}{1 + y_{EB}^0 \left(X_{TO} + X_{BZ} + X_{H_2}\right)} P_T$$

5.4   Parameter Estimation: Theory

5.4.1   Minimization Technique: Marquardt's Method

Estimation in algebraic or differential equations which are nonlinear in the parameters can be performed by minimizing the objective function by methods such as steepest descent, Newton-Gauss, and Marquardt algorithm. These methods are explained elsewhere.[99, 105, 106] Newton-Gauss and Marquardt methods will be presented below.

Let a nonlinear model be expressed by

$$y_i = f\left(x_i, \boldsymbol{\beta}\right) + \varepsilon_i \qquad (5.29)$$

where y_i are the dependent variables, x_i are the independent variables, β are the parameters, and ε are the experimental errors.

The minimization of the least squares criterion can be represented by

$$S\left(\boldsymbol{\beta}\right) = \sum_{i=1}^{n} \left[y_i - f\left(x_i, \boldsymbol{\beta}\right)\right]^2 \xrightarrow{\beta} \text{Min} \qquad (5.30)$$

To minimize the sum of squares of residuals the necessary conditions require taking the

partial derivative of $S(\boldsymbol{\beta})$ with respect to $\boldsymbol{\beta}$ and setting it equal to zero:

$$\frac{\partial S(\boldsymbol{\beta})}{\partial \boldsymbol{\beta}} = 0 \tag{5.31}$$

Because f is nonlinear with respect to the parameters, it is converted into a linear form by

Taylor series around an estimated value of the parameter vector $\boldsymbol{\beta}$:

$$f(x_i, \boldsymbol{\beta}) = f(x_i, \mathbf{b}_0) + \sum_{j=1}^{p} \frac{\partial f(x_i, \boldsymbol{\beta})}{\partial \beta_i}\bigg|_{\beta = \mathbf{b}_o} \cdot \Delta \mathbf{b}_j + \ldots + \varepsilon \tag{5.32}$$

where the Taylor series has been truncated after the second term. Eq. (5.32) can be

expanded into:

$$f(x_i, \boldsymbol{\beta}) - f(x_i, \mathbf{b}_0) = \frac{\partial f(x_i, \boldsymbol{\beta})}{\partial \beta_1}\bigg|_{\beta = \mathbf{b}_o} \cdot \Delta \mathbf{b}_1 + \frac{\partial f(x_i, \boldsymbol{\beta})}{\partial \beta_2}\bigg|_{\beta = \mathbf{b}_o} \cdot \Delta \mathbf{b}_2 + \ldots \frac{\partial f(x_i, \boldsymbol{\beta})}{\partial \beta_p}\bigg|_{\beta = \mathbf{b}_o} \cdot \Delta \mathbf{b}_p + \varepsilon \tag{5.33}$$

Eq. (5.33) is linear in $\Delta \mathbf{b}_j$ and the improvement of the parameter values are obtained

from

$$\Delta \mathbf{b} = \left(\mathbf{J}^T \mathbf{J} \right)^{-1} \mathbf{J}^T \mathbf{r} \tag{5.34}$$

where

$$\mathbf{r} = \begin{bmatrix} f(x_1, \boldsymbol{\beta}) - f(x_1, \mathbf{b}_0) \\ \vdots \\ f(x_n, \boldsymbol{\beta}) - f(x_n, \mathbf{b}_0) \end{bmatrix}, \ \Delta \mathbf{b} = \begin{bmatrix} \Delta \mathbf{b}_1 \\ \vdots \\ \Delta \mathbf{b}_n \end{bmatrix}, \ \mathbf{J} = \begin{bmatrix} \frac{\partial f(x_1, \boldsymbol{\beta})}{\partial \beta_1} & \cdots & \frac{\partial f(x_1, \boldsymbol{\beta})}{\partial \beta_p} \\ \vdots & \cdots & \vdots \\ \frac{\partial f(x_n, \boldsymbol{\beta})}{\partial \beta_1} & \cdots & \frac{\partial f(x_n, \boldsymbol{\beta})}{\partial \beta_p} \end{bmatrix}_{\beta = \mathbf{b}_0} \tag{5.35}$$

This procedure is called the Newton-Gauss method. This method works very well unless the model is highly nonlinear. But the linearization of nonlinear model may lead to such a large $\Delta\mathbf{b}$ that the method diverges.[99] To overcome this, Marquardt developed a compromise between the method of steepest descent and the method of Newton-Gauss.[107] Marquardt's compromise starts with a large value of λ, the Lagrangian multiplier, and the direction of search is close to that of steepest descent. λ is gradually decreased and the direction of search becomes that of Newton-Gauss. Mathematically $\Delta\mathbf{b}$ is determined using

$$\Delta\mathbf{b} = \left(\mathbf{J}^T\mathbf{J} + \lambda\mathbf{I}\right)^{-1}\mathbf{J}^T\mathbf{r} \tag{5.36}$$

where $\mathbf{I}$ is the unit matrix. It can be seen from Eq. (5.36) that the step size $\Delta\mathbf{b}$ is inversely proportional to λ and λ determines the orientation of the search.

When λ is very large, Eq. (5.36) reduces to

$$\Delta\mathbf{b} = \lambda^{-1}\mathbf{J}^T\mathbf{r} \tag{5.37}$$

The step size is very small and the search direction is that of the steepest descent.

When λ is very small,

$$\Delta\mathbf{b} = \left(\mathbf{J}^T\mathbf{J}\right)^{-1}\mathbf{J}^T\mathbf{r} \tag{5.38}$$

The step size reaches the maximum and the search direction is that of Newton-Gauss.

5.4.2   Reparameterization

The computational difficulties arising from the complexity of the kinetic models can be diminished by reparameterization.[99, 108, 109] Activation energy and pre-exponential factor are correlated by the Arrhenius equation.

$$k_i = A_i \exp\left(-\frac{E_i}{RT}\right)$$

(5.39)

$$i = 1, 2, 3, 4$$

where k_i is the rate coefficient of reaction i, A_i the preexponential factor of reaction i and E_i the activation energy of reaction i. The convergence of parameter estimation can be facilitated by reparameterization of Eq. (5.39).

$$k_i = A_i \exp\left(-\frac{E_i}{RT_r}\right) \exp\left[-\frac{E_i}{R}\left(\frac{1}{T} - \frac{1}{T_r}\right)\right]$$

$$= A_i^* \exp\left[-\frac{E_i}{R}\left(\frac{1}{T} - \frac{1}{T_r}\right)\right]$$

(5.40)

where A_i^* is the reparameterized preexponential factor of reaction i and T_r is the average temperature. The adsorption constants for ethylbenzene, styrene, and hydrogen are given by thermodynamics.

$$K_j = \exp\left(-\frac{\Delta S_{a,j}}{R}\right) \exp\left(-\frac{\Delta H_{a,j}}{RT}\right)$$

$$= A_j \exp\left(-\frac{\Delta H_{a,j}}{RT}\right)$$

(5.41)

$$j = EB, ST, H_2$$

where K_j is the adsorption equilibrium constant of species j, $\Delta S_{a,j}$ the standard entropy change of adsorption of species j and $\left(-\Delta H_{a,j}\right)$ heat of adsorption of species j. Eq. (5.41) can be rewritten in terms of reparameterized preexponential factors and heats of adsorptions.

$$K_j = A_j \exp\left(-\frac{\Delta H_{a,j}}{RT_r}\right) \exp\left[-\frac{\Delta H_{a,j}}{R}\left(\frac{1}{T}-\frac{1}{T_r}\right)\right]$$

$$= A_j^* \exp\left[-\frac{\Delta H_{a,j}}{R}\left(\frac{1}{T}-\frac{1}{T_r}\right)\right]$$

(5.42)

$$j = EB, ST, H_2$$

where A_j^* is the reparameterized preexponential factors for adsorption of species j and $\left(-\Delta H_{a,j}\right)$ is the heat of adsorption of component j. The reparameterized parameters, i.e., A_i^* and E_i for reactions and A_j^* and $\left(-\Delta H_{a,j}\right)$ for adsorbed species, will be estimated using the experimental data for all temperatures.

5.5   Results and Discussion

5.5.1   Model Parameter Estimation per Temperature

The ordinary differential equations, Eq. (5.23), were numerically integrated using Gear's method[110] because of the stiffness of the differential equations. The objective function to be minimized for the parameter estimation was based upon the difference between experimental and calculated conversions of ethylbenzene dehydrogenation products:

$$S = \sum_{h=1}^{n_{resp}} \sum_{k=1}^{n_{resp}} \sigma^{hk} \sum_{i=1}^{n_{exp}} \left(y_{ih} - \bar{y}_{ih}\right) \cdot \left(y_{ik} - \bar{y}_{ik}\right) \tag{5.43}$$

where σ^{hk} are the elements of the inverse of the ($n_{resp} \times n_{resp}$) error covariance matrix, n_{resp} is the number of responses, n_{exp} is the number of experiments, and $\bar{y}_{ih}$ is the calculated value of the hth response for the ith experiment. The minimization of the objective function was performed by means of Marquardt's nonlinear multiresponse regression algorithm.

The statistical analysis based upon the t-test is performed. The null hypothesis that the estimate b_j would be zero can be rejected when

$$t_c = \frac{|b_j - 0|}{s(b_j)} > t\left(n - p; 1 - \frac{\alpha}{2}\right) \tag{5.44}$$

where $s(b_j)$ is the standard deviation of estimated b_j and $t(n-p; 1-(\alpha/2))$ is the tabulated $\alpha/2$ percentage point of the t distribution with $n-p$ degree of freedom.[95] The parameters are significantly different from zero with the 95% confidence level if the calculated t values, t_c, are greater than the tabulated t value. Table 5.2 shows the parameter estimates

calculated from the simultaneous nonlinear regression of all the experimental data at 600°C along with the standard deviations, t values, and lower- and upper-values of 95% confidence interval. Since the calculated t values for all the parameters are greater than the corresponding tabulated t value, i.e. t (121; 0.025) = 1.980, all the parameters satisfy the statistical analysis. The results of the parameter estimation at 620°C and 640°C are given in Tables 5.3 and 5.4, respectively

Table 5.2. Parameter estimates, standard deviations, t values and 95% confidence intervals for the Hougen-Watson kinetic model at 600°C

Parameter	unit	estimate	standard deviation	t value	95% confidence interval	
					lower value	upper value
K_{EB}	1/bar	16.34	1.08	15.2	14.21	18.48
K_{ST}	1/bar	52.47	1.86	28.2	48.79	56.16
K_{H2}	1/bar	6.064	0.393	15.4	5.286	6.842
k_1	kmol/(kgcat·hr)	0.1412	0.00267	54.3	0.1359	0.1465
k_2	kmol/(kgcat·hr)	0.00188	0.000186	10.1	0.00151	0.00226
k_3	kmol/(kgcat·hr)	0.00634	0.00210	3.02	0.00219	0.0105
k_4	kmol/(kgcat·hr)	0.0105	0.00160	6.57	0.00733	0.0137

Table 5.3. Parameter estimates, standard deviations, t values and 95% confidence intervals for the Hougen-Watson kinetic model at 620°C

Parameter	unit	estimate	standard deviation	t value	95% confidence interval	
					lower value	upper value
K_{EB}	1/bar	8.466	1.01	8.37	6.460	10.47
K_{ST}	1/bar	34.00	1.51	22.6	31.02	36.99
K_{H2}	1/bar	3.091	0.447	6.91	2.204	3.977
k_1	kmol/(kgcat·hr)	0.2725	0.0171	15.9	0.2385	0.3065
k_2	kmol/(kgcat·hr)	0.00544	0.000504	10.8	0.00444	0.00644
k_3	kmol/(kgcat·hr)	0.0184	0.00874	2.11	0.001095	0.03571
k_4	kmol/(kgcat·hr)	0.0302	0.00565	5.66	0.0190	0.0413

Table 5.4. Parameter estimates, standard deviations, t values and 95% confidence intervals for the Hougen-Watson kinetic model at 640°C

Parameter	unit	estimate	standard deviation	t value	95% confidence interval	
					lower value	upper value
K_{EB}	1/bar	5.761	1.08	5.33	3.615	7.907
K_{ST}	1/bar	23.56	1.33	17.8	20.92	26.20
K_{H2}	1/bar	2.206	0.368	5.99	1.474	2.937
k_1	kmol/(kgcat·hr)	0.4779	0.0599	7.98	0.3587	0.5970
k_2	kmol/(kgcat·hr)	0.01331	0.00178	7.48	0.009766	0.01685
k_3	kmol/(kgcat·hr)	0.1151	0.0325	3.54	0.05051	0.1796
k_4	kmol/(kgcat·hr)	0.05274	0.00883	5.97	0.03519	0.07030

5.5.2   Model Parameter Estimation for all Temperatures

Table 5.5 shows the estimates of reparameterized parameters for all the temperature, i.e., 600$^{\text{o}}$C, 620$^{\text{o}}$C, and 640$^{\text{o}}$C. *t*-test illustrates that parameters are significantly different from zero. The preexponential factors A_i and A_j can be calculated using the Eqs. (5.40) and (5.42). The results are shown in Table 5.6. The temperature dependence of adsorption constants and rate coefficients is plotted in Figure 5.1. Symbols represent the values of kinetic parameters estimated per temperature (in Tables 5.2, 5.3, and 5.4) and lines represent the values calculated from the reparameterized parameters estimated at all the temperatures (in Table 5.6). It shows an excellent agreement between these values.

The kinetic model with the set of estimated kinetic parameters yields an excellent fit of the experimental data. The parity plots for the conversions to the products at all the experimental conditions used for the parameter estimation are shown in Figure 5.2.

Figures 5.3 and 5.4 show how good the fit of the experimental data are. Figure 5.3 shows the comparison of ethylbenzene conversion and conversions into styrene, benzene, and toluene between experimental and calculated values as a function of space time at 620$^{\text{o}}$C. In Figure 5.4 experimental and calculated selectivity to styrene is shown as a function of ethylbenzene conversion at 620$^{\text{o}}$C.

Table 5.5. Reparameterized parameter estimates, standard deviations, *t* values and 95% confidence intervals for the Hougen-Watson kinetic model at all temperatures

Parameter	unit	estimate	standard deviation	$\lvert t \text{ value}\rvert$	95% confidence interval	
					lower limit	upper limit
A_{EB}^{*}	1/bar	9.648	0.628	15.36	8.414	10.88
A_{ST}^{*}	1/bar	34.93	0.916	38.13	33.12	36.73
$A_{H_2}^{*}$	1/bar	3.577	0.242	14.78	3.100	4.054
$\Delta H_{a,EB}$	kJ/mol	-102.22	12.31	8.304	-126.44	-78.01
$\Delta H_{a,ST}$	kJ/mol	-104.56	7.308	14.31	-118.94	-90.18
$\Delta H_{a,H_2}$	kJ/mol	-117.95	20.75	5.684	-158.78	-77.12
A_{1}^{*}	kmol/(kgcat·hr)	0.2539	0.00822	30.89	0.2378	0.2701
A_{2}^{*}	kmol/(kgcat·hr)	0.00497	0.000278	17.88	0.00361	0.00634
A_{3}^{*}	kmol/(kgcat·hr)	0.02132	0.00557	3.828	0.01038	0.03228
A_{4}^{*}	kmol/(kgcat·hr)	0.02519	0.00237	10.63	0.02053	0.02985
E_1	kJ/mol	175.38	9.172	19.12	157.34	193.43
E_2	kJ/mol	296.29	20.64	14.36	255.08	336.91
E_3	kJ/mol	474.76	90.81	5.228	296.08	653.44
E_4	kJ/mol	213.78	31.59	6.767	151.62	275.94

Table 5.6. Values of the true kinetic parameters*

A_1	A_2	A_3	A_4	A_{EB}	A_{ST}	A_{H2}
4.594×10^{9}	1.060×10^{15}	1.246×10^{26}	8.024×10^{10}	1.014×10^{-5}	2.678×10^{-5}	4.519×10^{-7}
E_1	E_2	E_3	E_4	$\Delta H_{a,EB}$	$\Delta H_{a,ST}$	$\Delta H_{a,H_2}$
175.38	296.29	474.76	213.78	-102.22	-104.56	-117.95

* Units of parameters are the same as those in Table 5.5.
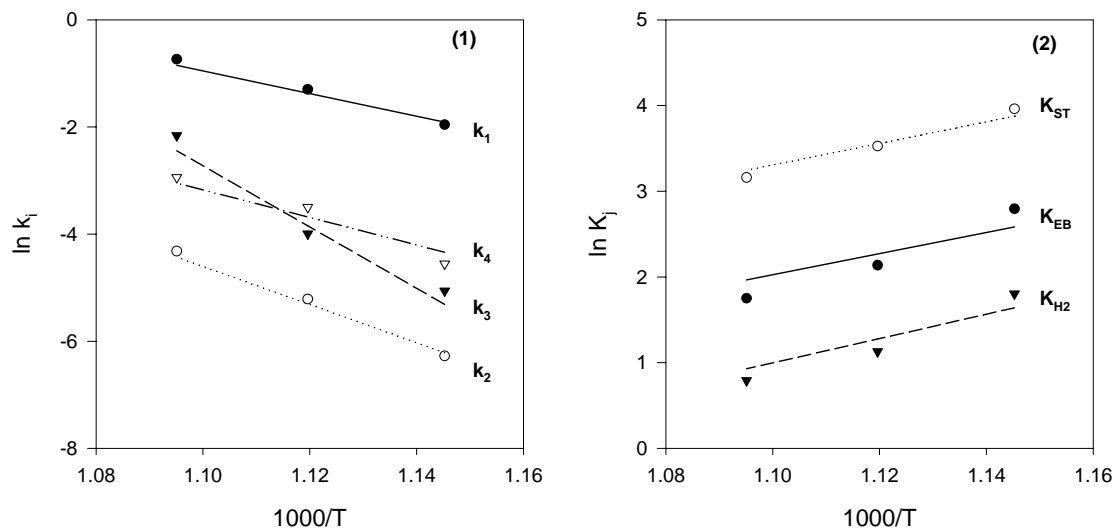
Figure 5.1. Effect of temperature on (1) rate coefficients, k_i, and (2) adsorption equilibrium constants, K_j: symbols, estimated values per temperature; lines, calculated values from estimates at all temperatures.
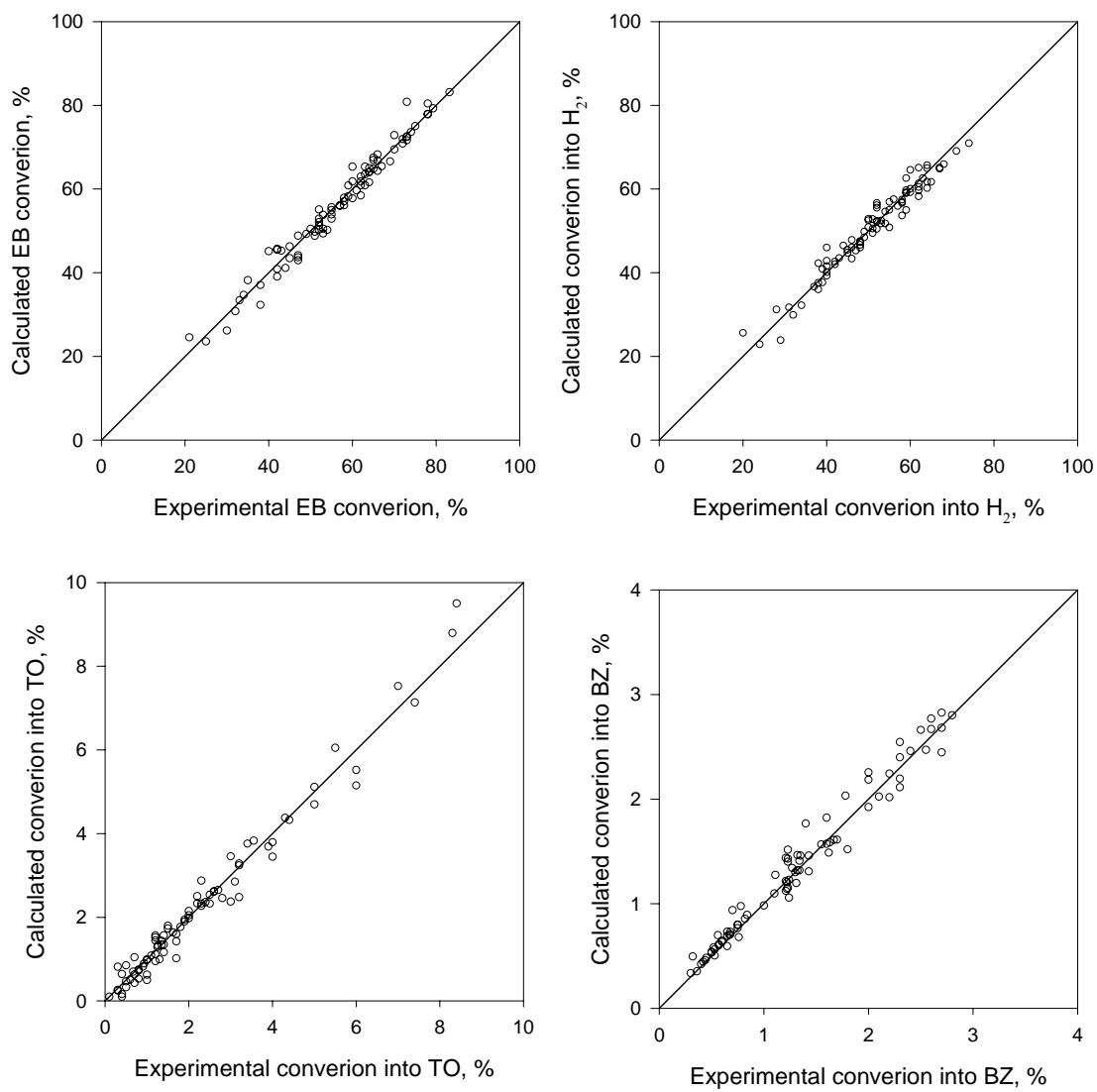
Figure 5.2. Comparison of experimental and calculated conversions for ethylbenzene, hydrogen, toluene, and benzene at all reaction conditions.
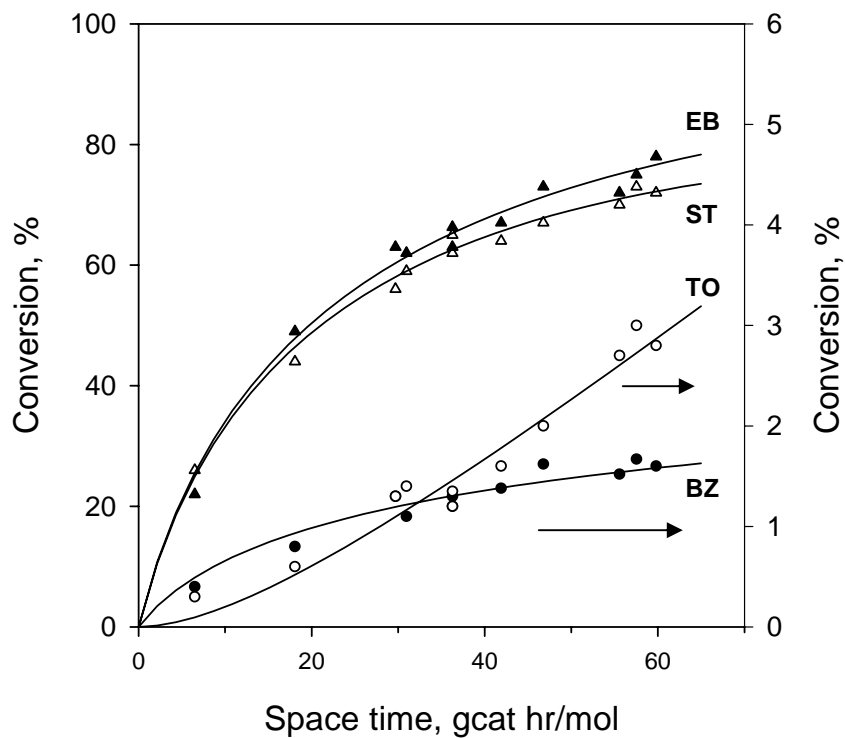
Figure 5.3. Comparison of calculated conversions and experimental conversions as a function of space time: Symbols represent experimental data and lines represent calculated values using the estimates of kinetic parameters obtained from all temperatures simultaneously: $T = 620^{\circ}C$; $H_2O/EB = 11$ (mol/mol); $P_T = 1.044$ bar; $P_{N2} = 0.432$ bar.
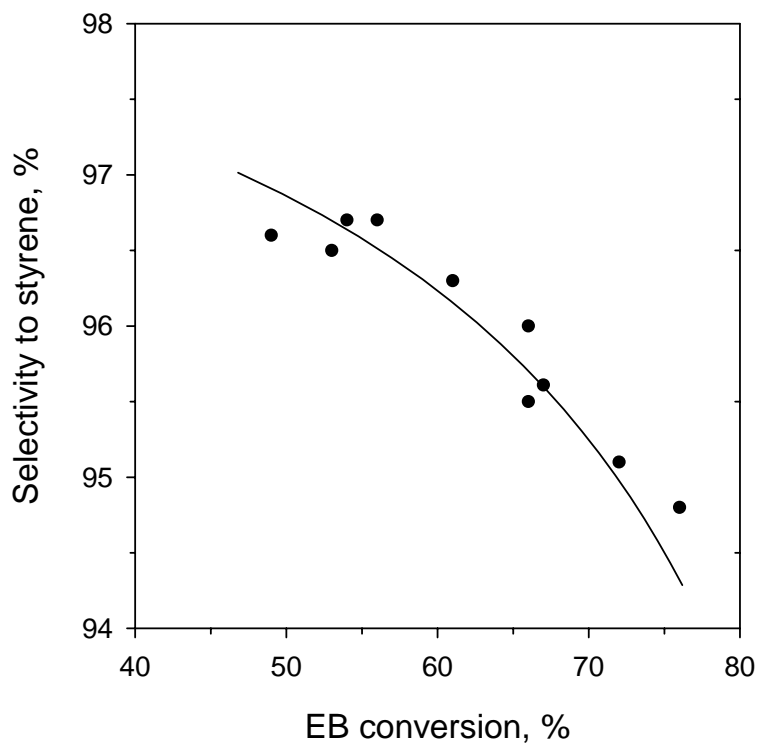
Figure 5.4. Comparison of calculated selectivity to styrene and experimental selectivity to styrene as a function of space time: Symbols represent experimental data and lines represent calculated values using the estimates of kinetic parameters obtained from all temperatures simultaneously: $T = 620^{\circ}C$; $H_2O/EB = 11$ (mol/mol); $P_T = 1.044$ bar; $P_{N2} = 0.432$ bar.

It is worthwhile to compare the results of this work to those in the literature. Schüle et al.[111] described kinetic modeling using surface science experiments for the catalytic dehydrogenation of ethylbenzene over unpromoted iron oxide. The rate-determining step was assumed to be a surface reaction of adsorbed ethylbenzene to give adsorbed styrene and gas phase hydrogen as shown in Eq. (5.45).

$$EBl \rightarrow STl + H_2 \qquad (5.45)$$

It turned out that on the active *unpromoted* Fe_2O_3 the activation energy of reaction Eq. (5.45) is 160 kJ/mol, and activation energy of *desorption* of ethylbenzene and styrene are 64 kJ/mol and 73 kJ/mol, respectively.[23, 111, 112] Since the adsorption is believed to be a non-activated process, the heat of adsorption of component j is equal to the activation energy of *desorption* of component j, $\left(-\Delta H_{a,j}\right) = -\left(E_{a,j} - E_{d,j}\right) = E_{d,j}$.[112] They also reported that on the *potassium-promoted* iron oxide, KFe_xO_y, the activation energy of *desorption* of ethylbenzene is 65 kJ/mol, which is almost the same as that of unpromoted Fe_2O_3, while the activation energy of *desorption* of styrene is decreased to 65 kJ/mol. Lebedev[37] showed that the heat of adsorption of styrene is 58.4 kJ/mol on a commercial styrene catalyst. More recently Dulamiţă et al[113] performed experiments using *potassium-promoted* iron catalyst and estimated the kinetic parameters of the kinetic model based on the Langmuir-Hinshelwood mechanism. The rate-determining step was assumed to be

$$EBl + l \rightleftharpoons STl + H_2l \qquad (5.46)$$

which is identical to the assumption made in Eq. (5.5). They found that the activation

energy of dehydrogenation of ethylbenzene on potassium-promoted iron catalyst, E_1, is

103.1 kJ/mol, and the heat of adsorptions of ethylbenzene, styrene, and hydrogen are

$\left(-\Delta H_{a,EB}\right) = 65.83$ kJ/mol, $\left(-\Delta H_{a,ST}\right) = 209.396$ kJ/mol, and $\left(-\Delta H_{a,H_2}\right) = 103.15$

kJ/mol, respectively. In our work the estimated activation energy of dehydrogenation of

ethylbenzene is $E_1 = 175.38$ kJ/mol and the heat of adsorptions of ethylbenzene, styrene,

and hydrogen are $\left(-\Delta H_{a,EB}\right) = 102.22$ kJ/mol, $\left(-\Delta H_{a,ST}\right) = 104.56$ kJ/mol, and

$\left(-\Delta H_{a,H_2}\right) = 117.95$ kJ/mol, respectively.

5.5.3   Physicochemical Tests

In section 5.2.2, the catalytic rate equations are developed with assuming that

surface reactions are the rate-determining step, which leads to include the adsorption

equilibrium constants in the final rate equations. In sections 5.5.1 and 5.5.2, those

parameters are estimated using experimental data. For many years if the adsorption

equilibrium constants showed negative values or did not decrease with temperature, the

corresponding rate equations were believed to be eliminated. Raghavan and

Doraiswamy[114] examined the validity of adsorption equilibrium constants directly for

gas phase catalytic isomerization of n-butene to isobutene. They compared adsorption

equilibrium constants of isobutene and n-butene at the reaction temperature with those

estimated from the Hougen-Watson model. They reported that the adsorption

equilibrium constants showed an excellent agreement within about 12% over the temperature range they studied.

More systematically, Boudart and co-authors[100, 101] have proposed well-established rules for testing the suitability of the estimated parameter values in the final rate equations. In this work the adsorption enthalpies and entropies are tested by the constraint rules presented by Boudart et al.[100] and Boudart.[115] The following test procedure is guided by Mears and Boudart[116], Van Trimpont et al.[117], Xu and Froment[90], and Froment and Bischoff.[95]

1. Thermodynamics requires the activation energy of reaction i to be greater than the heat of the reaction, $\Delta H_{r,i}$, for an endothermic reaction i. Therefore, the following relation must be obeyed.

$$E_i > \Delta H_{r,i} \tag{5.47}$$

As shown in Table 5.7, the activation energies for reactions 1 and 2, which are endothermic reactions, are indeed greater than the corresponding heats of reactions at 893.15K.

2. The heat of adsorption, $\left(-\Delta H_{a,j}\right)$, has to be greater than zero, because the adsorption is exothermic. All the estimates of heat of adsorption satisfy this constraint.

3. The adsorption entropy has to satisfy

$$0 < -\Delta S_{a,j}^o < S_g^o \tag{5.48}$$

The inequality comes from the relation:

$$\Delta S_a^o = S_a^o - S_g^o \tag{5.49}$$

where S_g^o is the standard entropy of the gas, and S_a^o is the entropy of the adsorbed

molecule. For adsorption, S_a^o is less than S_g^o because of the translational contribution to

S_g^o [116]. The standard entropies of ethylbenzene, styrene, and hydrogen in gas phase, $S_{g,j}^o$,

can be obtained from Stull et al.[118] $\Delta S_{a,j}^o$ is calculated by following relationship:

$$\Delta S_{a,j}^o = R \ \ln A_j \tag{5.50}$$

The result is presented in Table 5.8, and the rule is satisfied.

4.   The last criterion is:

$$41.8 < -\Delta S_{a,j}^o \leq 51 - 0.0014 \Delta H_{a,j} \tag{5.51}$$

Everett[119] obtained the equality relation in Eq. (5.51) by the linear regression between

standard entropy and enthalpy changes for physical adsorption on a gas-charcoal. This

equation can be extended to chemisorption.[116] Furthermore, Vannice et al.[101] showed

that it could be applicable to dissociative adsorption which was not included in the rule

proposed earlier by Boudart et al.[100] The verification of this rule is shown in Table 5.8.

This rule is satisfied as well.

Table 5.7. Activation energies and heat of reactions for reactions 1 and 2

	E_i (kJ/mol)*	$\Delta H_{r,i}$ (kJ/mol) at 298.15K**	$\Delta H_{r,i}$ (kJ/mol) at 893.15K**
Reaction 1 [¶]	175.38	117.7	124.8
Reaction 2 [§]	296.29	105.5	101.5

* Activation energies are shown in Table 5.6.
** Heat of reactions are calculated from thermodynamics.
[¶] Reaction 1 refers to dehydrogenation of ethylbenzene to styrene.
[§] Reaction 2 refers to formation of benzene from ethylbenzene.

Table 5.8. Adsorption entropies, standard entropies for ethylbenzene, styrene, and hydrogen

	$-\Delta S_{a,j}^o$ (J/mol/K)*	$S_{g,j}^o$ (J/mol/K)**	$51 - 0.0014\,\Delta H_{a,j}$ (J/mol)
ethylbenzene	95.61	361.65	194.1
styrene	87.53	346.25	197.4
hydrogen	121.5	186.1	216.1

* Values are calculated from Eq. (5.50).
** Values are obtained from Stull et al.[118]

CHAPTER VI

SIMULATION OF FIXED BED ADIABATIC REACTOR

WITH AXIAL FLOW: PSEUDOHOMOGENEOUS MODEL

6.1   Introduction

The *basic one-dimensional pseudohomogeneous* model for the simulation of fixed bed adiabatic reactor is discussed in this chapter. It is a simple model which does not explicitly account for the presence of catalyst and considers the fluid phase to be in plug flow in the axial direction.[120] The *heterogeneous* model leads to separate model equations for the fluid and the catalyst to account for the resistance to mass and heat transfer inside the catalyst particle and between particle and fluid. This topic will be discussed in chapter VII. The general classification of fixed bed reactor models is presented by Froment and Bischoff.[120]

Axial dispersion can be assumed to be negligible when the ratio of bed length to particle diameter is over 50.[121] A more accurate condition that axial dispersion is unimportant in a nonisothermal fixed bed reactor was developed by Young and Finlayson.[122] They showed that the criterion is independent of the reactor length, so that the importance of axial dispersion can be diminished not by increasing the reactor length but by increasing the flow rates. This condition is satisfied in industrial reactors.

6.2 Continuity, Energy, and Momentum Equations

The underlying assumption for the basic one-dimensional pseudohomogeneous model may be written:[120, 123]

1. Radial and axial dispersions are negligible.

2. Gradients of concentration and temperature within the catalyst particle are negligible.

3. Channeling or shortcut effects do not occur.

4. The reactor is run in the steady state.

5. The fluid phase is in plug flow.

6. The gas phase obeys the ideal gas law.

6.2.1 Continuity Equation

The steady state continuity equations for the reacting species accounting for both catalytic and thermal reactions in the catalyst bed and voids are given by

$$\frac{dX_{EB}}{d\left(W/F_{EB}^0\right)} = r_{c1} + r_{c2} + r_{c3} + \left(r_{t1} + r_{t2} + r_{t3}\right)\frac{\varepsilon_B}{\rho_B}$$

$$\frac{dX_{ST}}{d\left(W/F_{EB}^0\right)} = r_{c1} - r_{c4} + r_{t1}\frac{\varepsilon_B}{\rho_B}$$

$$\frac{dX_{BZ}}{d\left(W/F_{EB}^0\right)} = r_{c2} + r_{t2}\frac{\varepsilon_B}{\rho_B}$$

$$\frac{dX_{TO}}{d\left(W/F_{EB}^0\right)} = r_{c3} + r_{c4} + r_{t3}\frac{\varepsilon_B}{\rho_B}$$

(6.1)

As derived in chapter V, the rate equations for the catalytic reactions are

$$r_{c1} = \frac{k_1 K_{EB}\left(P_{EB} - P_{ST}P_{H_2}/K_{eq}\right)}{\left(1 + K_{EB}P_{EB} + K_{H_2}P_{H_2} + K_{ST}P_{ST}\right)^2}$$

$$r_{c2} = \frac{k_2 K_{EB}P_{EB}}{\left(1 + K_{EB}P_{EB} + K_{H_2}P_{H_2} + K_{ST}P_{ST}\right)^2}$$

$$r_{c3} = \frac{k_3 K_{EB}P_{EB}K_{H_2}P_{H_2}}{\left(1 + K_{EB}P_{EB} + K_{H_2}P_{H_2} + K_{ST}P_{ST}\right)^2}$$

$$r_{c4} = \frac{k_4 K_{ST}P_{ST}K_{H_2}P_{H_2}}{\left(1 + K_{EB}P_{EB} + K_{H_2}P_{H_2} + K_{ST}P_{ST}\right)^2}$$

(6.2)

The thermodynamic equilibrium constant, K_{eq}, is evaluated as a function of temperature, which will be explained in section 6.3.1. The rate equations for the thermal reactions are

$$r_{t1} = k_{t1}\left(P_{EB} - P_{ST}P_{H_2}/K_{eq}\right)$$

$$r_{t2} = k_{t2}P_{EB}$$

(6.3)

$$r_{t3} = k_{t3}P_{EB}$$

The values of the kinetic parameters in Eqs. (6.2) and (6.3) are shown in sections 5.5.1 and 5.2.1, respectively,

6.2.2   Energy Equation

The energy equation for a tubular reactor with plug flow in the steady state can be written:[80]

$$\sum_{j=1}^{6} \dot{m}_j c_{pj} \frac{dT}{dz} = \Omega \rho_B \sum_{i=1}^{4} \left(-\Delta H_{ri}\right) r_i, \quad j = \text{EB, ST, BZ, TO, } H_2, \text{ and } H_2O \qquad (6.4)$$

where $\dot{m}_j = \left(u_s \cdot \rho_g \cdot \Omega\right)$ and is the mass rate of component j in kg/hr, ρ_g is the gas density in kg/m³$_f$, c_{pj} is the specific heat of component j in kJ/(kg·K), $-\Delta H_{ri}$ is the heat of reaction i in kJ/kmol and Ω is the cross section of reactor in m²$_r$, ρ_B is the catalyst bed density in kgcat/m³$_r$, r_i is the rate of reaction i in kmol/(kgcat·hr). Since $W = \rho_B \cdot \Omega \cdot z$, Eq. (6.4) can be expressed with respect to space time:

$$\sum_{j=1}^{6} \dot{m}_j c_{pj} \frac{dT}{d\left(W/F_{EB}^0\right)} = F_{EB}^0 \sum_{i=1}^{4} \left(-\Delta H_{ri}\right) r_i \qquad (6.5)$$

Since the mass flow rates of the components change as the reactions proceed, they should be expressed in terms of the corresponding conversions.

$$
\begin{aligned}
\dot{m}_{EB} &= \text{Mw}_{EB} F_{EB}^0 \left(1 - X_{EB}\right) \\
\dot{m}_{ST} &= \text{Mw}_{ST} \left(F_{ST}^0 + F_{EB}^0 X_{ST}\right) \\
\dot{m}_{BZ} &= \text{Mw}_{BZ} \left(F_{BZ}^0 + F_{EB}^0 X_{BZ}\right) \\
\dot{m}_{TO} &= \text{Mw}_{TO} \left(F_{TO}^0 + F_{EB}^0 X_{TO}\right) \\
\dot{m}_{H_2} &= \text{Mw}_{H_2} \left(F_{H_2}^0 + F_{EB}^0 X_{H_2}\right) \\
\dot{m}_{H_2O} &= \text{Mw}_{H_2O} F_{H_2O}^0
\end{aligned}
\qquad (6.6)
$$

where Mw$_j$ is the molecular weight of component j in kg/kmol and F_j^0 is the feed molar flow rate of component j in kmol/hr.

To calculate the isobaric specific heats of the component j, c_{pj}, the following polynomial function from Reid et al.[124] is used.

$$C_{pj} = a_j + b_j T + c_j T^2 + d_j T^3 \tag{6.7}$$

The values of the constants are shown in Table 6.1.

Table 6.1. Constants of the specific heats of the components

Component, j	EB	ST	BZ	TO	H$_2$	H$_2$O
a_j, kJ/$(\text{kg}\cdot\text{K})$	-0.43426	-0.26436	-0.40599	-0.27127	13.57	1.79111
$b_j \times 10^3$, kJ/$(\text{kg}\cdot\text{K}^2)$	6.0671	5.564	6.6616	5.9142	4.637	0.1069
$c_j \times 10^6$, kJ/$(\text{kg}\cdot\text{K}^3)$	-3.8625	-3.0018	-4.5318	-3.8631	-6.905	0.58611
$d_j \times 10^{10}$, kJ/$(\text{kg}\cdot\text{K}^4)$	9.1282	5.3317	12.255	9.54	38.23	-1.998

6.2.3   Momentum Equation

The momentum equation is obtained from Froment and Bischoff:[120]

$$-\frac{dP_t}{dz} = f\alpha\frac{\rho_g u_s^2}{d_p} = f\frac{G^2}{\rho_g d_p} \tag{6.8}$$

Eq. (6.8) can be expressed with respect to space time, W/F_{EB}^o.

$$-\frac{dP_t}{d\left(W/F_{EB}^o\right)} = f\alpha\frac{u_s G F_{EB}^o}{\rho_B d_p \Omega} \tag{6.9}$$

where f is the friction factor, G is the superficial mass flow velocity in kg/(m^2_r·hr), α is the conversion factor, 7.7160×10^{-8} when P_t is in bar and G is in kg/(m^2_r·hr), u_s is the superficial velocity in m^3_f/(m^2_r·s), and d_p is the equivalent particle diameter in m$_p$ and is defined by the diameter of a sphere with the same surface area per unit volume as the actual particle:[120, 125]

$$S_v = \frac{a_v}{1-\varepsilon_B} = \frac{6}{d_p} \tag{6.10}$$

Therefore,

$$d_p = \frac{6\left(1-\varepsilon_B\right)}{a_v} \tag{6.11}$$

where S_v is the external particle surface area per unit volume of particle in m$^{-1}_p$ and a_v is the external particle surface area per unit reactor volume in m^2_p/m^3_r.

The friction factor, f, is calculated using Ergun relation:

$$f = \frac{1-\varepsilon_B}{\varepsilon_B^3}\left[a + \frac{b\left(1-\varepsilon_B\right)}{\text{Re}}\right] \tag{6.12}$$

with a = 1.75 and b = 150. Re is the Reynolds number, $(d_p \cdot u_s \cdot \rho_g)/\mu$. Handley and Heggs[126] measured the pressure drop for beds of various packings and plotted friction factors against Reynolds number. The linear fit by least square method yielded a = 1.24 and b = 368 for spherical packings. For cylindrical packings the coefficients a and b are 1.28 and 458, respectively, which are dependent on the particle size of packing. Hicks[127] showed that the Ergun equation is limited to Re/(1- ε) < 500 and the Handley and Heggs equation is recommended for use for 1000 < Re/(1-ε) < 5000.

6.3   Calculation of Physicochemical Properties

6.3.1   Thermodynamic Equilibrium Constant

The calculation of the thermodynamic equilibrium constant, K_{eq}, in Eqs. (6.2) and (6.3), at given temperatures requires the data of specific heats which can be expressed as a function of temperature.

$$C_{pj} = a_j + b_j T + c_j T^2 + d_j T^4 \tag{6.13}$$

where C_{pj} is in kJ/kmol. The polynomial constants are found from Reid et al.[124] The data of standard heats of formation and the standard Gibbs energies of formation for ethylbenzene, styrene, and hydrogen are also needed to calculate the equilibrium constant. Those data are shown in Table 6.2.

The heat of reaction at temperature T may be obtained through integration of the integrals illustrated in Eq. (6.14).[128]

$$\Delta H^o = \Delta H^o_{298} + \int_{298.15}^{T} \Delta C^o_p dT$$

$$= \Delta H^o_{298} + \Delta a (T - 298.15) + \frac{\Delta b}{2}(T^2 - 298.15^2) \qquad (6.14)$$

$$+ \frac{\Delta c}{3}(T^3 - 298.15^3) + \frac{\Delta d}{4}(T^4 - 298.15^4)$$

where

$$\Delta H^o_{298} = \sum v_i \Delta H^o_{f,i}$$

$$\Delta C^o_p = \sum v_i C^o_{p,i} = \Delta a + \Delta b T + \Delta c T^2 + \Delta d T^3$$

Since the entropy change of the reaction is known as a function of T, the entropy change

of the reaction at temperature T can be written as

$$\Delta S^0 = \Delta S^0_{298} + \int_{298.15}^{T} \Delta C^o_p \frac{dT}{T}$$

$$= \Delta S^0_{298} + \Delta a \ln\left(\frac{T}{298.15}\right) + \Delta b (T - 298.15) \qquad (6.15)$$

$$+ \frac{\Delta c}{2}(T^2 - 298.15^2) + \frac{\Delta d}{3}(T^3 - 298.15^2)$$

The Gibbs energy change of reaction is calculated from

$$\Delta G^o = \Delta H^o - T\Delta S^o \qquad (6.16)$$

Finally, the equilibrium constant is obtained from the definition:

$$\prod(\hat{a}_j)^{v_j} = \exp\left(-\Delta G^o / RT\right) \equiv K \qquad (6.17)$$

where $\hat{a}_j$ is the activity of component j.

Since the ethylbenzene dehydrogenation is performed under atmospheric

pressure and the temperature is in the range between 600°C and 640°C, the reaction

mixture behaves as an ideal gas. Therefore, the equilibrium constant at standard state becomes

$$K_{eq} = K \cdot \left(P^0\right)^\nu = \frac{P_{ST} P_{H_2}}{P_{EB}} \qquad (6.18)$$

where $\nu = \sum \nu_j$ and P^o is the standard state pressure, 1 bar. From this relation the equilibrium constant can be calculated as a function of temperature at each step of reactor integration. Table 6.3 shows the calculated values of the heat of reaction, the standard entropy change of reaction, the standard Gibbs energy change of reaction, the equilibrium constant, and equilibrium conversion at given temperatures with the molar feed ratio of $H_2O/EB = 11(mol/mol)$.

Table 6.2. Polynomial constants for the specific heat, the standard heats of formation, and the standard Gibbs energies for the formation of EB, ST, and H_2

Component, j	EB	ST	H_2
a_j, kJ/(kmol·K)	-43.1	-28.25	27.14
$b_j \times 10^3$, kJ/(kmol·K^2)	707.2	615.9	9.274
$c_j \times 10^5$, kJ/(kmol·K^3)	-48.11	-40.23	-1.381
$d_j \times 10^9$, kJ/(kmol·K^4)	130.1	99.35	7.645
$\Delta H_{f,i}{}^o \times 10^{-5}$, kJ/kmol	0.2981	1.475	-
$\Delta G_{f,i}{}^o \times 10^{-5}$, kJ/kmol	1.307	2.139	-

Table 6.3. Values of the heat of reaction, the standard entropy change of reaction, the standard Gibbs energy change of reaction, the equilibrium constant, and equilibrium ethylbenzene conversion at given temperatures with the feed ratio of H_2O/EB = 11(mol/mol)

T, °C	600	620	640
ΔH^o, kJ/kmol	124 747.08	124 833.54	124 911.51
ΔS^o, kJ/kmol	130.6	130.69	130.78
ΔG^o, kJ/(kmol·K)	10 716.88	8 103.96	5 489.19
K_{eq}, bar	0.228	0.336	0.485
X_{EB}	0.804	0.851	0.888

6.3.2 Heat of Reaction

The temperature dependence of the heat of reaction is given by[128]

$$
\begin{aligned}
\Delta H_{ri} = \Delta H^o_{298,i} + \Delta a_i \left(T - 298.15\right) + \frac{\Delta b_i}{2}\left(T^2 - 298.15^2\right) \\
+ \frac{\Delta c_i}{3}\left(T^3 - 298.15^3\right) + \frac{\Delta d_i}{4}\left(T^4 - 298.15^4\right)
\end{aligned}
\tag{6.19}
$$

where $\Delta H^0_{298,i}$ is the standard heat of reaction i at 298 K in kJ/kmol. Table 6.4 shows the values of constants of the specific heats of the reactions. The heats of reaction are evaluated as a function of temperature at each step of reactor integration.

Table 6.4. Constants of the specific heats of the reactions

Reaction i	1	2	3	4
Δa_i, kJ/(kmol$\cdot$K)	41.99	12.986	10.86	-31.13
$\Delta b_i \times 10^2$, kJ/(kmol$\cdot$K^2)	-8.2026	-7.67	-15.1844	-6.9818
$\Delta c_i \times 10^5$, kJ/(kmol$\cdot$K^3)	6.499	9.592	23.04	16.54
$\Delta d_i \times 10^8$, kJ/(kmol$\cdot$K^4)	-2.311	-4.125	-9.9955	-7.685
$\Delta H^0_{298,i}$, kJ/kmol	117 690	105 510	-54 680	-172 370

6.3.3   Viscosity of the Gas Mixture

The viscosity of a pure component is obtained using the equations from Reid.[129] For EB, ST, BZ, and TO the corresponding-states method by Thodos is used. The Thodos relation is:

$$\mu\xi = 4.610 T_r^{0.618} - 2.04\, e^{-0.449 T_r} + 1.94 e^{-4.058 T_r} + 0.1 \qquad (6.20)$$

where $\xi = T_c^{1/6} \mathrm{Mw}^{-1/2} P_c^{-2/3}$. Molecular weights and critical constants of the components are shown in Table 6.5.

For H_2 and H_2O the Chapman-Enskog viscosity equation is recommended to use by Reid et al. It is given by

$$\mu = 26.69 \frac{\sqrt{\mathrm{Mw}T}}{\sigma^2 \Omega_v} \qquad (6.21)$$

where μ is the viscosity in μP, Mw is the molecular weight, T is the temperature in K, σ is the hard-sphere diameter in Å, and Ω_v is the collision integral. Ω_v is unity if the molecules do not interact. It can be calculated from a potential energy of interaction $\psi(r)$. Lennard-Jones potential functions are useful for nonpolar molecules, such as H_2, and Stockmayer potential functions are more reasonable for polar compounds, such as H_2O. For H_2, Ω_v is given by

$$\Omega_v = \frac{A}{T^{*B}} + Ce^{-DT^*} + Ee^{-FT^*}$$

where $T^* = (k/\varepsilon)T$, $A = 1.16145$, $B = 0.14874$, $C = 0.52487$, $D = 0.77320$, $E = 2.16178$, $F = 2.43787$.

For H_2O, Ω_v (Stockmayer) is given by

$$\Omega_v \text{ (Stockmayer)} = \Omega_v \text{ (Lennard-Jones)} + 0.2\delta^2/T^*$$

The values of σ, ε/κ, and δ of H_2 and H_2O are shown in Table 6.6.

The viscosity of the gas mixture can be approximated by

$$\mu_m = \sum_{i=1}^{n} \frac{y_i\mu_i}{\sum_{j=1}^{n} y_j\phi_{ij}} \tag{6.22}$$

where μ_m is the viscosity of mixture, μ_i is the viscosity of pure component i, and y_i is the mole fraction of pure component i. Wilke's approximation yields

$$\phi_{ij} = \frac{\left[1 + \left(\mu_i/\mu_j\right)^{1/2}\left(\text{Mw}_j/\text{Mw}_i\right)^{1/4}\right]^2}{\left[8\left(1 + \text{Mw}_i/\text{Mw}_j\right)\right]^{1/2}} \tag{6.23}$$

ϕ_{ji} is found by interchanging subscripts or by

$$\phi_{ji} = \frac{\mu_j}{\mu_i} \frac{Mw_i}{Mw_j} \phi_{ij} \qquad (6.24)$$

with $\phi_{ij} = \phi_{ji} = 1$. Note that the viscosity of the gas mixture should be calculated at each integration step at the corresponding temperature, pressure, and conversions.

Table 6.5. Molecular weights and critical constants of EB, ST, BZ, and TO[129]

	Mw	T_c, K	P_c, bar
EB	106.16	617.2	36.0
ST	104.14	647.0	39.9
BZ	78.11	562.2	48.9
TO	92.11	591.8	41.0

Table 6.6. Values of σ, ε/κ, and δ of H_2 and H_2O[129]

	σ, Å	ε/κ, K	δ
H_2	2.827	59.7	-
H_2O	2.641	809.1	1.0

6.3.4 Physical Properties of the Catalyst

The physical properties of the catalyst used in this investigation are listed in Table 6.7. ρ_B is measured in the laboratory and ρ_s is given by the catalyst manufacturer. ε_B is calculated using the values of ρ_B and ρ_s as shown in section 5.3. The values of ε_s and τ are assumed and will be used for the heterogeneous model in chapter VII. d_p is calculated using Eq. (6.10).

Table 6.7. Physical properties of catalyst

Physical property	Notation	Value
Catalyst bulk density, $\mathrm{kgcat./m}_r^3$	ρ_B	1 422
Catalyst pellet density, $\mathrm{kgcat./m}_p^3$	ρ_s	2 500
Void fraction of the bed, $\mathrm{m}_f^3/\mathrm{m}_r^3$	ε_B	0.4312
Catalyst Internal void fraction, $\mathrm{m}_f^3/\mathrm{m}_p^3$	ε_s	0.4
Tortuosity of the catalyst	τ	3
Catalyst equivalent pellet diameter, m_p	d_p	0.0055

6.4 Results and Discussion

The continuity-, energy-, and momentum equations are solved numerically for the simulation of a 3-bed adiabatic reactor using the Gear's method with variable step size. Tables 6.8 and 6.9 shows the feed conditions, reactor dimension, and simulation results at different feed molar ratio of H_2O to EB, i.e., 11 and 9. The feed molar flow rate of EB, weight of catalyst, inlet temperatures for each bed, inlet pressure for the first bed were provided by Froment.[130] Note that these data are for a catalyst which is different from that used in the present investigation. The inner radius of the reactor is determined to avoid the failure of the pressure drop calculation because the small inner radius results in the high superficial velocity of gas which leads to an increase in the pressure drop in the reactor. The length of the reactor is calculated using the relation, $z = W/(\rho_B \cdot \Omega)$. As shown in Table 6.8, the inner radius and the length of the reactor utilized for the reactor simulation are 3.50m and 4.26m, respectively.

The reactor simulation is performed at two different H_2O/EB molar ratios, 11 and 9. First, the simulation performed at a molar ratio of H_2O/EB = 11 is shown in Table 6.8 and Figures 6.1 and 6.2. The profiles of ethylbenzene conversion and selectivity of styrene, benzene, and toluene are plotted against the space time in Figure 6.1. The plots of temperature profile and pressure drop profile in the reactor are represented in Figure 6.2. The total ethylbenzene conversion and styrene selectivity at the exit of the reactor are 86.82% and 91.43%. The conversion of ethylbenzene into styrene reaches 79.39% which is below the thermodynamic equilibrium conversion of ethylbenzene into styrene, 84% at 620°C. Since the optimum total ethylbenzene conversion and styrene selectivity

in industrial operation have been reported to lie in the range of 65% - 70% and 95% -
97%, respectively, the simulated values indicate that these conditions are not optimal for
the present catalyst.

Table 6.9 represents the simulation result carried out for a molar ratio of H_2O/EB
= 9 at the same space time as the case of H_2O/EB = 11. The ethylbenzene conversion
and styrene selectivity at the exit of the reactor are 82.83% and 88.92%. The decrease of
the styrene selectivity is due to the increase of the rate of toluene formation rather than
that of benzene formation as shown in (b) of Figure 6.1. Compared to the case of
H_2O/EB = 11, the total feed molar flow rate is substantially decreased, so that the
pressure drop, 0.53 bar through the reactor, becomes small.

The industrial styrene reactor simulation using the pseudohomogeneous model
together with the *intrinsic* kinetic parameters is a simple task but can mislead the
prediction of reactor performance. The pseudohomogeneous model has been often used
to calculate the *observed* reaction rates for simulation and optimization of an industrial
styrene reactor.[8-10, 32, 38, 131] Since the industrial styrene catalysts are reported to have
pore diffusion limitations,[11, 34, 89] the *observed* reaction rates are not *intrinsic*. The
intrinsic kinetic parameters should be used with the heterogeneous model, which
explicitly accounts for the presence of the porous catalyst pellet, for rigorous simulation
of an industrial styrene reactor. The application of the heterogeneous model will be
discussed in the next chapter.

Table 6.8. Simulation result of a 3-bed adiabatic reactor for the feed ratio of $H_2O/EB =$ 11mol/mol when using the *pseudohomogeneous model*

	BED1	BED2	BED3
Weight of catalyst, kg [*]	72 950	82 020	78 330
Space time [§]	103.18	219.19	329.98
X_{EB}, % [¶]	39.25	68.64	86.82
S_{ST}, % [¶]	98.84	96.09	91.43
S_{BZ}, %	0.94	1.34	1.67
S_{TO}, %	0.23	2.58	6.90
P_{in}, bar [3]	1.25	1.066	0.787
T_{in}, K [3]	886	898.2	897.6
T_{out}, K	806.2	843.6	873.7
Length of bed, m	1.33	1.50	1.43
Inner radius of reactor, m		3.50	
Feed molar flow rate, kmol/hr EB [*]		707	
ST		7.104	
BZ		0.293	
TO		4.968	
H_2O [†]		7 777	
Total feed molar flow rate, kmol/hr		8 496.37	

[§] Space time is cumulative and is in kgcat hr/kmol EB.
[¶] X_{EB} denotes the EB conversion and S_j denotes the selectivity of component j.
[*] The information was provided by personal communication with Froment.[130]
[†] The feed molar flow rate of H_2O was obtained from a molar ratio of $H_2O/EB=11$.

Table 6.9. Simulation result of a 3-bed adiabatic reactor for the feed ratio of $H_2O/EB = 9$ mol/mol when using the *pseudohomogeneous model*

	BED1	BED2	BED3
Weight of catalyst, kg[*]	72 950	82 020	78 330
Space time [§]	103.18	219.19	329.98
X_{EB}, % [¶]	37.09	64.85	82.83
S_{ST}, % [¶]	98.84	95.76	88.92
S_{BZ}, %	0.91	1.35	1.82
S_{TO}, %	0.25	2.88	9.26
P_{in}, bar [*]	1.25	1.11	0.92
T_{in}, K [*]	886	898.2	897.6
T_{out}, K	802.61	842.13	877.2
Length of bed, m	1.33	1.50	1.43
Inner radius of reactor, m		3.50	
Feed molar flow rate, kmol/hr EB [*]		707	
ST		7.104	
BZ		0.293	
TO		4.968	
H_2O [†]		6 363	
Total feed molar flow rate, kmol/hr		7 082.3	

[§] Space time is cumulative and is in kgcat hr/kmol EB.
[¶] X_{EB} denotes the EB conversion and S_j denotes the selectivity of component *j*.
[*] The information was provided by personal communication with Froment.[130]
[†] The feed molar flow rate of H_2O was obtained from a molar ratio of $H_2O/EB=9$.
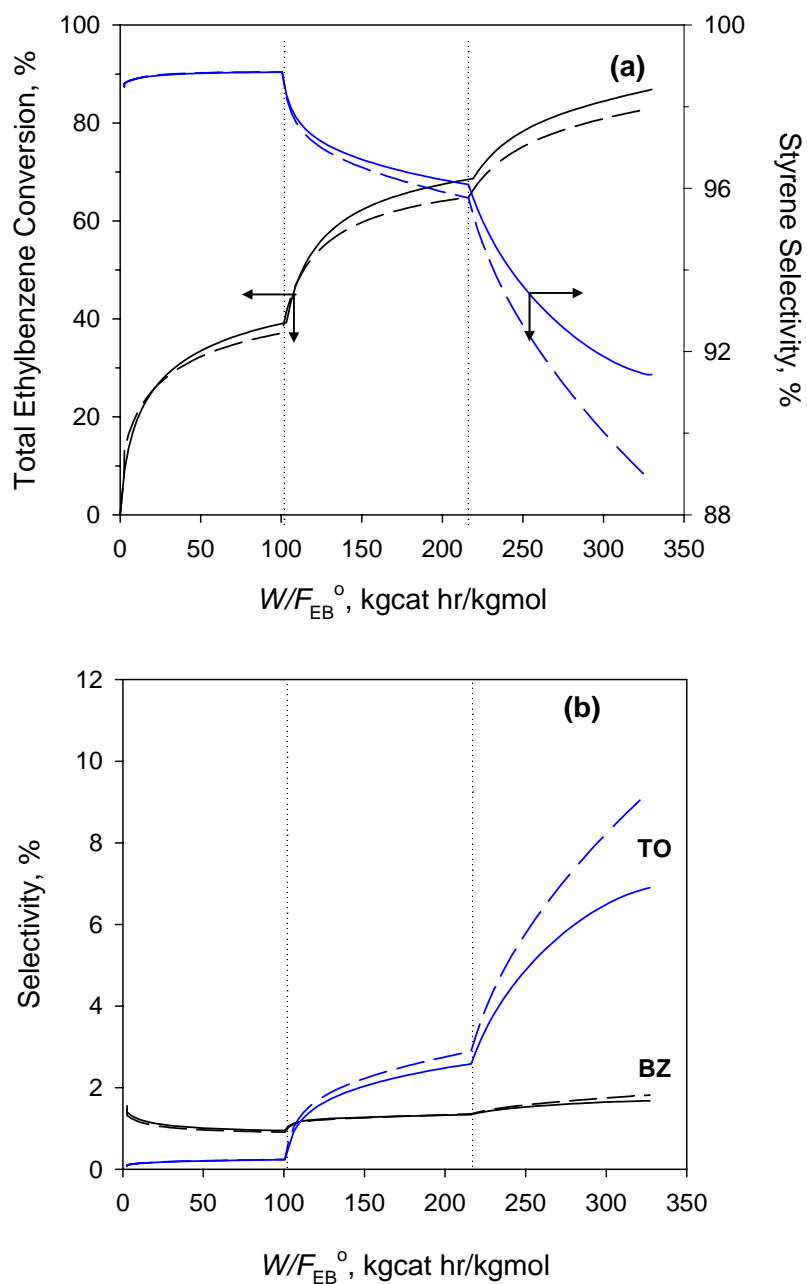
Figure 6.1. Effect of H₂O/EB feed molar ratios of 11 and 9 on the simulated total ethylbenzene conversion and styrene selectivity profiles (a) and benzene and toluene selectivity profiles (b) in a 3-bed adiabatic reactor using the pseudohomogeneous model for T_{in} = 886K, 898K, 897K; P_{in} = 1.25bar; F_{EB}^{o} = 707 kmol/hr. Solid line: H₂O/EB=11 mol/mol; dashed line: H₂O/EB=9 mol/mol.
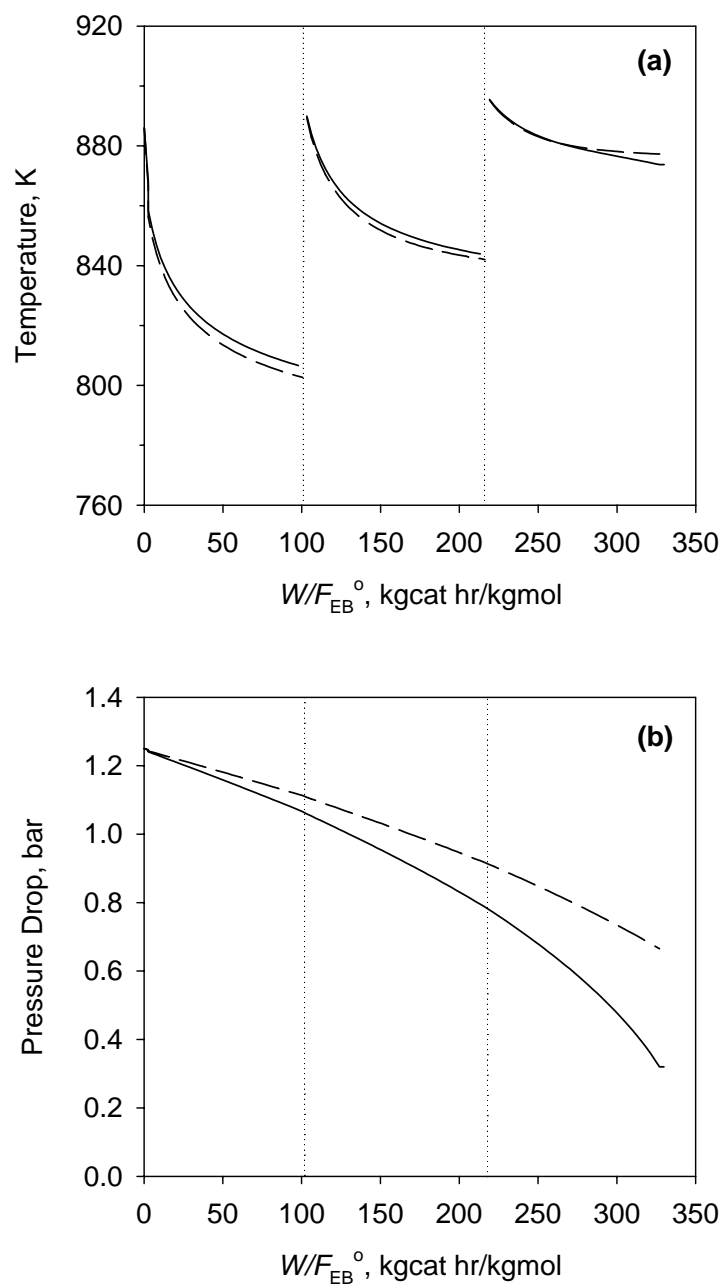
Figure 6.2. Effect of H_2O/EB feed molar ratios of 11 and 9 on the simulated temperature profiles (a) and pressure drop profiles (b) in a 3-bed adiabatic reactor using the pseudohomogeneous model for T_{in} = 886K, 898K, 897K; P_{in} = 1.25bar; F_{EB}^o = 707 kmol/hr. Solid line: H_2O/EB=11 mol/mol; dashed line: H_2O/EB=9 mol/mol.

CHAPTER VII

SIMULATION OF FIXED BED ADIABATIC REACTOR

WITH AXIAL FLOW: HETEROGENEOUS MODEL

7.1   Introduction

In heterogenous catalysis the transport processes may influence the overall reaction rate. These may be divided into two parts: heat and mass transfer between the fluid and the solid (interparticle transport), and inside the internal surface of the porous solid (intraparticle transport). This chapter deals with the resistance to transport inside the porous catalyst, because the high flow rates applied in industrial reactors lead to negligible interparticle gradients. The effect of intraparticle mass transfer is to reduce the reactant concentration within the pellet. Since all the intraparticle transport effects become less important with decreasing catalyst size, for fluidized bed and slurry reactors intraparticle transport can usually be neglibible.

The effect of intraparticle mass transfer on observed reaction characteristics were first studied by Thiele[132] in the U.S.A and Damköhler[133] in Germany independently. Thiele assumed isotropic geometry for a catalyst pellet model, be it a flat plate or sphere. Such models are proven to be quite good approximation to pratical catalyst. The early work was further developed by Wheeler,[134] Weisz,[135] and Wicke.[136] The most important result of these studies is to evaluate what determines the effectiveness of a porous catalyst. The concept of the effectiveness factor was introduced and is defined as the ratio of the reaction rate in the presence of diffusional resistances, averaged over the

particle, to the reaction rate at bulk conditions. Aris[137] showed a comprehensive mathematical treatment of the effectiveness factor problem which includes various type of kinetics, nonisothermal operation, effect of particle shape, and multiple reactions. Bischoff[138] developed a generalized Thiele type modulus for evaluating the effectiveness factor for any form of kinetics. The effectiveness factors for a number of catalytic reactions are listed by Satterfield.[139]

In *heterogeneous* model the differential model equations are written separately for the fluid and solid phases, and the differential equations involve the effective diffusivity. Integration of model equations, including intrinsic reaction rates and transport by internal diffusion throughout the pellet leads to the calculation of the effectiveness factor. Since the effectiveness factor varies along the reactor length, it has to be calculated at each integration step for simulation of an industrial reactor.

7.2   Diffusion: Theory

7.2.1   Diffusion in a Fluid

The molecular diffusion in gases results from the concentration gradients in the mixture. Diffusion tends to make the concentration difference uniform. In a binary gas mixture, the molar flux N_j is proportional to the concentration gradient in the direction of diffusion. The proportionality constant is called diffusivity. Most catalytic reactions involve multicomponent mixtures, so that the rigorous treatment of diffusivity becomes more complicated. In general, the flux of a given chemical species is given in Froment and Bischoff[84]

$$\mathbf{N}_j = -\sum_{k=1}^{N-1} C_t D_{jk} \nabla y_k + y_j \sum_{k=1}^{N} \mathbf{N}_k \qquad j = 1,\ 2,...,\ N\text{-}1 \tag{7.1}$$

where $\mathbf{N}_j$ is the molar flux, C_t is the total concentration, and D_{jk} are the binary diffusivities. It can be rearranged into the Stefan-Maxwell equation given in Bird, Stewart, and Lightfoot[140]

$$-C_t \nabla y_j = \sum_{\substack{k=1 \\ k \neq j}}^{N} \frac{1}{D_{jk}} \left(y_k \mathbf{N}_j - y_j \mathbf{N}_k \right) \tag{7.2}$$

According to Hsu and Bird[141], Eq. (7.1) can be extended to the multicomponent system using effective binary diffusivity D_{jm} for the diffusion of j in a multicomponent mixture.

$$\mathbf{N}_j = -C_t D_{jm} \nabla y_j + y_j \sum_{k=1}^{N} \mathbf{N}_k \tag{7.3}$$

Eq. (7.3) is solved for ∇y_j and then equating the result to ∇y_j in Eq. (7.2) gives

$$\frac{1}{D_{jm}} = \frac{\displaystyle\sum_{k=1}^{N} \frac{1}{D_{jk}} \left(y_k - y_j \frac{N_k}{N_j} \right)}{1 - y_j \displaystyle\sum_{k=1}^{N} N_k / N_j} \tag{7.4}$$

If species 1 diffuses through stagnant component 2, 3, …, m, Eq. (7.4) reduces to the Wilke equation:

$$\frac{1}{D_{1m}} = \frac{1}{1 - y_1} \sum_{k=2,3,...}^{N} \frac{y_k}{D_{1k}} \tag{7.5}$$

If the diffusing components in a mixture are in low concentrations, Eq. (7.5) works very well.[139] For a single chemical reaction, the steady-state flux ratios are obtained by the reaction stoichiometry since

$$\frac{N_i}{\alpha_i} = constant \tag{7.6}$$

where α_i is the stoichiometry coefficient of component i. Thus Eq. (7.4) reduces to

$$\frac{1}{D_{jm}} = \frac{\sum_{k=1}^{N} \frac{1}{D_{jk}} \left(y_k - y_j \frac{\alpha_k}{\alpha_j} \right)}{1 - y_j \sum_{k=1}^{N} \alpha_k / \alpha_j} \tag{7.7}$$

To predict the diffusion coefficients in a binary mixture both extensive experimental data and theoretical equations can be found in the literature.[124, 139] The diffusion coefficients for binary gas mixtures can be calculated from the following theoretical equation based upon the kinetic theory of gases and the Lennard-Jones potential:[124, 142]

$$D_{AB} = \frac{0.00143 T^{1.75}}{P M_{AB}^{1/2} \left[\left(\sum_v \right)_A^{1/3} + \left(\sum_v \right)_B^{1/3} \right]} \tag{7.8}$$

where D_{AB} is the binary diffusion coefficient, cm^2/s; T is the temperature in K; M_A, M_B are the molecular weights of A and B in g/gmol; and M_{AB} is $2[(1/M_A) + (1/M_B)]^{-1}$; P is the pressure in bar. $\sum_v$ is calculated for each component by summing atomic diffusion volumes. The product of coefficient and pressure, $D_{AB}P$, is frequently cited and in most catalytic processes the value is around 0.1cm^2/s at ambient temperature, except when hydrogen is present in the mixture.[143]

7.2.2   Diffusion in a Porous Catalyst

Diffusion inside catalysts may occur by one or more of following three process: molecular diffusion, Knudsen diffusion, and surface diffusion. If the pore size is large and the gas is relatively dense, the diffusion is dominated by molecular diffusion, which has been discussed in the previous section. However, when the pore size becomes small or the gas density is low, the collision of molecules with the pore wall is more significant than with each other. This is known as Knudsen diffusion. Surface diffusion is known as the transport by movement of molecules over a surface. It is not important when appreciable adsorption does not occur and molecules are adsorbed on the surface very strongly.

7.2.2.1   Knudsen Diffusivity

Knudsen diffusivity in gases in a straight cylindrical pore can be calculated from the kinetic theory:[80, 143]

$$D_{KA} = \frac{4}{3} r_e \sqrt{\frac{2RT}{\pi M_A}} = 9700 \, r_e \sqrt{\frac{T}{M_A}} \quad \left(\text{cm}^2/\text{s}\right) \tag{7.9}$$

where r_e is the pore radius in cm, T is the temperature in K, and M_A is the molecular weight in g/gmol. For practical purposes, the Knudsen diffusion coefficient in a porous solid can be obtained by defining a mean pore radius and using a tortuosity of the catalyst. From a parallel cylindrical pore model the mean pore radius is defined as

$$r_m = \frac{2V_g}{S_g} = \frac{2\varepsilon_s}{S_g \rho_p} \tag{7.10}$$

where S_g is the total surface area in cm^2/g, ρ_p is the pellet density in g/cm^3, ε_s is the catalyst internal void fraction. The Knudsen diffusion coefficient becomes

$$D_{e,KA} = \frac{D_K \varepsilon_s}{\tau} = \frac{8}{3} \frac{\varepsilon_s^2}{\tau\, S_g \rho_p} \sqrt{\frac{2RT}{\pi\, M_A}} = 19{,}400\, \frac{\varepsilon_s^2}{\tau\, S_g \rho_p} \sqrt{\frac{T}{M_A}} \quad \left(\text{cm}^2/\text{s}\right) \qquad (7.11)$$

Knudsen diffusivity is negligible in this research because of the large pore size of the catalyst.

7.2.2.2   Effective Diffusivity

In contrast to a homogeneous medium, a porous catalyst contains nonuniform pore structures which intersect with others to form a network where the fluid may follow the tortuous path. To take into account the texture properties of the porous catalyst, the effective diffusivity D_e for component A diffusing through a porous catalyst can be evaluated by[139]

$$D_{eA} = \frac{\varepsilon_s D_A(r)}{\tau} \qquad (7.12)$$

where τ is the tortuosity factor. $D_A(r)$ represents the molecular diffusivity, D_{AB}, in the bulk region and Knudsen diffusivity, D_{KA}, in the Knudsen region. If a pore size distribution is wide and diffusion is in the transition region, various models can be used to calculate the effective diffusivity. Wang and Smith[144] used a composite molecular diffusivity which is a function of the pore radius r when Knudsen diffusion is important. For uniform pressure, D_A is represented by the Bosanquet formula[145, 146]

$$\frac{1}{D_A(r)} = \frac{1}{D_{AB}} + \frac{1}{D_{KA}(r)} \tag{7.13}$$

The effective diffusivity for component A can be expressed by using Eqs. (7.12) and (7.13) as

$$\frac{1}{D_{eA}} = \frac{\tau}{\varepsilon_s} \frac{1}{D_A(r)} = \frac{\tau}{\varepsilon_s} \left(\frac{1}{D_{AB}} + \frac{1}{D_{KA}(r)} \right) \tag{7.14}$$

Parallel cylindrical pore model proposed by Johnson and Stewart[147] is

$$D_{eA} = \frac{\varepsilon}{\tau} \int_0^\infty \left[\frac{1 - a x_A}{D_{AB}} + \frac{1}{D_{KA}} \right]^{-1} f(r) dr \tag{7.15}$$

where $a = 1 - (M_A / M_B)^{1/2}$, M_A and M_B is the molecular weight of species A and B, $f(r)dr$ is the fraction of void volume in pores of radii between r and $r + dr$, and x_A is the mole fraction of diffusing component A in the mixture. In this model the tortuosity factor does not depend on the pore size and the diffusing species. Feng and Stewart[148] extended the structural model of porous solid of Johnson and Stewart to the cross-linked pore network.

Wakao and Smith[149] presented the random pore model that is useful to predict the diffusivities in porous material with a bimodal pore size distribution which has micropores and macropores.

$$D_{eA} = \varepsilon_a^2 D_a + \left(1-\varepsilon_a\right)^2 D_i + \frac{4\varepsilon_a\left(1-\varepsilon_a\right)}{1/D_a + 1/D_i}$$

with

(7.16)

$$D_a = \frac{D_{AB}}{1 - ax_A + D_{AB}/D_{KAa}}$$

$$D_i = \frac{D_{AB}\varepsilon_i^2}{\left(1-\varepsilon_a\right)^2\left(1 - ax_A + D_{AB}/D_{KAi}\right)}$$

where ε_a, ε_i, and D_{KAa}, D_{KAi} represent the void fractions and Knudsen diffusivities associated with the macro- and micropores, respectively. Since bimodal porous materials have two separate peaks, i.e., macro and micro, in the pore size distribution, the void fractions for macro- and micropores can be determined separately.

More recently, Beeckman and Froment[61] described the pore network in terms of a Bethe-lattice model. This approach, based on probability theory, has been applied to diffusion inside catalysts subject to deactivation by both site coverage and pore blockage. The predicted tortuosity of the pore network has a value of 4.

Satterfield and Cadle[150] measured the diffusivities of 17 commercial catalysts and catalyst supports and calculated tortuosity using the parallel-path pore model. This model is similar to the parallel cylindrical pore model proposed by Johnson and Stewart.[147] They showed the tortuosity lies between 3 and 7, except for materials which were calcined at very high temperature. Tables 7.1 and 7.2 show the tortuosity factors predicted from various pore models and determined from experiments, respectively.

Table 7.1. Comparison of tortuosity factors predicted from various models[84]

Tortuosity factor	Model	Reference
2	parallel-path pore	Wheeler[134]
$1/\varepsilon_s$ (2.5 – 3.5)	random pore	Wakao and Smith[149]
3	cross-linked pore	Feng and Stewart[148]
4	pore network	Beeckman and Froment[61]

Table 7.2. Comparison of tortuosity factors obtained from experiments[84]

Tortuosity factor	Catalysts	Reference
2.8 – 7.3	various industrial catalysts	Satterfield and Cadle[150]
4.6	alumina pellet	Feng and Stewart[148]
4 - 7	Ni/molybdate	Patel and Butt[151]
5	chromia/alumina	Dumez and Froment[152]
4.4 – 5.0	Ni/alumina	De Deken et al.[153]
6.1 -9.6	HDS catalysts	Wang and Smith[144]
2.0 – 11.2	various industrial catalysts	Sharma et al.[154]

7.2.3   Diffusion and Reaction in a Porous Catalyst

Since the total rate of reaction is proportional to the amount of surface in the catalyst, most practical catalysts have large surface areas. In order to obtain a large surface area a porous catalyst with many small pores is frequently used;[80] hence, an adequate gas transport model for a porous catalyst is necessary. A mathematical model, so-called 'dusty-gas' model, of mass transport in a porous catalyst was proposed by Mason and Evans,[155] in which the porous medium is composed of an array of dust particles held and uniformly distributed in space. The dust particles are treated as one of the gas molecules in the mixture. The model presents that the diffusional and viscous flow are independent and additive.

Due to the importance of gas transport and chemical reactions in porous catalysts, much theoretical and experimental research has been dedicated on these phenomena. Numerous literature studies are found for the study of diffusion with chemical reaction.[156-160] Mathematical equations developed to predict the diffusion and reaction in a porous catalyst lead to boundary-value problems. These problems form second order ordinary differential equations with two boundary conditions. The orthogonal collocation method has proved to be a useful and effective method for solving these problems.[161-163] The solution of two-point boundary value problems using the orthogonal collocation method will be discussed in the next section.

7.3 **Orthogonal Collocation Method: Theory**

The orthogonal collocation method was first developed by Villadsen and Stewart[161] to provide an efficient tool for solving ordinary differential equations. It chooses the collocation points automatically using the trial function as a series of orthogonal polynomials. Collocation points are the roots of the polynomial and the corresponding dependent variables are calculated at each collocation point.

In the following sections, the properties of orthogonal polynomials will be discussed first and then the application of orthogonal polynomials and collocation method to the solution of the boundary value problems will be presented. More details on this method and its application to the chemical engineering problems can be found in Villadsen,[164] Villadsen and Michelsen,[165] Finlayson,[166] Xu and Froment,[160] Coppens and Froment,[156] Abashar and Elnashaie,[167] Wang,[168] Constantinides and Mostoufi,[105] and Rice and Do.[169]

7.3.1 **Definition of Orthogonal Polynomials**

From Villadsen[164] Jacobi polynomials with specific weight function can be defined as follows:

"Let $W(x) = x^\alpha (1-x)^\beta$ where $\alpha > $ -1 and $\beta > $ -1, and let the range of orthogonality be [0, 1]. The set of approximation function is defined by Jacobi polynomials $P_n^{(\alpha,\beta)}(x)$:

$$\int_0^1 x^\beta (1-x)^\alpha P_n^{(\alpha,\beta)}(x) P_m^{(\alpha,\beta)}(x) dx = c_n \delta_{nm} \qquad (7.17)$$

where c_n is the value of the integral for $n = m$ and δ_{nm} the Kronecker delta function."

Since Jacobi polynomials are originally defined in the range of [-1, 1] and with a weight function $W(x) = (1-x)^\alpha (1+x)^\beta$, the polynomials in Eq. (7.17) is usually termed as "shifted" Jacobi polynomials. But the shorter term, Jacobi polynomials, is also used by Villadsen and Stewart.[161] The Jacobi polynomials have the form

$$P_n^{(\alpha,\beta)} = \gamma_n x^n + \ldots + (-1)^n x^0 = \sum_{i=0}^{n} (-1)^{n-i} \gamma_i x^i \qquad (7.18)$$

The coefficients γ_i are all positive.

7.3.2 Coefficients of Jacobi Polynomials

The Jacobi polynomials defined by Eqs. (7.17) and (7.18) can be expressed by using Rodrigues formula[164]

$$P_n^{(\alpha,\beta)} x^\beta (1-x)^\alpha = \frac{(-1)^n \Gamma(\beta+1)}{\Gamma(n+\beta+1)} \frac{d^n}{dx^n} \left[x^{n+\beta} (1-x)^{n+\alpha} \right] \qquad (7.19)$$

where Γ is the gamma function. The Rodrigues formula leads to the explicit formula for the coefficients in Eq. (7.18).

$$P_n^{(\alpha,\beta)}(x) = \sum_{k=0}^{n} \binom{n}{k} \frac{\Gamma(n+\alpha+1) + \Gamma(\beta+1)}{\Gamma(k+\beta+1) + \Gamma(n-k+\alpha+1)} x^k (x-1)^{n-k} \qquad (7.20)$$

where $\binom{n}{k}$ is the binomial coefficient, which is given by

$$_nC_k = \binom{n}{k} = \frac{n!}{(n-k)!k!} = \frac{\Gamma(n+1)}{\Gamma(n-k+1)\Gamma(k+1)}.$$

A simpler formula can be obtained by expanding the factor $x^k (x-1)^{n-k}$ in Eq. (7.20), which gives general form of γ_k in Eq. (7.18).[164]

$$\gamma_k = \binom{n}{n-k} \frac{\Gamma(n+k+\alpha+\beta+1)+\Gamma(\beta+1)}{\Gamma(n+\alpha+\beta+1)+\Gamma(k+\beta+1)} \tag{7.21}$$

with $\gamma_0 = 1$.

The application of Eq. (7.21) can be extended to the Legendre polynomials with $\alpha = \beta = 0$.[164]

$$\gamma_k = \binom{n}{n-k} \frac{\Gamma(n+k+1)}{\Gamma(n+1)+\Gamma(k+1)} \tag{7.22}$$

with $\gamma_0 = 1$.

7.3.3   Jacobi Polynomials in x^2

In many engineering problems, such as diffusion of heat or mass in catalyst pellets and flows in a cylindrical tube, the solution of ordinary differential equations is a symmetrical function of x, i.e., an even function of x. The construction of orthogonal polynomials as a function of x^2 permits faster convergence than a function defined in Eq. (7.18).[163, 164, 166] The Jacobi polynomials are defined by

$$\int_0^1 u^\beta (1-u)^\alpha P_n(u) P_m(u) du = c_n \delta_{nm} \tag{7.23}$$

Substituting $u = x^2$, $du = 2xdx$ gives

$$\int_0^1 \left(1-x^2\right)^\alpha x^{2\beta+1} P_n\left(x^2\right) P_m\left(x^2\right) dx = \frac{c_n}{2}\delta_{nm} \tag{7.24}$$

The orthogonal polynomial sets with $\alpha = 1$, and $2\beta + 1 = 0$, 1, and 2 were dealt with by

Villadsen and Stewart.[161] According to these authors, a more general formula yields

$$\int_0^1 \left(1-x^2\right) P_n\left(x^2\right) P_m\left(x^2\right) x^{a-1} dx = c_n^* \delta_{nm} \tag{7.25}$$

where $x^{a-1}dx$ can be replaced by the volume element dV. For slabs, cylinders, and

spheres geometry, a = 1, 2, and 3, respectively. For sphere geometry the formula for γ_k

is obtained by substituting α and β into 1 and 1/2 in Eq. (7.21).[164]

$$\gamma_k = \left(\frac{n}{n-k}\right)\frac{\Gamma\left(n+k+5/2\right)\Gamma\left(3/2\right)}{\Gamma\left(n+5/2\right)\Gamma\left(k+3/2\right)} \tag{7.26}$$

7.3.4 Solution Procedure of a Two-Point Boundary Value Problem of ODE Using the Orthogonal Collocation Method

Consider the following differential equation:

$$\frac{d^{(n)}y}{dx^{(n)}} = f\left(x,y\right) \tag{7.27}$$

Suppose that the solution of differential equation can be approximated in the form of a

Jacobi polynomial in x^2, as described in section 7.3.3.[161, 163]

$$y\left(x^2\right) = y\left(1\right) + \left(1-x^2\right)\sum_{i=1}^{N} a_i P_{i-1}\left(x^2\right) \tag{7.28}$$

where $P_{i-1}(x^2)$ are polynomials of degree i-1 in x^2 and a_i are constants to be determined.

Eq. (7.28) satisfies the boundary conditions

$$y = y(1) \quad \text{at} \quad x^2 = 1$$

$$\frac{dy}{dx} = 0 \quad \text{at} \quad x = 0$$

The orthogonal polynomials are defined by

$$\int_0^1 (1-x^2) P_n(x^2) P_m(x^2) x^{a-1} dx = c_n \delta_{nm} \tag{7.29}$$

where a = 1, 2, and 3 for planar, cylindrical, and spherical geometries, respectively. The gradient and Laplacian operators for the function $y(x^2)$ of Eq. (7.28) are expressed at the collocation points:[161]

$$x^{a-1} \frac{dy}{dx}\bigg|_{x=x_j} = \sum_{j=1}^{n+1} A_{ij} y(x_j) \tag{7.30}$$

$$x^{1-a} \frac{d}{dx}\left(x^{a-1} \frac{dy}{dx}\right)\bigg|_{x=x_j} = \sum_{j=1}^{n+1} B_{ij} y(x_j) \tag{7.31}$$

for i = 1, 2, …, n+1. The coefficients A_{ij} and B_{ij} can be calculated using the equations given by Villadsen and Stewart.[161] The ordinary differential equations can be transformed into a set of simultaneous algebraic equations, Eqs. (7.30) and (7.31), whose solutions can be obtained numerically.

7.4   Continuity, Energy, and Momentum Equations on the Reactor Scale

The steady state continuity equations for the reacting species along the reactor (or space time) are given by

$$\frac{dX_{EB}}{d\left(W/F_{EB}^0\right)} = \eta_1 r_{c1} + \eta_2 r_{c2} + \eta_3 r_{c3} + \left(r_{t1} + r_{t2} + r_{t3}\right)\frac{\varepsilon_B}{\rho_B}$$

$$\frac{dX_{ST}}{d\left(W/F_{EB}^0\right)} = \eta_1 r_{c1} - \eta_4 r_{c4} + r_{t1}\frac{\varepsilon_B}{\rho_B}$$

$$\frac{dX_{BZ}}{d\left(W/F_{EB}^0\right)} = \eta_2 r_{c2} + r_{t2}\frac{\varepsilon_B}{\rho_B} \tag{7.32}$$

$$\frac{dX_{H_2}}{d\left(W/F_{EB}^0\right)} = \eta_1 r_{c1} - \eta_3 r_{c3} - 2\eta_4 r_{c4} + \left(r_{t1} - r_{t2}\right)\frac{\varepsilon_B}{\rho_B}$$

where η_i is the effectiveness factor of a reference component in the reaction i. The effectiveness factor is calculated from:[160]

$$\eta_i = \frac{\int_0^V r_{ci}\left(P_{s,j}\right)\rho_s dV}{r_{ci}\left(P_j\right)\rho_s V} \tag{7.33}$$

where r_{ci} is the rate of catalytic reaction i in kmol/(kgcat·hr), $P_{s,j}$ is the partial pressure of component j in the catalyst in bar, P_j is the partial pressure of j in the bulk fluid in bar, ρ_s is the catalyst pellet density in kgcat/m_p^3, V is the catalyst pellet volume in m_p^3. Accounting for the thermal reactions in the void space inside the porous catalyst, the effectiveness factor can be calculated from:

$$\eta_i = \frac{\int_0^V \left[r_{ci}\left(P_{s,j}\right)\rho_s + r_{ti}\left(P_{s,j}\right)\varepsilon_s\right] dV}{\left[r_{ci}\left(P_j\right)\rho_s + r_{ti}\left(P_j\right)\varepsilon_s\right] V} \tag{7.34}$$

where r_{ti} is the rate of thermal reaction i in kmol/($m_f^3 \cdot$hr) and ε_s is the catalyst internal

void fraction in m_f^3/m_p^3.

The energy equation is written

$$\sum_{j=1}^{6} \dot{m}_j c_{pj} \frac{dT}{d\left(W/F_{EB}^0\right)} = F_{EB}^0 \left[-\Delta H_{r1}\left(\eta_1 r_{c1} + r_{t1}\frac{\varepsilon_B}{\rho_B} \right) - \Delta H_{r2}\left(\eta_2 r_{c2} + r_{t2}\frac{\varepsilon_B}{\rho_B} \right) \right.$$
$$\left. -\Delta H_{r3}\left(\eta_3 r_{c3} + r_{t3}\frac{\varepsilon_B}{\rho_B} \right) - \Delta H_{r4}\eta_4 r_{c4} \right]$$

(7.35)

The momentum equation is

$$-\frac{dP_t}{d\left(W/F_{EB}^o\right)} = f\alpha \frac{u_s GF_{EB}^o}{\rho_B d_p \Omega}$$

(7.36)

The friction factor, f, is calculated using the Ergun relation:

$$f = \frac{1-\varepsilon_B}{\varepsilon_B^3}\left[a + \frac{b\left(1-\varepsilon_B\right)}{\text{Re}} \right]$$

(7.37)

For cylindrical packings the coefficients a and b are 1.28 and 458, respectively, which

are dependent on the particle size of packing.[126] The pressure drops between the beds are

neglected.

7.5   Continuity Equations for the Componets inside a Porous Catalyst

7.5.1   Formulaton of Continuity Equations for the Components in a Porous

      Catalyst

      The continuity equations for ethylbenzene inside the porous catalyst are derived

under the following assumptions.[139]

1. Interparticle diffusion resistance is negligible.

2. The catalyst pellet is isothermal.

3. Diffusion of a species in a pellet obeys Fick's first law and the effective diffusivities

are invariant inside the particle.

4. The total pressure in the catalyst is uniform.

5. Steady-state condition holds.

The molar balance equation for ethylbenzene on a spherical shell of thickness Δr is:

$$-N_{EB}\big|_{r+\Delta r} \cdot 4\pi\left(r+\Delta r\right)^2 - \left(-N_{EB}\big|_r \cdot 4\pi r^2\right) = r_{EB} \cdot 4\pi r^2 \cdot \Delta r \cdot \rho_s \qquad (7.38)$$

where N_{EB} is the molar flux in $\text{kmol}/\left(\text{m}^2 \text{ hr}\right)$, r_{EB} is the rate of disappearance of EB in

$\text{kmol}/\left(\text{kg}_{\text{cat}} \text{ hr}\right)$, ρ_s is the catalyst density in $\text{kgcat/m}_\text{p}^3$. Ethylbenzene diffuses through

the shell thickness to the center of the sphere. ($r_{EB} \cdot 4\pi r^2 \cdot \Delta r \cdot \rho_s$) gives the number of

moles of EB per unit time being consumed by dehydrogenation.

Dividing by $4\pi \cdot r^2 \cdot \Delta r$ and taking $\Delta r \to 0$,

$$-\frac{1}{r^2}\frac{d}{dr}\left(r^2 N_{EB}\right) = r_{EB} \cdot \rho_s \qquad (7.39)$$

The effective diffusivity for ethylbenzene can be defined in a porous solid by

$$N_{EB} = -D_{e,EB} \frac{dC_{EB}}{dr} \qquad (7.40)$$

Substitution of Eq. (7.40) into Eq. (7.39) yields

$$\frac{1}{r^2} \frac{d}{dr}\left(r^2 D_{e,EB} \frac{dC_{EB}}{dr}\right) = r_{EB} \cdot \rho_s \qquad (7.41)$$

Applying the ideal gas law to express C_{EB} in terms of P_{EB} gives

$$\frac{1}{r^2} \frac{d}{dr}\left(r^2 \frac{dP_{EB}}{dr}\right) = \frac{\rho_s R_g T}{D_{e,EB}} r_{EB} \qquad (7.42)$$

Styrene diffuses through a spherical shell to the surface of the porous catalyst. The molar balance equation for styrene on a spherical shell of thickness Δr gives the following differential equations.

$$\frac{1}{r^2} \frac{d}{dr}\left(r^2 N_{ST}\right) = r_{ST} \cdot \rho_s \qquad (7.43)$$

Further manipulation leads to the formula:

$$\frac{1}{r^2} \frac{d}{dr}\left(r^2 \frac{dP_{ST}}{dr}\right) = -\frac{\rho_s R_g T}{D_{e,ST}} r_{ST} \qquad (7.44)$$

The complete set of continuity equations for the components in the porous catalyst in terms of partial pressure of component j inside the catalyst, $P_{s,j}$, gives

$$\frac{1}{r^2}\frac{d}{dr}\left(r^2\frac{dP_{s,EB}}{dr}\right)=\frac{\rho_s R_g T}{D_{e,EB}}\left(r_{c1}+r_{c2}+r_{c3}\right)$$

$$\frac{1}{r^2}\frac{d}{dr}\left(r^2\frac{dP_{s,ST}}{dr}\right)=-\frac{\rho_s R_g T}{D_{e,ST}}\left(r_{c1}-r_{c4}\right)$$

$$\frac{1}{r^2}\frac{d}{dr}\left(r^2\frac{dP_{s,BZ}}{dr}\right)=-\frac{\rho_s R_g T}{D_{e,BZ}}r_{c2}$$

(7.45)

$$\frac{1}{r^2}\frac{d}{dr}\left(r^2\frac{dP_{s,H_2}}{dr}\right)=-\frac{\rho_s R_g T}{D_{e,H_2}}\left(r_{c1}-r_{c3}-2r_{c4}\right)$$

Also accounting for the thermal reactions taking place in the void space inside the catalyst particle, Eq.(7.45) becomes

$$\frac{1}{r^2}\frac{d}{dr}\left(r^2\frac{dP_{s,EB}}{dr}\right)=\frac{R_g T}{D_{e,EB}}\left[\rho_s\left(r_{c1}+r_{c2}+r_{c3}\right)+\varepsilon_s\left(r_{t1}+r_{t2}+r_{t3}\right)\right]$$

$$\frac{1}{r^2}\frac{d}{dr}\left(r^2\frac{dP_{s,ST}}{dr}\right)=-\frac{R_g T}{D_{e,ST}}\left[\rho_s\left(r_{c1}-r_{c4}\right)+\varepsilon_s r_{c1}\right]$$

(7.46)

$$\frac{1}{r^2}\frac{d}{dr}\left(r^2\frac{dP_{s,BZ}}{dr}\right)=-\frac{R_g T}{D_{e,BZ}}\left(\rho_s r_{c2}+\varepsilon_s r_{t2}\right)$$

$$\frac{1}{r^2}\frac{d}{dr}\left(r^2\frac{dP_{s,H_2}}{dr}\right)=-\frac{R_g T}{D_{e,H_2}}\left[\rho_s\left(r_{c1}-r_{c3}-2r_{c4}\right)+\varepsilon_s\left(r_{t1}-r_{t3}\right)\right]$$

7.5.2   **Transformation of Continuity Equations for the Components inside a**

         Porous Catalyst into the Dimensionless Form

The continuity equations, Eq. (7.45), are transformed into the dimensionless form

using the following dimensionless variables:

$$\xi = \frac{r}{d_p/2}$$

$$P_j^* = \frac{P_{s,j}}{P_j}$$

(7.47)

where d_p is the equivalent particle diameter in m_p and P_j is the partial pressure of

component j on the *surface* of the porous catalyst. P_j is also the partial pressure of

component j in the *bulk condition* because the interparticle diffusion resistance is

assumed to be negligible. The dimensionless continuity equations for the components

can be written as follows:

$$\frac{1}{\xi^2}\frac{d}{d\xi}\left(\xi^2 \frac{dP_{EB}^*}{d\xi}\right) = \frac{d_p^2}{4}\frac{\rho_s}{D_{e,EB}}\frac{R_g T}{P_{EB}}(r_{c1} + r_{c2} + r_{c3})$$

$$\frac{1}{\xi^2}\frac{d}{d\xi}\left(\xi^2 \frac{dP_{ST}^*}{d\xi}\right) = -\frac{d_p^2}{4}\frac{\rho_s}{D_{e,ST}}\frac{R_g T}{P_{ST}}(r_{c1} - r_{c4})$$

(7.48)

$$\frac{1}{\xi^2}\frac{d}{d\xi}\left(\xi^2 \frac{dP_{BZ}^*}{d\xi}\right) = -\frac{d_p^2}{4}\frac{\rho_s}{D_{e,BZ}}\frac{R_g T}{P_{BZ}}r_{c2}$$

$$\frac{1}{\xi^2}\frac{d}{d\xi}\left(\xi^2 \frac{dP_{H_2}^*}{d\xi}\right) = -\frac{d_p^2}{4}\frac{\rho_s}{D_{e,H_2}}\frac{R_g T}{P_{H_2}}(r_{c1} - r_{c3} - 2r_{c4})$$

with boundary conditions

$$\text{at } \xi = 1, \ P_i^* = 1$$

$$\text{at } \xi = 0, \ \frac{dP_i^*}{d\xi} = 0$$

Accounting for the thermal reactions taking place in the void space inside the catalyst particle Eq.(7.46) can be transformed into

$$\frac{1}{\xi^2}\frac{d}{d\xi}\left(\xi^2 \frac{dP_{EB}^*}{d\xi}\right) = \frac{d_p^2}{4}\frac{1}{D_{e,EB}}\frac{R_g T}{P_{EB}}\left[\rho_s\left(r_{c1}+r_{c2}+r_{c3}\right)+\varepsilon_s\left(r_{t1}+r_{t2}+r_{t3}\right)\right]$$

$$\frac{1}{\xi^2}\frac{d}{d\xi}\left(\xi^2 \frac{dP_{ST}^*}{d\xi}\right) = -\frac{d_p^2}{4}\frac{1}{D_{e,ST}}\frac{R_g T}{P_{ST}}\left[\rho_s\left(r_{c1}-r_{c4}\right)r_{c1}+\varepsilon_s r_{c1}\right]$$

$$\frac{1}{\xi^2}\frac{d}{d\xi}\left(\xi^2 \frac{dP_{BZ}^*}{d\xi}\right) = -\frac{d_p^2}{4}\frac{1}{D_{e,BZ}}\frac{R_g T}{P_{BZ}}\left(\rho_s r_{c2}+\varepsilon_s r_{t2}\right)$$

(7.49)

$$\frac{1}{\xi^2}\frac{d}{d\xi}\left(\xi^2 \frac{dP_{H_2}^*}{d\xi}\right) = -\frac{d_p^2}{4}\frac{1}{D_{e,H_2}}\frac{R_g T}{P_{H_2}}\left[\rho_s\left(r_{c1}-r_{c3}-2r_{c4}\right)+\varepsilon_s\left(r_{t1}-r_{t3}\right)\right]$$

7.5.3 Transformation of Continuity Equations for the Components inside a Porous Catalyst into the Algebraic Equations

According to Eq. (7.31), the ordinary differential equations of Eq.(7.48) can be reduced to algebraic equations.

$$\sum_{i=1}^{N+1} B_{ji} P_{EB,i}^* - \beta_1 \left(r_{c1,j} + r_{c2,j} + r_{c3,j} \right) = 0 \qquad j = 1, 2, ..., N$$

$$\sum_{i=1}^{N+1} B_{ji} P_{ST,i}^* + \beta_2 \left(r_{c1,j} - r_{c4,j} \right) = 0 \qquad j = 1, 2, ..., N$$

$$\sum_{i=1}^{N+1} B_{ji} P_{BZ,i}^* + \beta_3 r_{c2,j} = 0 \qquad j = 1, 2, ..., N \tag{7.50}$$

$$\sum_{i=1}^{N+1} B_{ji} P_{H_2,i}^* + \beta_4 \left(r_{c1,j} - r_{c3,j} - 2r_{c4,j} \right) = 0 \qquad j = 1, 2, ..., N$$

where

$$\beta_1 = \frac{d_p^2}{4} \frac{R_g T \rho_s}{D_{e,EB} P_{EB}}$$

$$\beta_2 = \frac{d_p^2}{4} \frac{R_g T \rho_s}{D_{e,ST} P_{ST}}$$

$$\beta_3 = \frac{d_p^2}{4} \frac{R_g T \rho_s}{D_{e,BZ} P_{BZ}} \tag{7.51}$$

$$\beta_4 = \frac{d_p^2}{4} \frac{R_g T \rho_s}{D_{e,H_2} P_{H_2}}$$

The algebraic equations for Eq. (7.49) can be easily derived in the same manner. Eqs. (7.50) and (7.51) form a set of $4N$ algebraic equations, where N is number of interior collocation points. The effective diffusivity of each component in Eq. (7.51) is calculated using Eq. (7.14) without accounting for the Knudsen diffusivity. The diffusivity of component j in the mixture is calculated from the Wilke's equation of Eq.

(7.5). Wilke's equation works well if the diffusing components in a mixture are dilute.[139] The binary molecular diffusivity is calculated using Eq. (7.8).

7.6   Results and Discussion

The continuity-, energy-, and momentum equations, Eqs. (7.32), (7.35), and (7.36), are solved numerically using Gear's method. At each integration step along the reactor length the effectiveness factors for 4 reactions are calculated from the particle equations, Eqs. (7.50) and (7.51), which are solved using the orthogonal collocation method with 6 interior collocation points whose coefficients are obtained numerically from the Jacobian orthogonal polynomials. The feed conditions and reactor geometry are shown in Table 7.3, which is identical to that of the reactor simulation when using the pseudohomogeneous model.

The simulation results are shown in Table 7.3 and Figures 7.1 through 7.3. The profiles of ethylbenzene conversion and selectivity of styrene, benzene, and toluene are plotted against the space time in Figure 7.1. The ethylbenzene conversion and styrene selectivity at the exit of the reactor are 83.76% and 90.43%. Compared to the simulation results using the pseudohomogeneous model, the ethylbenzene conversion (86.82% in pseudohomogeneous model) and styrene selectivity (91.43% in pseudohomogeneous model) decreased. The decrease of ethylbenzene conversion can be explained that the effectiveness factors are lower than 1 as shown in Figure 7.2. At the entrance of a reactor, the temperature is high and the intrinsic reaction rate is very fast; accordingly, the effectiveness factors for reaction 1 and 2 (ethylbenzene dehydrogenation into styrene

and ethylbenzene conversion into benzene, respectively) are very small, which means that the process is diffusion controlled. These effectiveness factors increase along the bed length as the intrinsic reaction rates decrease. On the contrary, the effectiveness factor for reaction 4 (formation of toluene from styrene) is very high at the entrance because this is a consecutive reaction. The plots of temperature profiles and pressure drop profiles in the reactor are represented in Figure 7.3. The temperature variation in a reactor was smaller than that of the pseudohomogeneous model. The change of pressure drop between two models is negligible.

To ensure that 6 internal collocation points are sufficient for the accurate calculation of intraparticle profiles at the entrance of the reactor, where the intrinsic reaction rates are very high, simulation was performed with 9 collocation points. The ethylbenzene conversion and product selectivities at the end of each bed are found to be exactly the same for both cases. Table 7.4 compares the effectiveness factors at the entrance of the reactor between 6 internal collocation points and 9 internal collocation points. The difference of the effectiveness factors between both cases is negligible. Consequently, 6 internal collocation points are enough for solving the particle equations.

Table 7.3. Simulation result of a 3-bed adiabatic reactor for the feed ratio of H_2O/EB=11mol/mol when using the *heterogeneous model*

	BED1	BED2	BED3
Weight of catalyst, kg [*]	72 950	82 020	78 330
Space time [§]	103.18	219.19	329.98
X_{EB}, % [¶]	36.89	65.78	83.76
S_{ST}, % [¶]	98.49	95.10	90.43
S_{BZ}, %	1.000	1.423	1.754
S_{TO}, %	0.507	3.480	7.809
P_{in}, bar [*]	1.25	1.06	0.783
T_{in}, K [*]	886	898.2	897.6
T_{out}, K	811.36	845.71	873.6
Length of bed, m	1.33	1.50	1.43
Inner radius of reactor, m		3.50	
Feed molar flow rate, kmol/hr EB [*]		707	
ST		7.104	
BZ		0.293	
TO		4.968	
H_2O [†]		7 777	
Total feed molar flow rate, kmol/hr		8 496.37	

[§] Space time is cumulative and is in kgcat hr/kmol EB.
[¶] X_{EB} denotes the EB conversion and S_j denotes the selectivity of component *j*.
[*] The information was provided by personal communication with Froment.[130]
[†] The feed molar flow rate of H_2O was obtained from a molar ratio of H_2O/EB=11.

Figure 7.1. Comparison of simulated total ethylbenzene conversion profiles (a) and styrene selectivity profiles (b) in a 3-bed adiabatic reactor between the heterogeneous model and the pseudohomogeneous model for T_{in} = 886K, 898K, 897K; P_{in} = 1.25bar; H_2O/EB = 11 mol/mol; F_{EB}^o = 707 kmol/hr. Solid line: heterogeneous model; dashed line: pseudohomogeneous model.
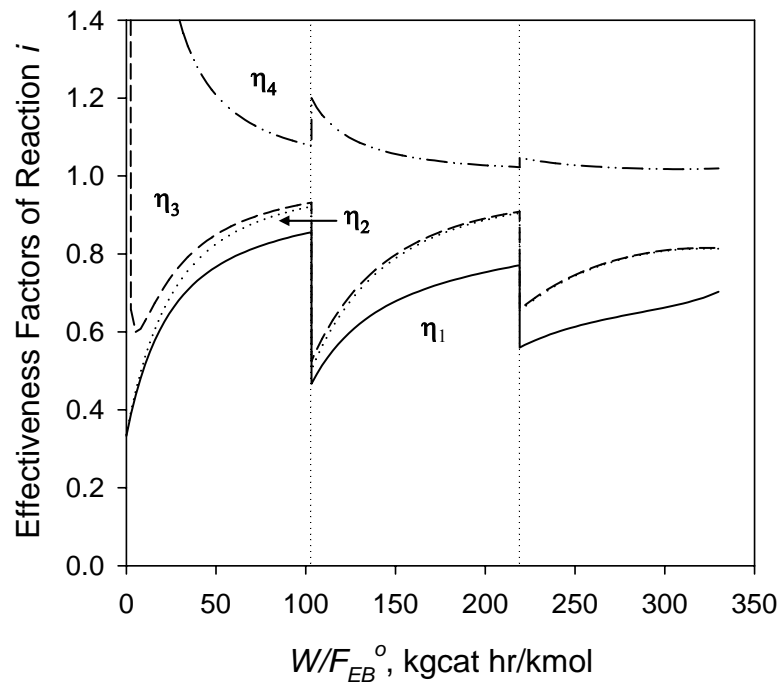
Figure 7.2. Evolution of effectiveness factors in a 3-bed adiabatic reactor for T_{in} = 886K, 898K, 897K; P_{in} = 1.25bar; H_2O/EB = 11 mol/mol; F_{EB}^o = 707 kmol/hr.
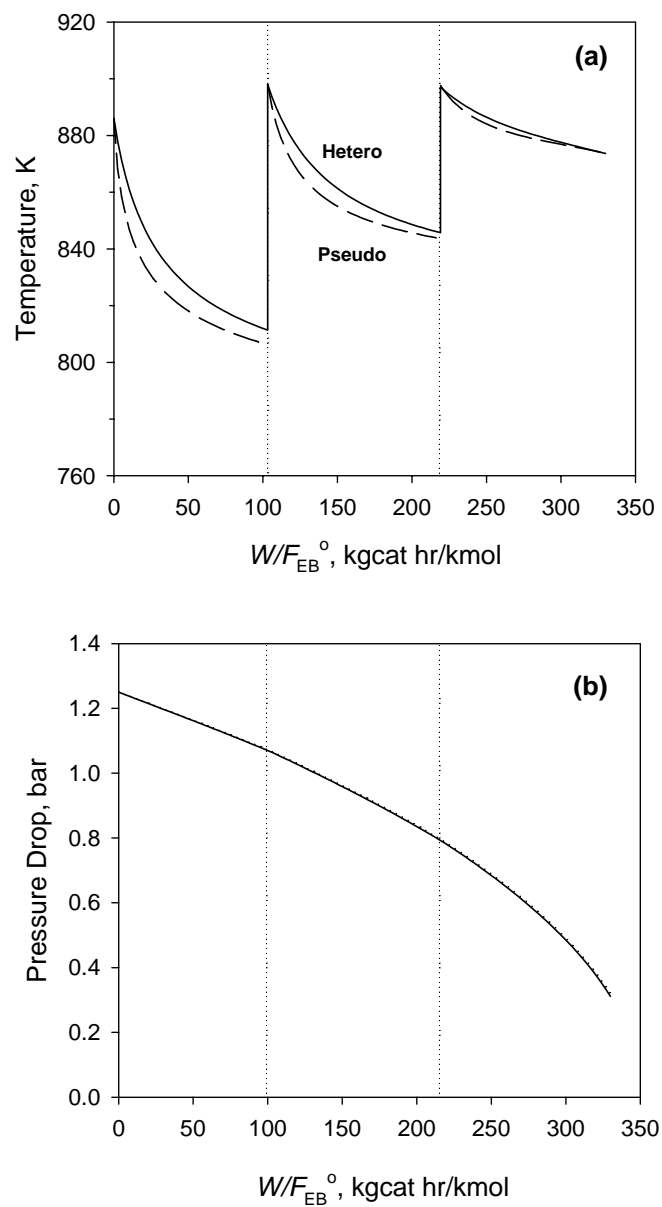
Figure 7.3. Comparison of simulated temperature profiles (a) and pressure drop profiles (b) in a 3-bed adiabatic reactor between the heterogeneous model and the pseudohomogeneous model for T_{in} = 886K, 898K, 897K; P_{in} = 1.25bar; H_2O/EB = 11 mol/mol; F_{EB}^o = 707 kmol/hr. Solid line: heterogeneous model; dashed line: pseudohomogeneous model.

Table 7.4. Effect of number of internal collocation points on effectiveness factors at the entrance of the reactor

Space time*	N = 6				N = 9			
	η_1	η_2	η_3	η_4	η_1	η_2	η_3	η_4
0.001	0.31614	0.31916	9.8993	770.00	0.31612	0.31914	9.8985	769.92
2.6466	0.34229	0.34692	0.84125	19.568	0.34228	0.34692	0.84113	19.566
5.2922	0.36674	0.37315	0.64879	8.6842	0.36674	0.37314	0.64868	8.6834
7.9378	0.38962	0.39792	0.59747	5.6469	0.38962	0.39792	0.59736	5.6463
10.583	0.41107	0.42135	0.58172	4.2873	0.41107	0.42136	0.58161	4.2868

* Space time is in kgcat hr/kmol EB.
The simulation conditions are the same as those in Table 7.3.

7.6.1 Effect of the Thermal Reactions in the Void Space inside the Catalyst

To account for the thermal reactions in the void space inside the catalyst, particle equations, Eq. (7.49), are solved with the reactor equations simultaneously. Eq. (7.34) is used to calculate the effectiveness factors. At the entrance of the reactor, the simulation result shows that effectiveness factors do not change much, except η_3 which shows a large difference between two cases (Table 7.5).

Table 7.5. Comparison of effectiveness factors at the entrance of the reactor without accounting for the thermal reactions and accounting for the thermal reactions

	w/o thermal reaction				w/thermal reaction			
Space time*	η_1	η_2	η_3	η_4	η_1	η_2	η_3	η_4
0.001	0.3161	0.3192	9.8993	770.00	0.3161	0.3210	3.7861	770.43
2.6466	0.3423	0.3469	0.8413	19.5680	0.3423	0.3487	0.8190	19.5630
5.2922	0.3667	0.3732	0.6488	8.6842	0.3668	0.3749	0.6487	8.6829
7.9378	0.3896	0.3979	0.5975	5.6469	0.3896	0.3996	0.6014	5.6464
10.583	0.4111	0.4214	0.5817	4.2873	0.4111	0.4230	0.5871	4.2870

* Space time is in kgcat hr/kmol.
The simulation conditions are the same as those in Table 7.3.

7.6.2 Effect of Feed Temperature

Figure 7.4 shows the effect of feed temperature to each bed on the ethylbenzene conversion and the styrene selectivity. The *reference* feed temperatures, 886 K, 898 K, and 897 K to bed1, bed2, and bed3, respectively, are denoted by '2' in the figure. Case 1 indicates feed temperatures 10 K higher than the reference. Case 3 indicates feed temperatures 10 K lower than the reference. As the feed temperatures increase, the ethylbenzene conversions increase and the styrene selectivities decrease. The reduction of styrene selectivities at higher temperatures results from the enhanced side reactions which form benzene and toluene. The styrene yields, which are not shown in Figure 7.4, at each feed temperature are: case 1, 75.48%; case 2, 75.75%; case 3, 73.24%. Case 2

yields the highest styrene throughput among these three cases. The styrene selectivity is also an important factor to determine the plant economics.

7.6.3 Effect of Feed Molar Ratios of H_2O/EB

Figure 7.5 shows the influence of feed molar ratios of H_2O/EB on the ethylbenzene conversions and styrene selectivity. The higher feed molar ratios of H_2O/EB give higher ethylbenzene conversion and styrene selectivity. Since ethylbenzene dehydrogenation into styrene is a reversible reaction with increasing number of moles, higher feed molar ratios of H_2O/EB promote the formation of styrene. Furthermore, the formation of styrene is kinetically enhanced at higher feed molar ratios of H_2O/EB because the lower partial pressures make the denominator of the rate equation for ethylbenzene dehydrogenation into styrene smaller and leads to higher rate of styrene formation.

$$r_{c1} = \frac{k_1 K_{EB} \left(P_{EB} - P_{ST} P_{H_2}/K_{eq} \right)}{\left(1 + K_{EB} P_{EB} + K_{EB} P_{EB} + K_{EB} P_{EB} \right)^2}$$

Less use of steam is preferred in terms of plant economics because the cost required to produce steam is decreased. However, there is a H_2O/EB ratio below which dynamic equilibrium coke content substantially increases and eventually the catalyst is deactivated.[52] Since steam continuously removes the coke deposits on the catalyst surface by gasification reactions which produce CO and CO_2, a steady-state coke content (3-6 wt.%) is obtained, which permits continuous operation for 1 or 2 years under typical
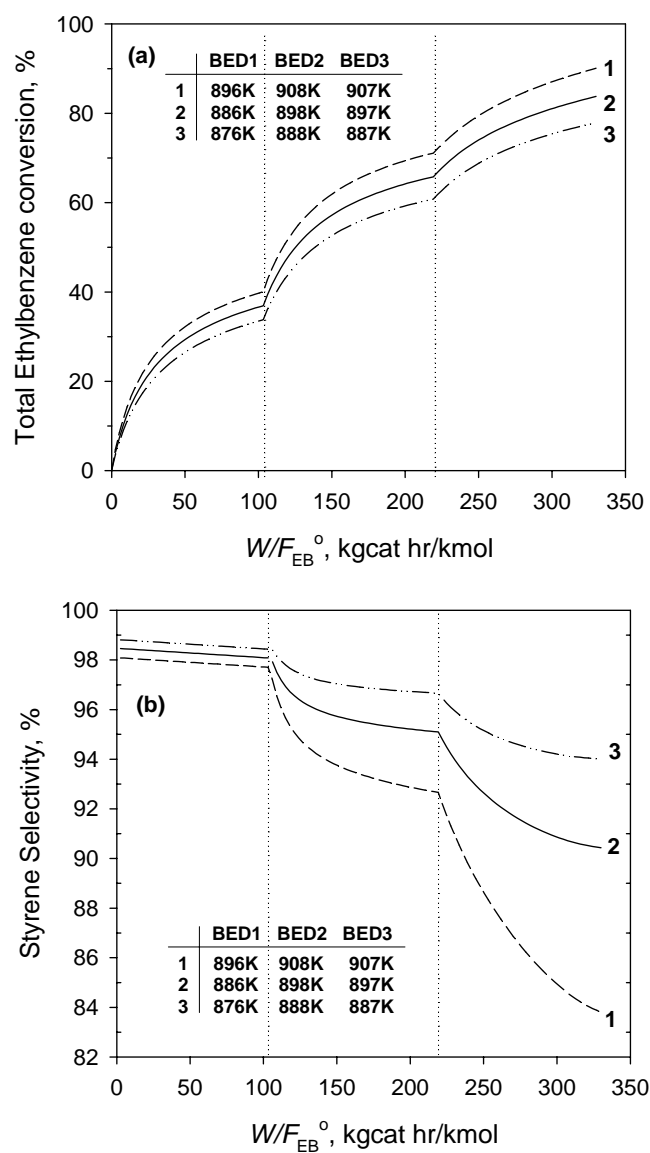
Figure 7.4. Effect of feed temperatures to each bed on ethylbenzene conversion (a) and styrene selectivity (b) in a 3-bed adiabatic reactor using the heterogeneous model for P_{in} = 1.25bar; H_2O/EB = 11 mol/mol; F_{EB}^o = 707 kmol/hr.
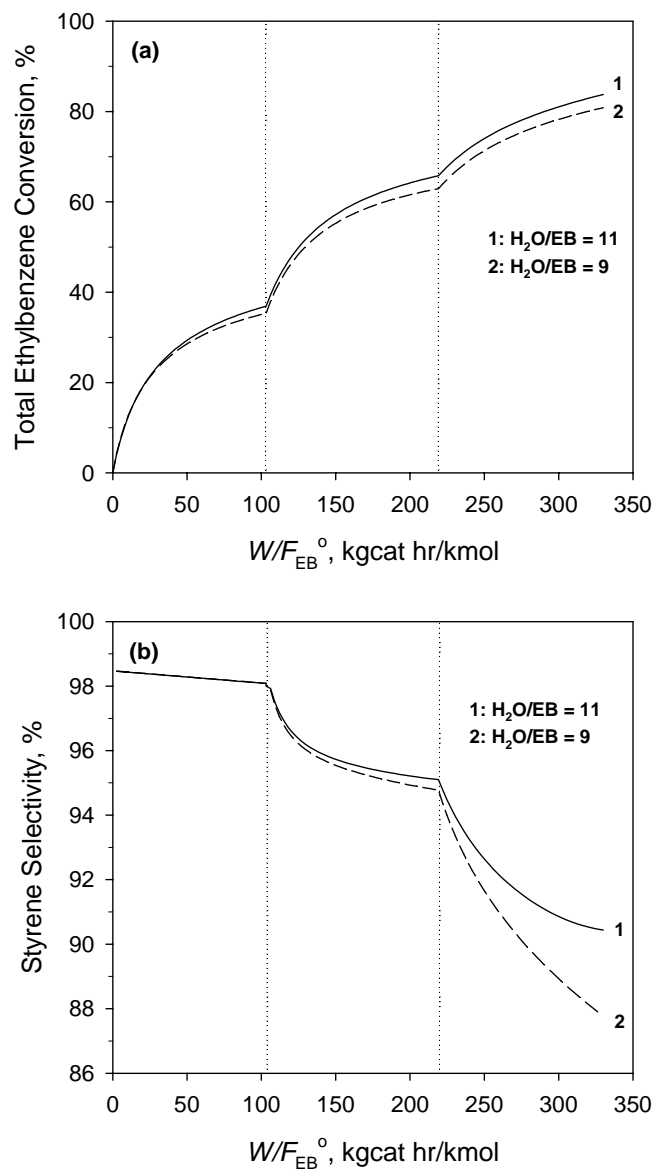
Figure 7.5. Effect of feed molar ratios of H_2O/EB on the ethylbenzene conversion (a) and styrene selectivity (b) in a 3-bed adiabatic reactor using the heterogeneous model for T_{in} = 886K, 898K, 897K; P_{in} = 1.25bar; F_{EB}^o = 707 kmol/hr.

operating conditions with a single catalyst charge.[11, 170] The effect of coke formation and gasification on the reactor performance will be discussed in the next chapter.

7.6.4   Effect of Feed Pressure

Figure 7.6 shows the effect of feed pressure on the ethylbenzene conversion and styrene selectivity. The feed pressure refers to the inlet pressure to the first bed. As the feed pressures decrease, both the ethylbenzene conversions and styrene selectivities increase. The decrease of feed pressure has little influence on the ethylbenzene conversions. However, its effect on the styrene selectivity is quite prominent. The increase of feed pressure from 1.25 bar to 1.40 bar leads to the decrease of styrene selectivity from 90.44% to 87.02%. The feed pressure much lower than 1.25 bar, such as 1 bar, is not allowed in this simulation because of the large pressure drop in a reactor. Since the pressure drop is lower in a radial flow reactor, it enables the use of lower feed pressure than the axial flow reactor. The new generation of ethylbenzene dehydrogenation reactors operates with radial flow and below atmospheric pressure. In chapter IX, we will discuss the effect of operating conditions on the radial flow reactor.

Before this chapter is closed, it may be interesting to simulate the axial flow reactor at isobaric condition, which means that no pressure drop occurs in the reactor. This condition is very close to that of radial flow reactor. Two different pressures are considered: 0.70bar and 1.25bar. As shown in Figure 7.7, when the total pressure decreases from 1.25bar to 0.70bar, the styrene selectivity increases from 82.18% to

90.13%. The total ethylbenzene conversion also increases from 81.09% to 82.18%. One

can conclude that the low feed pressure will be preferred in a radial flow reactor.
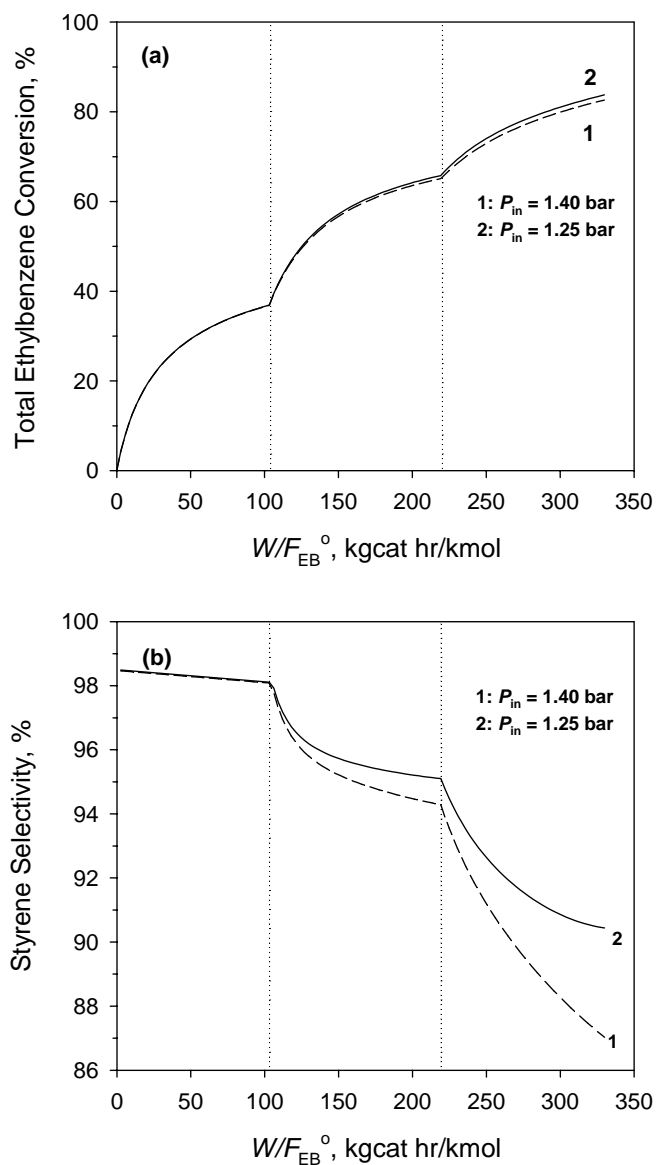
Figure 7.6. Effect of feed pressure on the total ethylbenzene conversion (a) and styrene selectivity (b) in a 3-bed adiabatic reactor using the heterogeneous model for $T_{in} = 886K$, 898K, 897K; $H_2O/EB = 11$ mol/mol; $F_{EB}^o = 707$ kmol/hr.
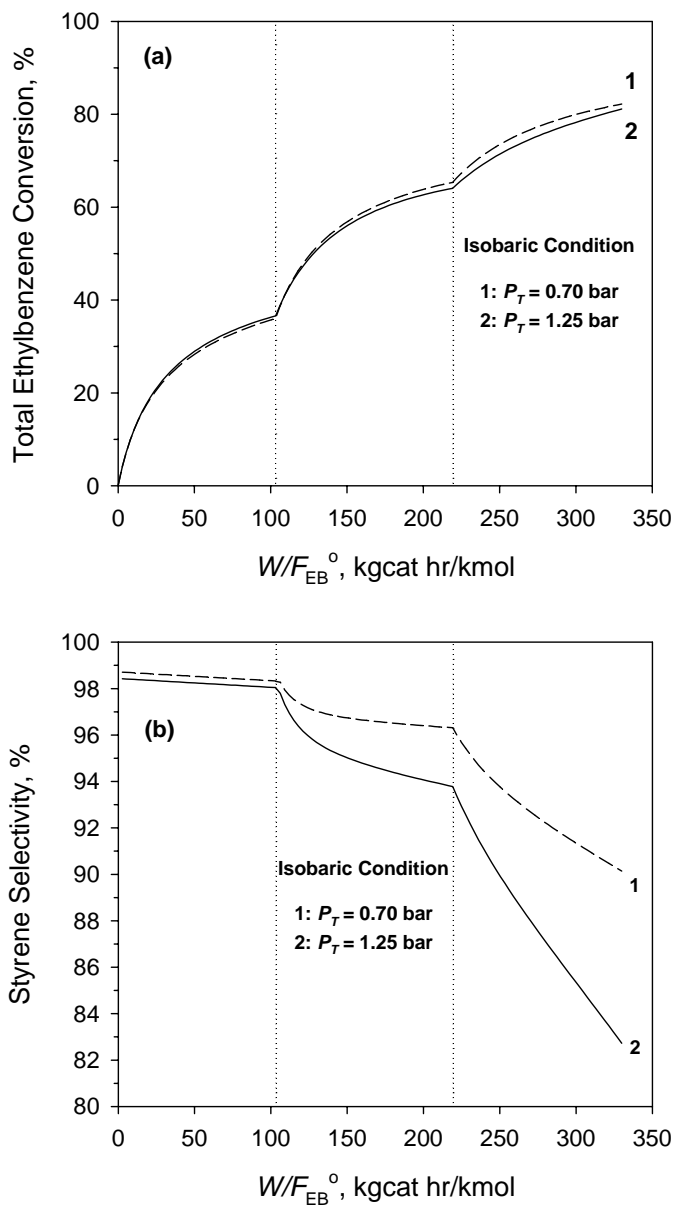
Figure 7.7. Effect of total pressure on the total ethylbenzene conversion (a) and styrene selectivity (b) in a 3-bed adiabatic reactor using heterogeneous model at isobaric condition (no pressure drop) in a reactor for T_{in} = 886K, 898K, 897K; H_2O/EB = 11 mol/mol; F_{EB}^o = 707 kmol/hr.

CHAPTER VIII

SIMULATION OF FIXED BED ADIABATIC REACTOR

WITH AXIAL FLOW: COKE FORMATION AND GASIFICATION

8.1   Introduction

Coke formation is frequently encountered in the hydrocarbon processing at medium or high (above 400°C) temperatures.[171] The coke formed on the potassium-promoted iron oxide catalysts during ethylbenzene dehydrogenation is continuously gasified by steam which is present in excess in the reaction mixture.[3] The kinetic models for the reactor simulation and process optimization have ignored the mechanistic approach to model the coke formation and coke gasification until Devoldere and Froment[52] first developed a detailed kinetic model for the coke formation and gasification during ethylbenzene dehydrogenation. The model for the coke formation is based on a two step mechanism: coke precursor formation and coke growth.[59] The gasification reaction occurs at the edges of the carbon, which is oxidized by the water.[172] The "dynamic equilibrium coke content" is attained when the net rates of coke precursor formation and coke growth are zero. In this chapter we will discuss how the catalyst coke content is affected by the operating conditions during coke formation and gasification and how the dynamic equilibrium coke content varies with the feed conditions along the 3-bed adiabatic reactor.

8.2 Formulation of Model Equations

8.2.1 Rate Equation for the Coke Precursor Formation

Let the coke precursor be formed by a parallel reaction to the main reaction (coke precursor formation from the adsorbed ethylbenzene) and also by a consecutive reaction (coke precursor formation from adsorbed styrene).[53] The adsorbed ethylbenzene and styrene intermediates are assumed to be in equilibrium with the corresponding gas phase species. The formation of irreversibly adsorbed coke precursor from adsorbed ethylbenzene and styrene on the n_s sites is assumed to be the rate-determining step.[173] The following mechanism for the coke precursor formation was proposed by Devoldere and Froment.[52]

$$EB + l \underset{k_{-EB}}{\overset{k_{EB}}{\rightleftharpoons}} EB\text{-}l \qquad with\ C_{EBl} = K_{EB}P_{EB}C_l \tag{8.1}$$

$$ST + l \underset{k_{-ST}}{\overset{k_{ST}}{\rightleftharpoons}} ST\text{-}l \qquad with\ C_{STl} = K_{ST}P_{ST}C_l \tag{8.2}$$

$$EB\text{-}l + (n_s\text{-}1)l \overset{k'_{EB,p}}{\rightarrow} C\text{-}l + (n_s\text{-}1)l \tag{8.3}$$

$$ST\text{-}l + (n_s\text{-}1)l \overset{k'_{ST,p}}{\rightarrow} C\text{-}l + (n_s\text{-}1)l \tag{8.4}$$

$$C\text{-}l \underset{k_{-Cl}}{\overset{k_{Cl}}{\rightleftharpoons}} C + l \tag{8.5}$$
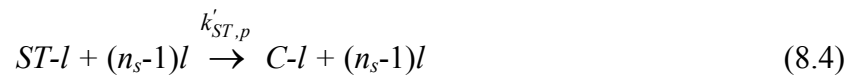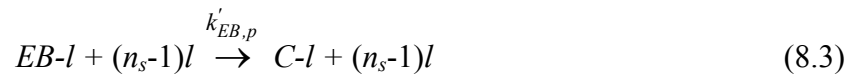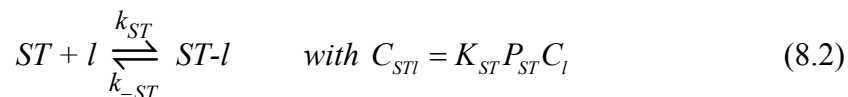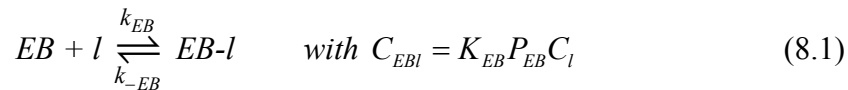
where *EB-l* is the adsorbed ethylbenzene on the surface, *ST-l* is the adsorbed styrene on the surface, *C-l* is the irreversibly adsorbed coke precursor, and n_s is the number of

active sites deactivated by the coke precursor formation. The rate of coke precursor formation is then given by

$$\frac{dC_{C_p}}{dt} = k'_{EB,p} C_{EBl} C_l^{n_s-1} + k'_{ST,p} C_{STl} C_l^{n_s-1} \tag{8.6}$$

Introducing the adsorption equilibrium constants of Eqs. (8.1) and (8.2) leads to

$$\frac{dC_{C_p}}{dt} = k'_{EB,p} K_{EB} P_{EB} C_l^{n_s} + k'_{ST,p} K_{ST} P_{ST} C_l^{n_s} \tag{8.7}$$

The total number of sites on the catalyst is given by

$$C_t = C_l + C_{Cl} + C_{EBl} + C_{STl} \tag{8.8}$$

Since C_{EBl} and C_{STl} are not accessible, they may be eliminated by using Eqs. (8.1) and (8.2).

$$C_t = C_{Cl} + C_l + K_{EB} P_{EB} C_l + K_{ST} P_{ST} C_l$$

$$= C_{Cl} + C_l \left(1 + K_{EB} P_{EB} + K_{ST} P_{ST}\right) \tag{8.9}$$

The coke precursor is not a measurable variable because it is strongly adsorbed on the surface.[173] Therefore, to eliminate C_l substitution of Eq.(8.9) into Eq.(8.7) leads to

$$r_s = \frac{dC_{C_p}}{dt} = \delta r_s^0 \Phi_{C_p} = \delta \frac{k_{EB,p} K_{EB} P_{EB} + k_{ST,p} K_{ST} P_{ST}}{\left(1 + K_{EB} P_{EB} + K_{ST} P_{ST}\right)^{n_s}} \Phi_{C_p} \tag{8.10}$$

where C_{cp} is the coke precursor content in kgcoke/kgcat, r_s is the rate of site coverage in kgcoke/(kgcat·hr), r_s^0 is the initial rate of site coverage in kgcoke/(kgmol·hr), δ is the

conversion factor in kmol/kgcat, $\Phi_{C_p} = \left(\dfrac{C_t - C_{Cl}}{C_t} \right)^{n_s} = \left(1 - \alpha_p C_p \right)^{n_s}$, $k_{EB,p} = C_t^{n_s} k_{EB,p}'$,

$k_{ST,p} = C_t^{n_s} k_{ST,p}'$, and Φ_{C_p} is the deactivation function for the site coverage. The value is

between 0 and 1.[53, 174] The values of n_s, α_p, $k_{EB,p}$, and $k_{ST,p}$ were estimated by Devoldere

and Froment.[52, 130]

8.2.2   Rate Equation for the Coke Growth

Further dehydrogenation of coke precursor yields the formation of the sites

active for the coke growth. The coke builds up on the active site. Devoldere and

Froment[52] expressed the intrinsic rate of coke growth as the product of three parts: the

intrinsic rate of coke growth for an active center; the total number of active sites on the

growing coke; and a deactivation function for coke growth.

$$r_{gr} = r_{gr}^0 C_{tgr} \Phi_{gr} \tag{8.11}$$

where r_{gr} is the rate of coke growth in kgcoke/(kgcat·hr), r_{gr}^0 is the initial rate of coke

growth per active center in kgcoke/(kgmol·hr), C_{tgr} is the total number of active sites for

gasification in kmol/kgcat, and Φ_{gr} is the deactivation function for the coke growth.

The model for the coke growth derived by Devoldere and Froment is

$$r_{gr} = \frac{dC_{gr}}{dt} = \frac{k_{EB,gr} P_{EB}^{n_{EB}} + k_{ST,gr} P_{ST}^{n_{ST}}}{\left(1 + K_{H_2O} P_{H_2O}/P_{H_2} + K_{H_2} \sqrt{P_{H_2}} \right)^{n_3}} \frac{C_c^{n_1}}{P_{H_2}^{n_2}} \left(1 - \alpha_{gr} C_{gr} \right)^{n_{gr}} \tag{8.12}$$

The values of n_{EB}, n_{ST}, n_1, n_2, n_3, n_{gr}, α_{gr}, $k_{EB,gr}$, and $k_{ST,gr}$ were estimated by Devoldere and Froment.[52, 130] From Eqs. (8.10) and (8.12), the intrinsic rate of coke formation which accounts for the coke precursor formation and coke growth is expressed as follows:

$$r_C = \delta r_s^o \Phi_{C_P} + r_{gr}^o C_{tgr} \Phi_{Cgr}$$

$$= \delta \frac{k_{EB,p} K_{EB} P_{EB} + k_{ST,p} K_{ST} P_{ST}}{\left(1 + K_{EB} P_{EB} + K_{ST} P_{ST}\right)^{n_s}} \left(1 - \alpha_s C_p\right)^{n_s}$$

$$+ \frac{k_{EB,gr} P_{EB}^{n_{EB}} + k_{ST,gr} P_{ST}^{n_{ST}}}{\left(1 + K_{H_2O} P_{H_2O}/P_{H_2} + K_{H_2} \sqrt{P_{H_2}}\right)^{n_3}} \frac{C_c^{n_1}}{P_{H_2}^{n_2}} \left(1 - \alpha_{gr} C_{gr}\right)^{n_{gr}}$$

(8.13)

8.2.3   Rate Equation for the Gasification

Devoldere and Froment[52] observed from the coke gasification experiments using the electrobalance that the rate of coke gasification increases with increasing steam partial pressures and temperature, but that it decreases with increasing hydrogen partial pressure. The four rival models for coke gasification were discriminated based on the F test.[52] The model which showed the best agreement with experimental data was derived with applying the following mechanism: a carbon atom with a free site (C_f) reacts with water to form oxidized surface complex, and this step is assumed to be in equilibrium.[175] Gas phase CO is then released and the oxidized surface complex is regenerated to a free site.[175, 176] The competitive dissociative adsorption of hydrogen on a carbon atom should be taken into account as well.[176]

$$H_2O + C_f \underset{k_{-1}}{\overset{k_1}{\rightleftharpoons}} C_f(O) + H_2$$

$$C_f(O) \overset{k_2}{\rightarrow} CO + C_f$$

$$1/2\ H_2 + C_f \underset{k_{-3}}{\overset{k_3}{\rightleftharpoons}} C_f(H)$$
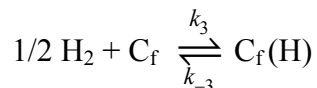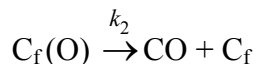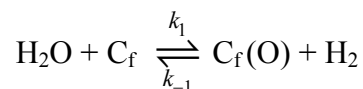
The model was developed assuming that the irreversible reaction is the rate-determining step. The application of pseudo-steady-state approximation for all the surface intermediates yields

$$r_G = \frac{k_2 P_{H_2O}}{\left(1 + K_3\sqrt{P_{H_2}}\right)\left(P_{H_2}/K_1 + k_2/k_1\right) + P_{H_2O}} C_{tG} \qquad (8.14)$$

where r_G is the rate of gasification in kgcoke/(kgcat·hr) and C_{tG} is the number of active sites for the gasification in kmol/kgcoke.

8.2.4   Coke Formation and Gasification: Dynamic Equilibrium Coke Content

The coke content of the catalyst reaches a certain value corresponding to an equilibrium between coke formation and coke gasification. The conversions of the main reactions decrease until the coke content reaches a stabilized state. The stabilization process is very fast. Once it is reached, the coke content, which is called the dynamic equilibrium coke content and depends only on the temperature and the compositions, does not change any more and no deactivation effect is observed from then onwards.[52] The catalyst has been practically deactivated in a very early stage of operation to an extent depending on the operating conditions. At dynamic equilibrium the net rates of

coke precursor formation and of coke growth are zero. Therefore, the dynamic equilibrium coke content can be obtained from the following equation.

$$\frac{dC_p}{dt} = \delta r_s^o \Phi_{C_P} - r_G = 0$$

$$\frac{dC_{gr}}{dt} = r_{gr}^o C_{tgr} \Phi_{gr} - r_G = 0$$

(8.15)

The kinetic model for coke formation was coupled to the kinetic model for the main reactions to simulate the 3-bed adiabatic industrial reactor using the heterogeneous model. The effectiveness factors for the coke formation were assumed to be one.

Eq. (8.16) shows the continuity equations for the components accounting for the coke formation from ethylbenzene and styrene.

$$\frac{dX_{EB}}{d\left(W/F_{EB}^0\right)} = \eta_1 r_{c1} + \eta_2 r_{c2} + \eta_3 r_{c3} + \left(r_{t1} + r_{t2} + r_{t3}\right)\frac{\varepsilon_B}{\rho_B} + \frac{r_c\left(EB\right)}{8}$$

$$\frac{dX_{ST}}{d\left(W/F_{EB}^0\right)} = \eta_1 r_{c1} - \eta_4 r_{c4} + r_{t1}\frac{\varepsilon_B}{\rho_B} - \frac{r_c\left(ST\right)}{8}$$

(8.16)

$$\frac{dX_{BZ}}{d\left(W/F_{EB}^0\right)} = \eta_2 r_{c2} + r_{t2}\frac{\varepsilon_B}{\rho_B}$$

$$\frac{dX_{H_2}}{d\left(W/F_{EB}^0\right)} = \eta_1 r_{c1} - \eta_3 r_{c3} - 2\eta_4 r_{c4} + \left(r_{t1} - r_{t2}\right)\frac{\varepsilon_B}{\rho_B} + 21\frac{r_c\left(EB\right)}{8} + 20\frac{r_c\left(ST\right)}{8}$$

where η_i are the effectiveness factors which are obtained as already explained in chapter VII. r_c(EB) represents the rate of coke formation from ethylbenzene and r_c(ST)

represents the rate of coke formation from styrene. The stoichiometries for the coke formation from ethylbenzene, the subsequent coke gasification and global reaction are

coke formation: $EB \rightarrow 8C + 5H_2$

gasification: $8C + 16H_2O \rightarrow 8CO_2 + 16H_2$

global reaction: $EB + 16H_2O \rightarrow 8CO_2 + 21H_2$
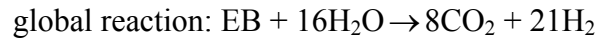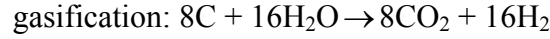
The stoichiometries for the coke formation from styrene, the subsequent coke gasification and global reaction are
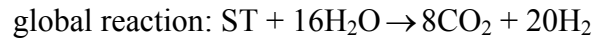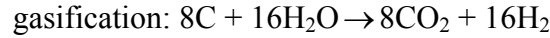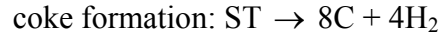
coke formation: $ST \rightarrow 8C + 4H_2$

gasification: $8C + 16H_2O \rightarrow 8CO_2 + 16H_2$

global reaction: $ST + 16H_2O \rightarrow 8CO_2 + 20H_2$

The energy equation is

$$\sum_{j=1}^{6} \dot{m}_j c_{pj} \frac{dT}{d\left(W/F_{EB}^0\right)} = F_{EB}^0 \left[-\Delta H_{r1}\left(\eta_1 r_{c1} + r_{t1}\frac{\varepsilon_B}{\rho_B}\right) - \Delta H_{r2}\left(\eta_2 r_{c2} + r_{t2}\frac{\varepsilon_B}{\rho_B}\right) \right.$$
$$\left. - \Delta H_{r3}\left(\eta_3 r_{c3} + r_{t3}\frac{\varepsilon_B}{\rho_B}\right) - \Delta H_{r4}\eta_4 r_{c4} \right.$$
$$\left. -\Delta H_{C,EB}\frac{r_c\left(EB\right)}{8} - \Delta H_{C,ST}\frac{r_c\left(ST\right)}{8} \right] \qquad (8.17)$$

The momentum equation is

$$-\frac{dP_t}{d\left(W/F_{EB}^o\right)} = f\alpha\frac{u_s GF_{EB}^o}{\rho_B d_p \Omega}$$
(8.18)

The set of continuity equations, energy equation, and momentum equation was integrated simultaneously along the reactor length. At each integration step the partial pressures and temperature were calculated and then these operating variables were substituted into Eq. (8.15) to evaluate the dynamic equilibrium coke content.

8.3   Results and Discussion

8.3.1   Coke Formation

Figure 8.1 shows the effect of operating conditions on the calculated catalyst coke content during coke formation only. The evolution of coke content was calculated by integrating Eq. (8.13) with respect to time at a particular position in the reactor. At the position the partial pressures and temperature were assumed to be constant during the run length. The kinetic parameters of coke formation (site coverage and growth) and coke gasification were estimated by Devoldere and Froment[52, 130] and are used in this simulation. Note that the values of kinetic parameters are for a catalyst which is different from that in the present investigation.

Three different sets of operating conditions were considered: (1) P_{EB} = 0.0757 bar, P_{ST} = 0.0018 bar, P_{H2} = 0.0010 bar, P_{H2O} = 0.8441 bar; (2) P_{EB} = 0.0716 bar, P_{ST} = 0.0055 bar, P_{H2} = 0.0047 bar, P_{H2O} = 0.8410 bar; (3) P_{EB} = 0.0554 bar, P_{ST} = 0.0202 bar, P_{H2} = 0.0193 bar, P_{H2O} = 0.8283 bar. The rate of coke formation at operating condition (3) is much slower than that at conditions (1) and (2). This behavior can be explained by
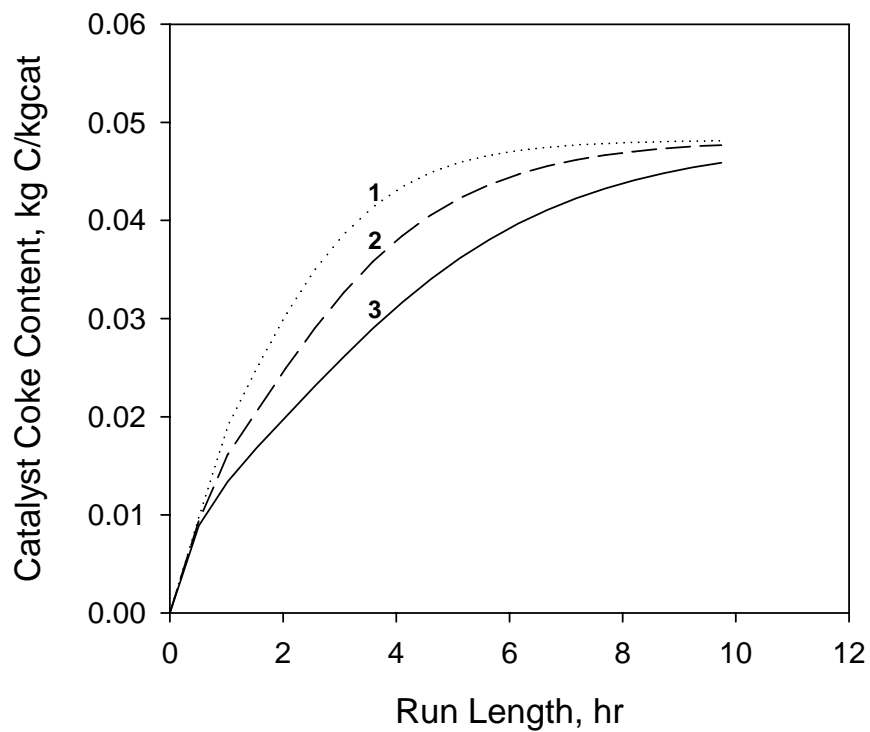
Figure 8.1. Effect of operating conditions on calculated catalyst coke content profiles during the coke formation only. Operating conditions: $T = 893$ K; $P_{total} = 1$ bar;

(1) $P_{EB} = 0.0757$ bar; $P_{ST} = 0.0018$ bar; $P_{H2} = 0.0010$ bar; $P_{H2O} = 0.8441$ bar;

(2) $P_{EB} = 0.0716$ bar; $P_{ST} = 0.0055$ bar; $P_{H2} = 0.0047$ bar; $P_{H2O} = 0.8410$ bar;

(3) $P_{EB} = 0.0554$ bar; $P_{ST} = 0.0202$ bar; $P_{H2} = 0.0193$ bar; $P_{H2O} = 0.8283$ bar.

the model equation of coke growth, Eq. (8.12), which shows that the higher partial pressure of hydrogen yields a slower rate of coke growth. According to Devoldere and Froment[52] the high partial pressure of hydrogen causes a decrease in the number of active sites for coke growth because sites for coke growth are produced by dehydrogenation/ dehydrocyclization. Furthermore, the rate of coke growth is decreased by competitive dissociative adsorption of hydrogen on active sites for coke growth.

8.3.2   Coke Gasification

Figure 8.2 shows the effect of operating conditions on the calculated catalyst coke content profiles during the coke gasification only. The operating conditions are the same as those in Figure 8.1. The initial catalyst coke content, 0.048 kgcoke/kgcat, is obtained from the asymptotic coke content in Figure 8.1. As the hydrogen partial pressure increases and the steam partial pressure decreases, the rate of coke gasification reaction decreases. Since coke gasification is the removal of adsorbed coke on the catalyst surface by reacting with steam, ethylbenzene and styrene partial pressures play no role in the rate of gasification.

8.3.3   Coke Formation and Gasification: Dynamic Equilibrium Coke Content

Coke formation and the continuous gasification reaction occur simultaneously during the ethylbenzene dehydrogenation, which leads to the calculation of dynamic equilibrium coke contents along the reactor length as discussed in section 8.2.4. The effect of feed temperatures on the dynamic equilibrium coke content in a 3-bed adiabatic
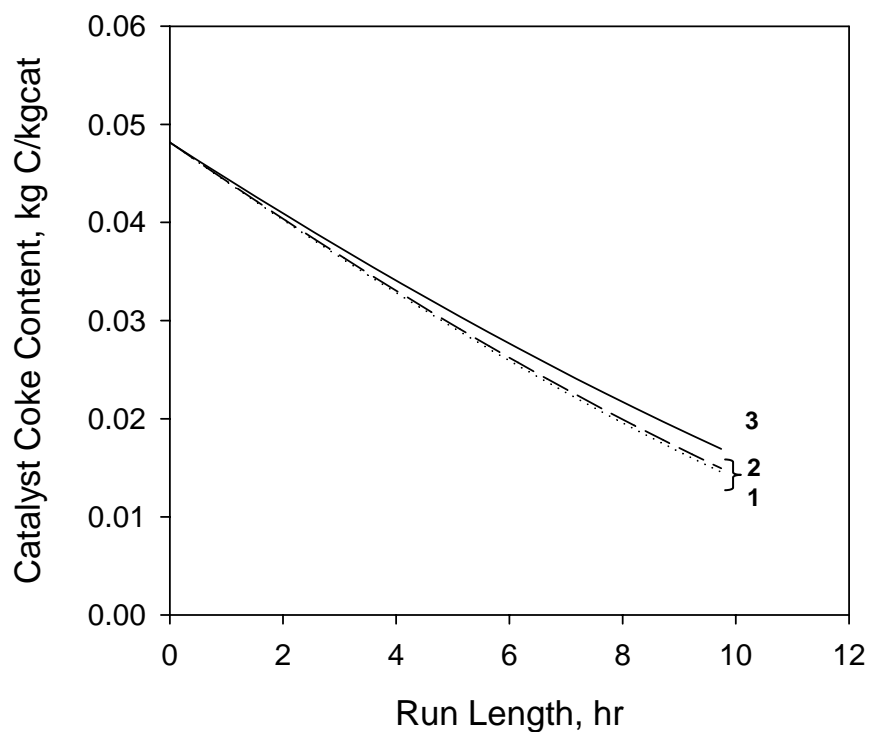
Figure 8.2. Effect of operating conditions on the calculated catalyst coke content profiles during the coke gasification only. Initial coke content = 0.048 kgcoke/kgcat. (obtained from the asymptotic value in Figure 8.1). Operating conditions: T = 893 K; P_{total} = 1 bar;

(1) P_{EB} = 0.0757 bar; P_{ST} = 0.0018 bar; P_{H2} = 0.0010 bar; P_{H2O} = 0.8441 bar;

(2) P_{EB} = 0.0716 bar; P_{ST} = 0.0055 bar; P_{H2} = 0.0047 bar; P_{H2O} = 0.8410 bar;

(3) P_{EB} = 0.0554 bar; P_{ST} = 0.0202 bar; P_{H2} = 0.0193 bar; P_{H2O} = 0.8283 bar.

reactor is illustrated in Figure 8.3. The higher feed temperatures result in the higher dynamic equilibrium coke content. The dynamic equilibrium coke content decreases with the bed length, which is due to the temperature drop over the adiabatic reactor.

Figure 8.4 shows the effect of feed molar ratios of H_2O/EB on the dynamic equilibrium coke content. The dynamic equilibrium coke content decreases as the feed molar ratios of H_2O/EB increases. Figures 8.3 and 8.4 indicate that the low dynamic equilibrium coke content can be obtained at low temperatures and high H_2O/EB feed ratios. As discussed in section 7.6.3, the higher steam to ethylbenzene ratio is not always preferred in industrial operation due to the cost of steam generation. At this point, the optimization is required to obtain the optimum steam to ethylbenzene feed ratio which also allows the longest catalyst activity.

We have shown that a dynamic equilibrium coke content is always present on the surface of the catalyst during ethylbenzene dehydrogenation under normal operating conditions. When the operating conditions need to be altered, the calculation of dynamic equilibrium coke content provides a crucial guideline for the selection of the steam to ethylbenzene feed ratio leading to optimum operating conditions.
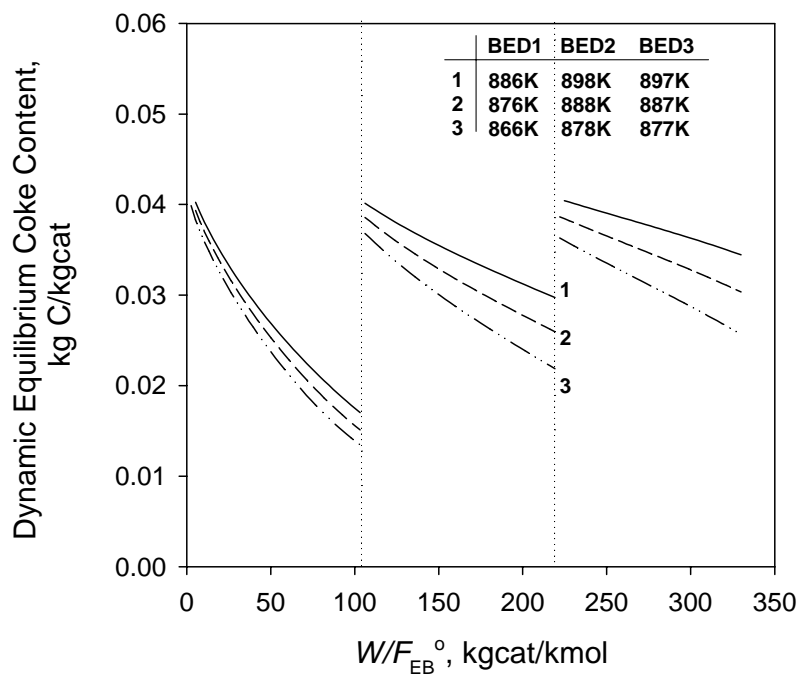
Figure 8.3 Effect of feed temperatures to each bed on dynamic equilibrium coke content profiles in a 3-bed adiabatic reactor for P_{in} = 1.25bar; H_2O/EB = 11 mol/mol; F_{EB}^o = 707 kmol/hr.
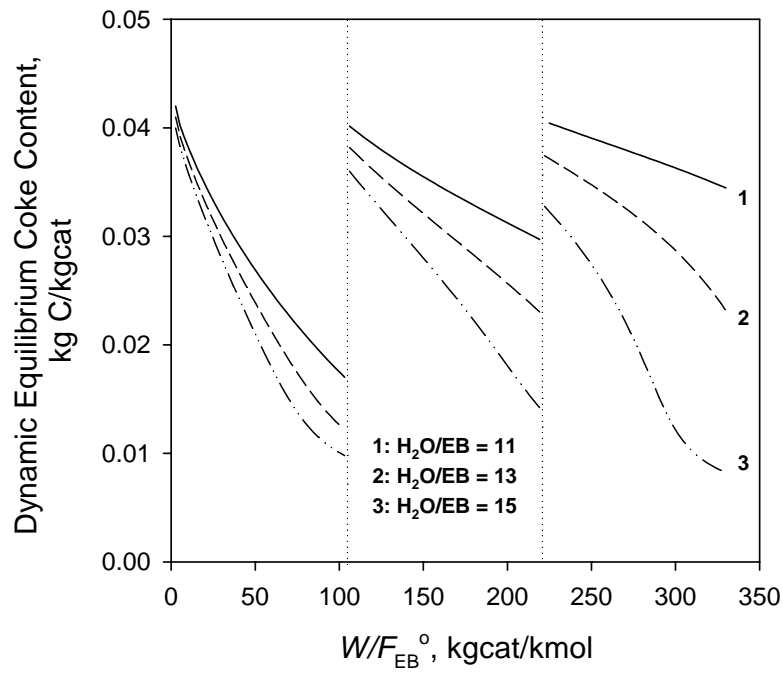
Figure 8.4 Effect of feed molar ratios of H_2O/EB on dynamic equilibrium coke content profiles in a 3-bed adiabatic reactor for T_{in} = 886K, 898K, 897K; P_{in} = 1.25bar; F_{EB}^{o} = 707 kmol/hr.

CHAPTER IX

SIMULATION OF FIXED BED ADIABATIC REACTOR

WITH RADIAL FLOW: HETEROGENEOUS MODEL

9.1   Introduction

Scale up of fixed bed adiabatic reactors is difficult because of the significant pressure drop for the higher production capacity. In order to overcome this problem the Haldor Topsøe Company developed a radial flow reactor for ammonia synthesis.[123] The radial flow reactor enables the decrease in the pressure drop in a reactor because of the high cross-sectional area and achieve high effectiveness factor by using small catalyst particles.[177] Pozi and Kaye[178] showed the design of a radial flow reactor with uniform gas distribution to the catalyst bed is very important because the uniformity of gas distribution affects the selectivities and conversions during the reaction. Fogler[179] showed that the radial flow reactor has an advantage for exothermic reactions because the high radial velocities at the entrance to the reactor can help reduce hot spots within the reactor. The industrial application of radial flow reactor includes ethylbenzene dehydrogenation,[5, 7] ammonia synthesis,[178, 180] and catalytic reforming.[181-183] A radial flow reactor was also recommended for use in methanol synthesis. However, it faces the serious problem that ammonia and methanol catalysts undergo shrinkage, which leads to breakage of the seal at the top of the bed.[184] Liu et al.[72, 185] reported several drawbacks associated with the radial flow reactor and proposed a honeycomb-type monolith reactor for ethylbenzene dehydrogenation. An axial-radial reactor is a new configuration of

fixed-bed reactor for ammonia systhesis.[180, 186, 187]   In this chapter the derivation of continuity equations for the components will be presented first. The effect of the feed conditions on the reactor performance, i.e., ethylbenzene conversion, styrene selectivity, temperature variation, and pressure drop will be discussed.

9.2   Continuity, Energy, and Momentum Equations

9.2.1   Continuity Equation

To derive the model equations the following assumptions are made:[123, 131]

1. Axial flow by convection or dispersion is negligible.

2. Radial dispersion is negligible.

3. The concentration and temperature gradients in axial and angular direction are negligible.

4. The fluid phase is in plug flow.

5. Channeling or shortcut effects do not occur.

6. The reactor is run in the steady state.

7. The gas mixture obeys the ideal gas law.

Figure 9.1 illustrate a radial flow reactor configuration. Gas flows in a centrifugal direction across the catalyst bed in a cylindrical reactor. The radial reactor with a centripetal flow reaction is used for ammonia synthesis. The mass balance over the differential cross-section of a cylindrical shell for reactant j can be written

$$\left(u_s C_j\right)_r 2\pi r L - \left(u_s C_j\right)_{r+\Delta r} 2\pi\left(r+\Delta r\right)L = \left(2\pi r L\right)\Delta r \rho_B R_j \tag{9.1}$$
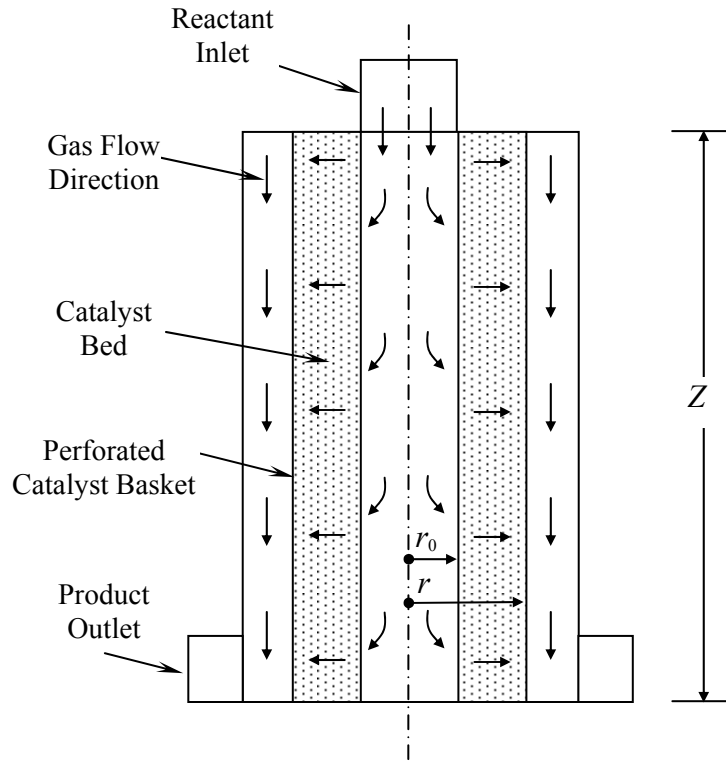
Figure 9.1. Simplified radial flow reactor configuration.

where r is the radial coordinate in m_r, C_j is the molar concentration of component j in kmol/ m_f^3, u_s is the superficial velocity in $m_f^3/(m_r^2 \cdot hr)$, ρ_B is the bed density in kgcat/ m_r^3 and R_j is the total rate of change of the amount of j in kmol/(kgcat$\cdot$ hr).

In the limit after some rearrangements, the continuity equation reduces to

$$-\frac{d}{dr}\left(r u_s C_j\right) = r \rho_B R_j \qquad (9.2)$$

Introducing ρ_g, gas density, and following the manipulation presented in Froment and Bischoff,[80]

$$-\frac{d}{dr}\left(r u_s \rho_g \frac{C_j}{\rho_g}\right) = -r u_s \rho_g \frac{d}{dr}\left(\frac{C_j}{\rho_g}\right) - \left(\frac{C_j}{\rho_g}\right)\frac{d}{dr}\left(r \rho_g u_s\right)$$

$$= r \rho_B R_j \tag{9.3}$$

where C_j/ρ_g is in kgmol/kg.

The total continuity equation yields

$$\frac{d}{dr}\left(r \rho_g u_s\right) = 0 \tag{9.4}$$

The superficial velocity in the reactor can be calculated from Eq. (9.4).

$$u_s = \frac{r_0 \rho_g^0 u_s^0}{r \rho_g} \tag{9.5}$$

where superscript 0 denotes the feed condition. Eq. (9.5) shows that the superficial velocity varies inversely with the radial coordinate, r. Eq. (9.3) reduced to

$$-r u_s \rho_g \frac{d}{dr}\left(\frac{C_j}{\rho_g}\right) = r \rho_B R_j \tag{9.6}$$

Eq. (9.6) is rewritten in terms of conversion, X_j using the relationship $C_j/\rho_B = (1 - X_j)$ ($C_{EB}/\rho_B)^0$ and Eq. (9.5)

$$\frac{dX_j}{dr} = \frac{1}{u_s^0 C_{EB}^0} \cdot \frac{r}{r_0} \rho_B R_j$$

$$= \frac{\Omega^0}{F_{EB}^0 r_0} \cdot r \rho_B R_j \tag{9.7}$$

where r_o is the inner radius of reactor in m_r^2, F_{EB}^0 is the molar feed rate of ethylbenzene, $u_s^0 C_{EB}^0 \Omega^0$, in kmol/hr and Ω^0 is the cross-section area at r_0, $2\pi r_0 z$, in m_r^2. Note that for the

radial flow reactor the cross-section area is not constant but varies with the radial coordinate r. Eq. (9.7) can be expressed in terms of space time, W/F_{EB}^0, using $W = \pi z \rho_B (r^2 - r_o^2)$

$$\frac{dX_j}{d\left(W/F_{EB}^0\right)} = R_j \tag{9.8}$$

When internal diffusion limitations are accounted for, Eq. (9.8) reduces to

$$\frac{dX_{EB}}{d\left(W/F_{EB}^0\right)} = \eta_1 r_{c1} + \eta_2 r_{c2} + \eta_3 r_{c3} + \left(r_{t1} + r_{t2} + r_{t3}\right)\frac{\varepsilon_B}{\rho_B}$$

$$\frac{dX_{ST}}{d\left(W/F_{EB}^0\right)} = \eta_1 r_{c1} - \eta_4 r_{c4} + r_{t1}\frac{\varepsilon_B}{\rho_B}$$

$$\frac{dX_{BZ}}{d\left(W/F_{EB}^0\right)} = \eta_2 r_{c2} + r_{t2}\frac{\varepsilon_B}{\rho_B} \tag{9.9}$$

$$\frac{dX_{H_2}}{d\left(W/F_{EB}^0\right)} = \eta_1 r_{c1} - \eta_3 r_{c3} - 2\eta_4 r_{c4} + \left(r_{t1} - r_{t2}\right)\frac{\varepsilon_B}{\rho_B}$$

9.2.2   Energy Equation

The energy equation can be written in the steady state:

$$\sum_{j=1}^{6} \dot{m}_j c_{pj} \frac{dT}{dr} = \Omega \rho_B \sum_{i=1}^{4} \left(-\Delta H_{ri}\right) r_i \tag{9.10}$$

Eq. (9.10) can be expressed with respect to W/F_{EB}^0 and accounting for internal diffusion limitations

$$\sum_{j=1}^{6} \dot{m}_j c_{pj} \frac{dT}{d\left(W/F_{EB}^0\right)} = F_{EB}^0 \sum_{i=1}^{4} \left(-\Delta H_{ri}\right) \eta_i r_i \tag{9.11}$$

9.2.3   Momentum Equation

The momentum equation is

$$-\frac{dP_t}{dr} = f\alpha\frac{\rho_g u_s^2}{d_p} = f\alpha\frac{G^2}{\rho_g d_p} \tag{9.12}$$

where f is the friction factor, G is the superficial mass flow velocity in kg/(m²ᵣ·hr), α is the conversion factor, 7.7160×10^{-8} when P_t is in bar and G is in kg/(m²ᵣ·hr).

In terms of W/F_{EB}^0, Eq. (9.11) is given by

$$-\frac{dP_t}{d\left(W/F_{EB}^0\right)} = f\alpha\frac{F_{EB}^0\rho_g u_s^2}{2\pi zr\rho_B d_p}$$

$$\text{where} \quad r = \left[r_0^2 + \frac{F_{EB}^0}{\rho_B\pi z}\left(\frac{W}{F_{EB}^0}\right)\right]^{1/2} \tag{9.13}$$

$$f = \frac{1-\varepsilon_B}{\varepsilon_B^3}\left[1.28 + \frac{458\left(1-\varepsilon_B\right)}{\text{Re}}\right]$$

9.3   Results and Discussion

The continuity-, energy-, and momentum equations, Eqs.(9.9), (9.11), and (9.13) are integrated simultaneously using the heterogeneous model as discussed in Chapter VII. With the radial flow reactor the cross section of the catalyst bed depends upon the space time, i.e., radial position, so that the superficial velocity, u_s, has to be adapted in each integration step through the reactor. The feed conditions and reactor geometry are shown in Table 9.1. The length of each reactor and inner radius of the catalyst bed are assumed to be 7m and 1.5m, respectively.

Table 9.1 and Figures 9.2 and 9.3 show the comparison of simulated results using the heterogeneous model between a 3-bed adiabatic radial flow reactor and a 3-bed adiabatic axial flow reactor. The same operating conditions were used for the simulation of two types of reactors. In the radial flow reactor the total ethylbenzene conversion amounted to 81.19%, compared to 83.76% in an axial flow reactor. The decrease of the total ethylbenzene conversion in the radial flow reactor is attributed to the small pressure drop as discussed in section 7.6.4 for the axial flow reactor. The styrene selectivity decreased from 90.43% to 83.24%. This is mainly due to the substantial increase of toluene selectivity (7.89% versus 14.60%). The difference of benzene selectivity between two types of reactors was insignificant (1.75% versus 2.12%). In Table 9.1 and Figure 9.3 the pressure drop in the three beds was 0.04 bar while it was 0.95bar in the axial flow reactor (Figure 7.3 in section 7.6). The reduction of pressure drop results from the large cross-section area in a radial flow reactor. Since the total ethylbenzene conversion was extremely high under the present operating conditions, simulation results performed at different operating conditions will be discussed to find out more reasonable total ethylbenzene conversion and styrene selectivity for a 3-bed radial reactor.

Figure 9.4 shows the effect of feed temperatures on the total ethylbenzene conversion and styrene selectivity. As the feed temperatures increase, the total ethylbenzene conversions increase but the styrene selectivity decrease. Decreasing the feed temperatures to each reactor (876K, 888K, and 887K) is preferred in order to decrease the total ethylbenzene conversion, which reached 74.31% at the end of the third bed. The styrene selectivity increased to 89.91%.

Table 9.1. Simulation result of a 3-bed adiabatic radial flow reactor for the feed ratio of $H_2O/EB = 11$mol/mol when using the heterogeneous model

	BED 1	BED 2	BED 3
Weight of catalyst, kg [*]	72 950	82 020	78 330
Space time [§]	103.18	219.19	329.98
X_{EB}, % [¶]	36.59	64.18	81.19
S_{ST}, % [¶]	98.43	93.92	83.24
S_{BZ}, %	1.01	1.53	2.12
S_{TO}, %	0.56	4.54	14.60
P_{in}, bar [*]	1.25	1.22	1.21
T_{in}, K [*]	886	898.2	897.6
T_{out}, K	812.04	850.26	890.37
Catalyst bed depth, m	0.614	0.708	0.681
Inner radius of catalyst bed, m	1.5		
Length of each reactor, m	7		
Feed molar flow rate, kmol/hr EB [*]	707		
ST	7.104		
BZ	0.293		
TO	4.968		
H_2O [†]	7 777		
Total feed molar flow rate, kmol/hr	8 496.37		

[§] Space time is cumulative and is in kgcat hr/kmol EB.
[¶] X_{EB} denotes the EB conversion and S_j denotes the selectivity of component j.
[*] The information was provided by personal communication with Froment.[130]
[†] The feed molar flow rate of H_2O was obtained from a molar ratio of H_2O/EB=11.

Figure 9.2. Comparison of simulated total ethylbenzene conversion profiles (a) and styrene selectivity profiles (b) using the heterogeneous model between a 3-bed adiabatic *radial* flow reactor and a 3-bed adiabatic *axial* flow reactor for T_{in} = 886K, 898K, 897K; P_{in} = 1.25bar; H_2O/EB = 11 mol/mol; F_{EB}^o = 707 kmol/hr. Solid line: radial flow reactor; dashed line: axial flow reactor.
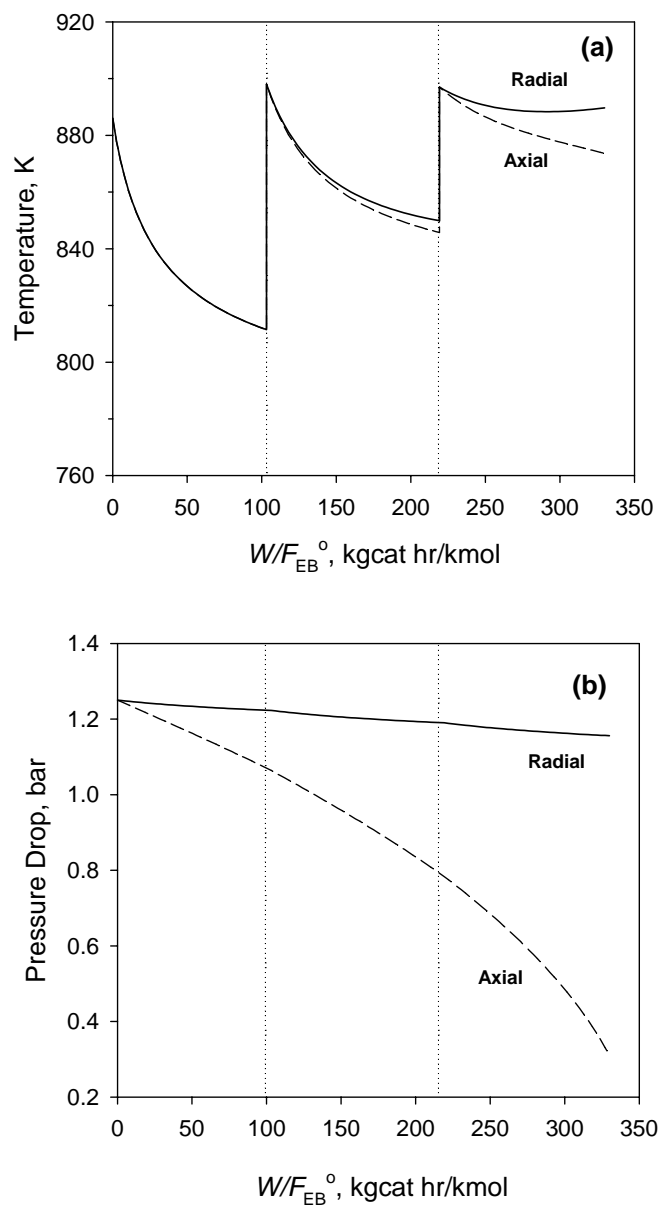
Figure 9.3. Comparison of simulated temperature profiles (a) and pressure drop profiles (b) using the heterogeneous model between a 3-bed adiabatic *radial* flow reactor and a 3-bed adiabatic *axial* flow reactor for T_{in} = 886K, 898K, 897K; P_{in} = 1.25bar; H_2O/EB = 11 mol/mol; F_{EB}^o = 707 kmol/hr. Solid line: radial flow reactor; dashed line: axial flow reactor.
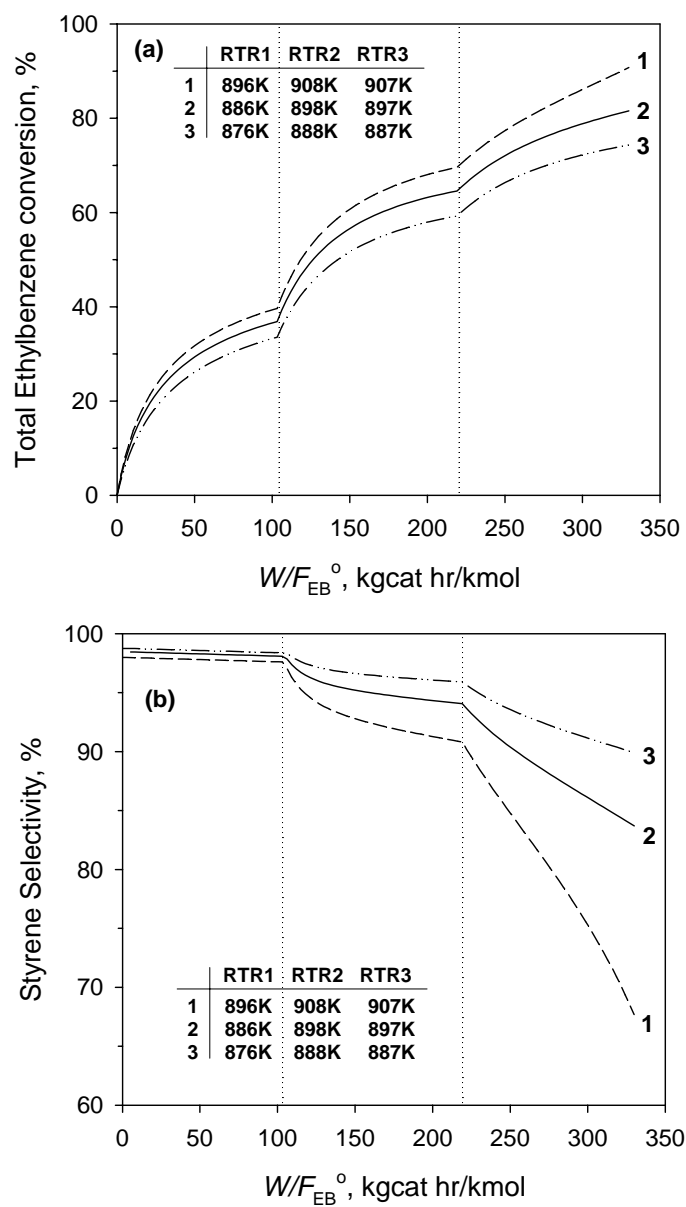
Figure 9.4. Effect of feed temperature on the total ethylbenzene conversion profiles (a) and styrene selectivity profiles (B) in a 3-stage adiabatic radial flow reactor for P_{in} = 1.25bar; H_2O/EB = 11 mol/mol; F_{EB}^o = 707 kmol/hr.

Figure 9.5 shows the influence of feed molar ratios of H_2O/EB. Three cases were considered: 9, 11, and 13. The total ethylbenzene conversion and the styrene selectivity were not affected very much by the feed molar ratios of H_2O/EB. The most significant effect on the styrene selectivity was the feed pressure as shown in Figure 9.6. The two feed pressures were used for the simulation: 0.70bar and 1.25bar. At 0.70bar the styrene selectivity increased to 91.32%. The change of total ethylbenzene conversion was not significant. This result is quite similar to the axial flow reactor simulation for the isobaric condition.

Among the operating conditions mentioned above the following conditions were selected to have the total ethylbenzene conversion and styrene selectivity closer to the optimum: T_{in} = 876K, 888K, 887K; P_{in} = 0.7bar; H_2O/EB = 9 mol/mol. The simulated total ethylbenzene conversion was 74.86% and the styrene selectivity was 94.40% (Figure 9.7). The pressure drop was 0.07bar (Figure 9.8). The optimal ethylbenzene conversion and styrene selectivity in the commercial operation have been known to be in the range 65%-70% and 95%-97%, respectively. Therefore, the simulated values are still not optimal at the selected operating conditions for the present catalyst. Instead of a 3-bed radial reactor, a 2-bed radial reactor has also been utilized for ethylbenzene dehydrogenation.[7, 131] In this case the total ethylbenzene conversion of 64.18% and styrene selectivity of 93.62% was obtained in Table 9.1 and Figure 9.2 without further searching for the optimal operating conditions. The use of a 2-bed radial reactor has the benefit to reduce the operating cost.
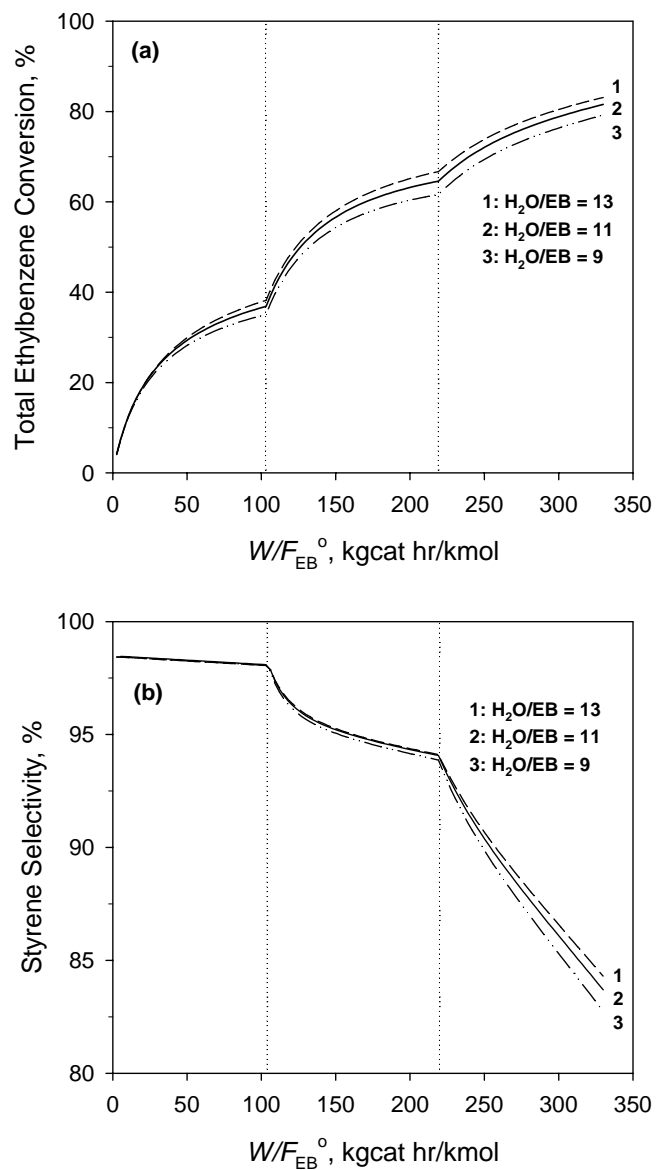
Figure 9.5. Effect of feed molar ratios of H_2O/EB on the total ethylbenzene conversion profiles (a) and styrene selectivity profiles (b) in a 3-stage adiabatic radial flow reactor for T_{in} = 886K, 898K, 897K; P_{in} = 1.25bar; F_{EB}^o = 707 kmol/hr.
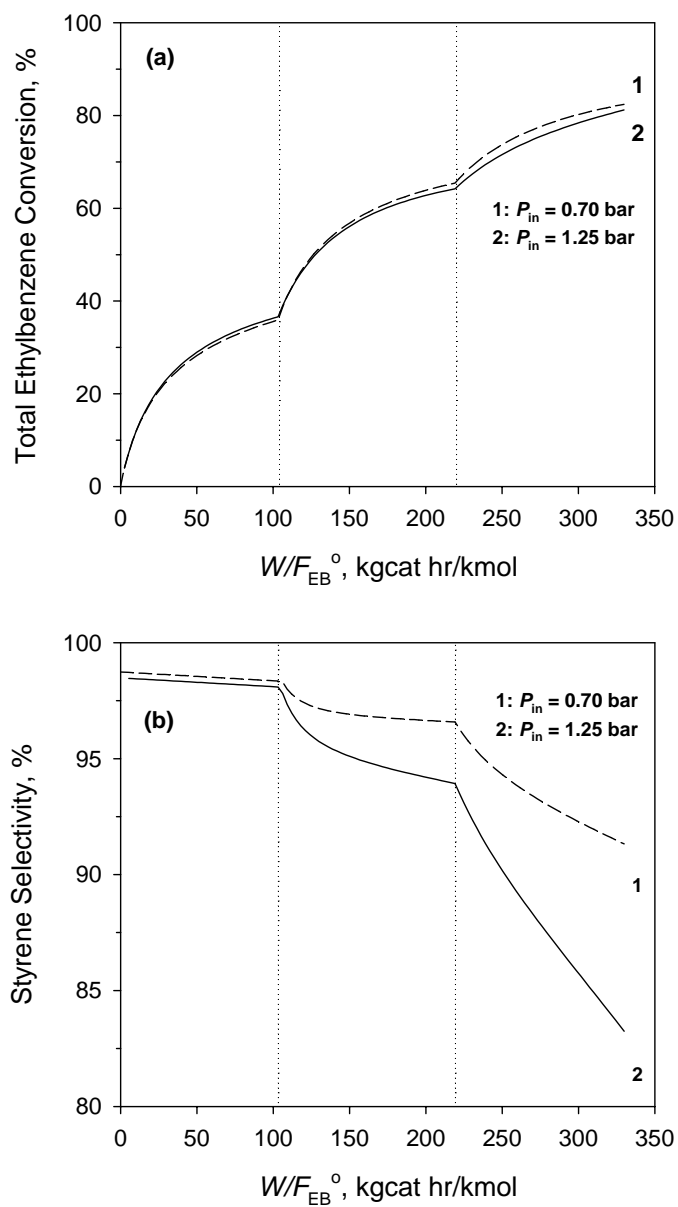
Figure 9.6. Effect of feed pressure on the total ethylbenzene conversion profiles (a) and styrene selectivity profiles (b) in a 3-stage adiabatic radial flow reactor for T_{in} = 886K, 898K, 897K; H_2O/EB = 11 mol/mol; F_{EB}^o = 707 kmol/hr.
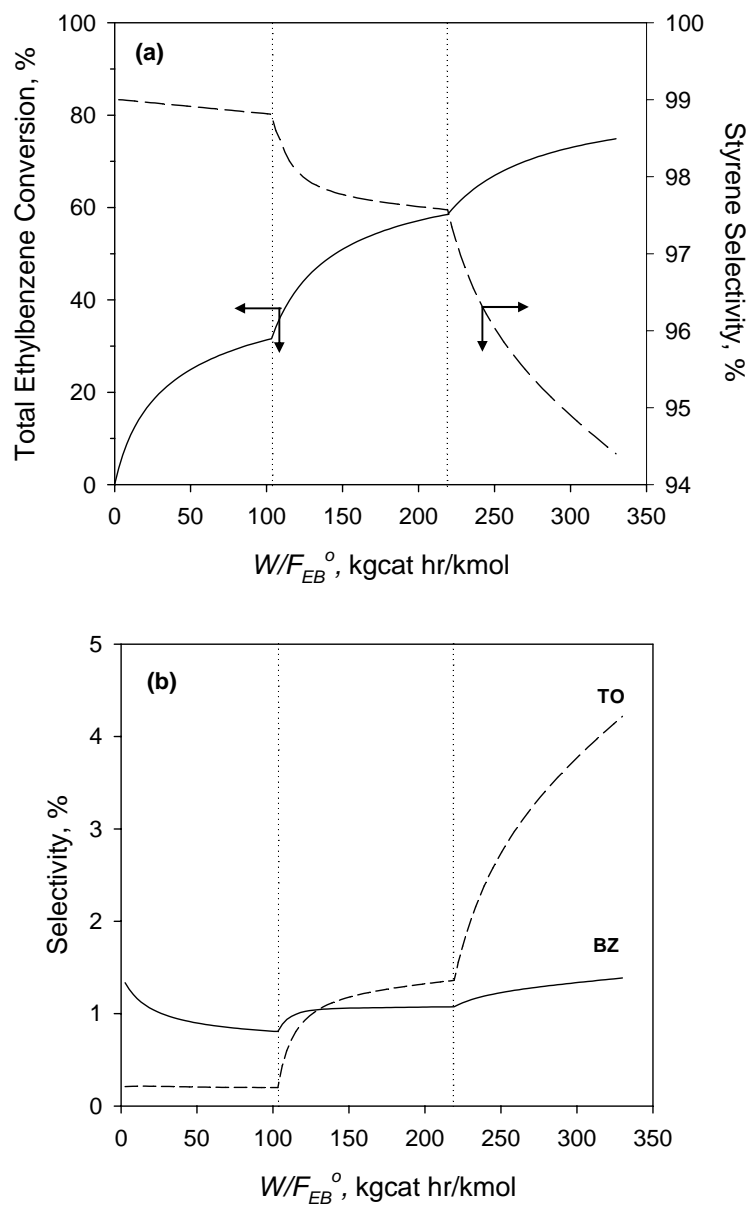
Figure 9.7. Simulated total ethylbenzene conversion and styrene selectivity profiles (a) and benzene and toluene selectivity profiles (b) in a 3-stage adiabatic radial flow reactor for the selected operating conditions: T_{in} = 876K, 888K, 887K; P_{in} = 0.7bar; H_2O/EB = 9 mol/mol; F_{EB}^o = 707 kmol/hr.
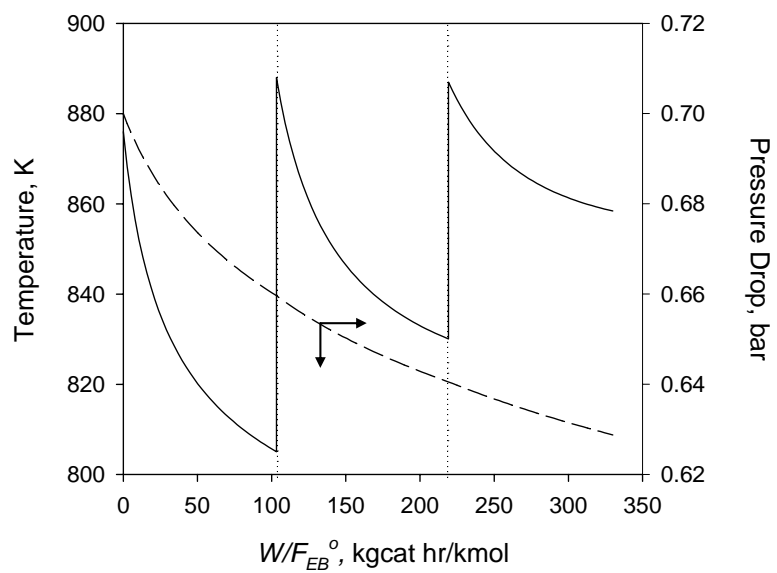
Figure 9.8. Simulated temperature and pressure drop profiles in a 3-stage adiabatic radial flow reactor for the selected operating conditions: T_{in} = 876K, 888K, 887K; P_{in} = 0.7bar; H_2O/EB = 9 mol/mol; F_{EB}^{o} = 707 kmol/hr.

CHAPTER X

CONCLUSION AND RECOMMENDATIONS

The catalytic dehydrogenation of ethylbenzene into styrene was investigated in a tubular reactor over commercial potassium-promoted iron oxide catalyst under atmospheric pressure. The extensive kinetic experiments covered a wide range of operating conditions and allowed the development of a fundamental kinetic model. The kinetic study showed that the higher feed molar ratio of H_2O/EB give higher total ethylbenzene conversion and styrene selectivity. The total ethylbenzene conversion and styrene selectivity decreased as the addition of styrene or H_2 to the feed mixture increased. The addition of styrene or H_2 leads to fast catalyst deactivation.

The intrinsic kinetics for the formation of styrene, benzene, and toluene has been modeled using the Hougen-Watson formula. The data analysis was based on the integral method of kinetic analysis. The mathematical model developed for the ethylbenzene dehydrogenation consists of nonlinear simultaneous differential equations in multiple dependent variables. The parameters were estimated from the minimization of the multiresponse objective function which was performed by means of the Marquardt algorithm.

The significance of the individual model parameters was tested by comparing the estimate b_j with its standard deviation. The estimate was significantly different from zero and effectively contributes to the model. The kinetic model with set of estimated

parameters yielded an excellent fit of the experimental data. The final estimated values of the adsorption enthalpies and entropies was tested and validated using the physicochemical criteria proposed by Boudart.

The intrinsic kinetic parameters were used to simulate 3-bed adiabatic industrial reactor with axial flow and radial flow using the heterogeneous fixed bed reactor model. The differential model equations were written separately for the fluid and solid phase. The differential equations for the solid involve the effective diffusivity. Integration of model equations, including intrinsic reaction rates and transport by internal diffusion in the porous catalyst, was solved using the orthogonal collocation method with 6 internal collocation points whose coefficients were obtained form the Jacobian orthogonal polynomials. The solution of particle equations leads to the calculation of the effectiveness factor. It was calculated at each integration step along the reactor length for the industrial reactor simulation. The effectiveness factors for the formation of styrene from ethylbenzene, formation of benzene, and formation of toluene were lower than 1. It indicates that the process is diffusion controlled. The effectiveness factor for the formation of toluene from styrene was greater than 1 because this is a consecutive reaction.

The dynamic equilibrium coke content was calculated using a detailed kinetic model for coke formation and gasification, which was coupled to the kinetic model for the main reactions. The calculation of the dynamic equilibrium coke content provided a crucial guideline for the selection of the molar of H_2O/EB leading to optimum operating conditions.

Kinetic experiments for the formation of minor by-products, such as phenylacetylene, α-methylstyrene, β-methylstyrene, cumene, n-propylbenzene, divinylbenzene, and stilbene revealed that the phenylacetylene selectivity did not depend on the total ethylbenzene conversion. The selectivity of stilbene was highly increased with increasing temperature. The selectivity of divinylbenzene was so low (below 0.01%) at all the reaction conditions that no correlation with the ethylbenzene conversion was made. The selectivities of other minor by-products decreased with increasing the total ethylbenzene conversion.

More research efforts can be contributed to the following recommendations for future work:

1.   Experimental study for the coke formation and gasification using an electrobalance to estimate the kinetic parameters for the coke formation and gasification, which leads to determine the dynamic equilibrium coke content.

2.   Process optimization of ethylbenzene dehydrogenation to determine an optimal reactor configuration and operating conditions, such as a molar ratio of steam to ethylbenzene, pressure, and temperature.

3.   Empirical kinetic model for the production of minor by-products which correlates the selectivity with the total ethylbenzene conversion.

NOMENCLATURE

A_i Preexponential factor of catalytic reaction i, $\text{kmol}/(\text{kgcat.} \cdot \text{hr})$

A_j Preexponential factor for adsorption of species j, $1/\text{bar}$

A_i^* Reparameterized preexponential factor of catalytic reaction i,

           $\text{kmol}/(\text{kgcat.} \cdot \text{hr})$

A_j^* Reparameterized preexponential factor for adsorption of species j, $1/\text{bar}$

A_{ti} Preexponential factor of thermal reaction i, $\text{kmol}/(\text{m}^3 \cdot \text{hr} \cdot \text{bar})$

a_v External particle surface are per unit reactor volume, $\text{m}_p^2/\text{m}_r^3$

$\mathbf{b}$ Vector of parameter estimates

b_j Estimates of parameter j

C_A, C_B, C_i Molar concentration of species A, B, i, kmol/m_f^3

C_{Al}, C_{Bl} Molar concentration of adsorbed A, B, $\text{kmol}/\text{kgcat.}$

C_{C_p} Coke precursor content, kgcoke/kgcat

C_l Molar concentration of vacant active sites of catalyst, $\text{kmol}/\text{kgcat.}$

C_t Total molar concentration of active sites, $\text{kmol}/\text{kgcat.}$

C_{tgr} Total number of active site for gasification, kmol/kgcat

c_p Specific heat of fluid, $\text{kJ}/(\text{kg} \cdot \text{K})$

D_A Molecular diffusivity of A, $\text{m}_f^3/(\text{m}_f \cdot \text{s})$

D_{AB} Molecular diffusivity for A in a binary mixture of A and B, $\text{m}_f^3/(\text{m}_f \cdot \text{s})$

$D_{e,j}$ Effective diffusivity of component j, $\text{m}_f^3/(\text{m}_r \cdot \text{s})$

D_K Knudsen diffusivity, $\text{m}_f^3/(\text{m}_f \cdot \text{s})$

d_p Catalyst equivalent pellet diameter, m_p

E_i Activation energy of catalytic reaction i, kJ/kmol

E_{ti}	Activation energy of thermal reaction i, kJ/kmol
F_j	Molar flow rate of j, kmol/hr
F_j^o	Feed molar flow rate of j, kmol/hr
f	Friction factor in momentum equation
G	Superficial mass flow velocity, $kg/\left(m_r^2 \cdot hr\right)$
$-\Delta H_{a,j}$	Adsorption enthalph of adsorbed species j, kJ/mol
$-\Delta H_r$	Heat of reaction, kJ/kmol
I	Unit matrix
J	Matrix of partial derivatives of function with respect to parameters
$K_A, K_j,...$	Adsorption equilibrium constants of species A, j,... , $1/$ bar
K_{eq}	Equilibrium constant, bar
k_i	Rate coefficient of reaction i, $kmol/\left(kgcat. \cdot hr\right)$
k_{ti}	Rate coefficient of thermal reaction i, $kmol/\left(m^3 \cdot hr \cdot bar\right)$
L	Reactor length, m
l	Vacant active site
$\dot{m}_j$	Mass rate of component j, kg/hr
$P_A, P_i,...$	Partial pressures of species A, i,..., bar
P_j^*	Dimensionless variable of partial pressure of j inside the catalyst
Pe_{ma}	Peclet number based on particle diameter, $\varepsilon u_s d_p / D_{ea}$
P_t	Total pressure, bar
$R\left(\text{or } R_g\right)$	Gas constant, $8.314 \ J/\left(mol \cdot K\right)$
R_j	Total rate of change of the component j, kmol/(kgcat·hr)
Re	Reynolds number based on particle diameter, $d_p u_s \rho_g / \mu$
r	Radial coodinate, m_r

r_0	Inner radius of catalyst bed in a radial reactor, m_r
r_c	Rate of coke formation, kgcoke/(kgcat·hr)
r_{ci}	Rate of catalytic reaction i, $kmol/(kgcat.\cdot hr)$
r_G	Rate of coke gasification, kgcoke/(kgcat·hr)
r_{gr}	Rate of coke growht, kgcoke/(kgcat·hr)
r_{gr}^0	Initial rate of site coverage, kgcoke/(kmol·hr)
r_s	Rate of site coverage, kgcoke/(kgcat·hr)
r_s^0	Initial rate of site coverage, kgcoke/(kmol·hr)
r_{ti}	Rate of thermal reaction i, $kmol/(m^3 \cdot hr)$
$S(\beta)$	Objective function
S_v	Specific surface, surface area of solids per unit volume of solids, m_p^{-1}
$-\Delta S_{a,j}^o$	Standard entropy of adsorption of species j, $kJ/(kmol \cdot K)$
S_g^o	Standard entropy of the gas, $kJ/(kmol \cdot K)$
S_a^o	Standard entropy of the adsorbed molecule, $kJ/(kmol \cdot K)$
$s(b_j)$	Standard deviation of estimated parameter b_j
T	Temperature in K
$t(n$ - $p;$ 1 - $\alpha/2)$	Tabulated $\alpha/2$ percentage point of the t distribution with n-p degree of freedom
t_c	Calculated t statistics, $\|b_j - 0\|/s(b_j)$
u_i	Interstitial velocity $(=u_s/\varepsilon_B)$, m_r/s
u_s	Superficial velocity, $m_f^3/(m_r^2 \cdot s)$
W	Weight of catalyst, kgcat
X_{EB}	Conversion of ethylbenzene

X_j	Conversion into species j
$\bar{y}$	Calculated values of dependent variables
z	Axial coordinate in reactor, m_r

Greek Letters

α_j	Stoichiometry coefficient of component j
α	Conversion factor in momentum equation
β	Parameter
δ	Conversion factor in the rate of coke site coverage, kmol/kgcat
ε_B	Void fraction of bed, m_f^3/m_r^3
ε_s	Internal void fraction, m_f^3/m_p^3
Φ_{C_p}	Deactivation function for site coverage
Φ_{gr}	Deactivation function for coke growth
η	Effectiveness factor
λ	Lagrangian multiplier in Marquardt method
ξ	Dimensionless variable of radial coordinate
ρ_B	Catalyst bulk density, kgcat./m_r^3
ρ_g	Gas density, kg/m_f^3
ρ_s	Catalyst pellet density, kgcat./m_p^3
Ω	Cross section of reactor, m_r^3

LITERATURE CITED

(1)   Product Focus: Styrene. *Chemical Week,* May 15, 2002, p. 36.

(2)   Chemical Profile. *Chemical Market Reporter,* May 14, 2001, p. 37.

(3)   James, D. H.; Castor, W. M. Styrene. In *Ullmann's Encyclopedia of Industrial Chemistry*; Campbell, F. T.,Pfefferkorn, R.,Rounsaville, J. F., Eds.; Wiley-VCH: Weinheim, 1994; Vol. A25, p. 329.

(4)   Kerby, K. K. US Patent 2,370,797, 1945.

(5)   Sundaram, K. M.; Sardina, H.; Fernandez-Baujin, J. M.; Hildreth, J. M., Styrene Plant Simulation and Optimization. *Hydrocarbon Process.,* January 1991, p. 93.

(6)   Kolios, G.; Eigenberger, G. Styrene Synthesis in a Reverse-Flow Reactor. *Chem. Eng. Sci.* **1999,** *54*, 2637.

(7)   Savoretti, A. A.; Borio, D. O.; Bucala, V.; Porras, J. A. Non-adiabatic Radial-flow Reactor for Styrene Production. *Chem. Eng. Sci.* **1999,** *54*, 205-213.

(8)   Yee, A. K. Y.; Ray, A. K.; Rangaiah, G. P. Multiobjective Optimization of an Industrial Styrene Reactor. *Comput. Chem. Eng.* **2003,** *27*, 111-130.

(9)   Sheel, J. G. P.; Crowe, C. M. Simulation and Optimization of an Existing Ethylbenzene Dehydrogenation Reactor. *Can. J. Chem. Eng.* **1969,** *47*, 183.

(10)   Clough, D. E.; Ramirez, W. F. Mathematical-Modeling and Optimization of Dehydrogenation of Ethylbenzene to Form Styrene. *AIChE J.* **1976,** *22*, 1097-1105.

(11)   Lee, E. H. Iron-Oxide Catalysts for Dehydrogenation of Ethylbenzene in Presence of Steam. *Catal. Rev.-Sci. Eng.* **1973,** *8*, 285-305.

(12)   Shibata, K.; Kiyoura, T. Effect of Potassium Promoter on Iron Oxide Catalysts for Dehydrogenation of Ethylbenzene to Styrene. *Bull. Chem. Soc. Jpn.* **1969,** *42*, 871.

(13)   Coulter, K.; Goodman, D. W.; Moore, R. G. Kinetics of the Dehydrogenation of Ethylbenzene to Styrene over Unpromoted and K-Promoted Model Iron-Oxide Catalysts. *Catal. Lett.* **1995,** *31*, 1-8.

(14)   Addiego, W. P.; Estrada, C. A.; Goodman, D. W.; Rosynek, M. P. An Infrared Study of the Dehydrogenation of Ethylbenzene to Styrene over Iron-Based Catalysts. *J. Catal.* **1994,** *146*, 407-414.

(15)   Shekhah, O.; Ranke, W.; Schlogl, R. Styrene Synthesis: In situ Characterization and Reactivity Studies of Unpromoted and Potassium-Promoted Iron Oxide Model Catalysts. *J. Catal.* **2004,** *225*, 56.

(16)   Stobbe, D. E.; van Buren, F. R.; van Dillen, A. J.; Geus, J. W. Potassium Promotion of Iron-Oxide Dehydrogenation Catalysts Supported on Magnesium-Oxide. 1. Preparation and Characterization. *J. Catal.* **1992,** *135*, 533.

(17)   Muhler, M.; Schlogl, R.; Reller, A.; Ertl, G. The Nature of the Active Phase of the Fe/K-Catalyst for Dehydrogenation of Ethylbenzene. *Catal. Lett.* **1989,** *2*, 201-210.

(18)   Hirano, T. Active Phase in Potassium-Promoted Iron-Oxide Catalyst for Dehydrogenation of Ethylbenzene. *Appl. Catal.* **1986,** *26*, 81-90.

(19)   Hirano, T. Roles of Potassium in Potassium-Promoted Iron-Oxide Catalyst for Dehydrogenation of Ethylbenzene. *Appl. Catal.* **1986,** *26*, 65-79.

(20)   Hirano, T. Dehydrogenation of Ethylbenzene over Potassium-Promoted Iron-Oxide Containing Cerium and Molybdenum Oxides. *Appl. Catal.* **1986,** *28*, 119-132.

(21)   Muhler, M.; Schutze, J.; Wesemann, M.; Rayment, T.; Dent, A.; Schlogl, R.; Ertl, G. The Nature of the Iron Oxide-Based Catalyst for Dehydrogenation of Ethylbenzene to Styrene .1. Solid-State Chemistry and Bulk Characterization. *J. Catal.* **1990,** *126*, 339-360.

(22)   Kuhrs, C.; Arita, Y.; Weiss, W.; Ranke, W.; Schlogl, R. Understanding Heterogeneous Catalysis on an Atomic Scale: A Combined Surface Science and Reactivity Investigation for the Dehydrogenation of Ethylbenzene over Iron Oxide Catalysts. *Top. Catal.* **2001,** *14*, 111-123.

(23)   Shaikhutdinov, S. K.; Joseph, Y.; Kuhrs, C.; Ranke, W.; Weiss, W. Structure and Reactivity of Iron Oxide Surfaces. *Faraday Discuss.* **1999**, 363-380.

(24)   Kuhrs, C.; Swoboda, M.; Weiss, W. Single Crystal Flow Reactor for Studying Reactivities on Metal Oxide Model Catalysts at Atmospheric Pressure to Bridge the Pressure Gap to the Adsorption Properties Determined under UHV Conditions. *Top. Catal.* **2001,** *15*, 13-18.

(25)   Emig, G.; Hofmann, H. Action of Zirconium-Phosphate as a Catalyst for the Oxydehydrogenation of Ethylbenzene to Styrene. *J. Catal.* **1983,** *84*, 15-26.

(26)   Hirano, T. Dehydrogenation of Ethylbenzene on Potassium-Promoted Iron-Oxide Catalyst Containing Magnesium-Oxide. *Bull. Chem. Soc. Jpn.* **1986,** *59*, 2672-2674.

(27)   Ndlela, S. C.; Shanks, B. H. Reducibility of Potassium-Promoted Iron Oxide under Hydrogen Conditions. *Ind. Eng. Chem. Res.* **2003,** *42*, 2112.

(28)   Miyakoshi, A.; Ueno, A.; Ichikawa, M. XPS and TPD Characterization of Manganese-substituted Iron-potassium Oxide Catalysts Which Are Selective for Dehydrogenation of Ethylbenzene into Styrene. *Appl. Catal. A-Gen.* **2001,** *219*, 249-258.

(29)   Miyakoshi, A.; Ueno, A.; Ichikawa, M. Mn-substituted Fe-K Mixed Oxide Catalysts for Dehydrogenation of Ethylbenzene towards Styrene. *Appl. Catal. A-Gen.* **2001,** *216*, 137-146.

(30)   Muhler, M.; Schlogl, R.; Ertl, G. The Nature of the Iron Oxide-Based Catalyst for Dehydrogenation of Ethylbenzene to Styrene. *J. Catal.* **1992,** *138*, 413-444.

(31)   Kotarba, A.; Kruk, I.; Sojka, Z. How the Iron Oxide Catalyst for EBDH is Stabilized via Mn Addition. *J. Catal.* **2004,** *221*, 650-652.

(32)   Wenner, R. R.; Dybdal, E. C. Catalytic Dehydrogenation of Ethylbenzene. *Chem. Eng. Prog.* **1948,** *44*, 275.

(33)   Carra, S.; Forni, L. Kinetics of Catalytic Dehydrogenation of Ethylbenzene to Styrene. *Ind. Eng. Chem. Proc. Des. Dev.* **1965,** *4*, 281.

(34)   Elnashaie, S. S. E. H.; Abdalla, B. K.; Hughes, R. Simulation of the Industrial Fixed-Bed Catalytic Reactor for the Dehydrogenation of Ethylbenzene to Styrene - Heterogeneous Dusty Gas-Model. *Ind. Eng. Chem. Res.* **1993,** *32*, 2537-2541.

(35)   Dittmeyer, R.; Hollein, V.; Quicker, P.; Emig, G.; Hausinger, G.; Schmidt, F. Factors Controlling the Performance of Catalytic Dehydrogenation of Ethylbenzene in Palladium Composite Membrane Reactors. *Chem. Eng. Sci.* **1999,** *54*, 1431-1439.

(36)   Majumdar, S.; Mitra, K. Modeling of a Reaction Network and its Optimization by Genetic Algorithm. *Chem. Eng. J.* **2004,** *100*, 109-118.

(37)   Lebedev, N. N.; Odabashyan, G. V.; Lebedev, V. V.; Makorov, M. G. Mechanism and Kinetics of Ethylbenzene Dehydrogenation and By-product Formation. *Kinet. Catal.* **1977,** *18*, 1177-1182.

(38)   Sheppard, C. M.; Maier, E. E. Ethylbenzene Dehydrogenation Reactor Model. *Ind. Eng. Chem. Proc. Des. Dev.* **1986,** *25*, 207-210.

(39)   Butt, J. B. Catalyst Deactivation and Regeneration. In *Catalysis Science and Technology*; Springer-Verlag: New York, 1984; Vol. 6, p. 2.

(40)   Appleby, W. G.; Gibson, J. W.; Good, G. M. Coke Formation in Catalytic Cracking. *Ind. Eng. Chem. Proc. Des. Dev.* **1962,** *1*, 102.

(41)   Voorhies, A. Carbon Formation in Catalytic Cracking. *Ind. Eng. Chem.* **1945,** *37,* 318.

(42)   Ozawa, Y.; Bischoff, K. B. Coke Formation Kinetics on Silica-alumina Catalyst. *Ind. Eng. Chem. Proc. Des. Dev.* **1968,** *7*, 67.

(43)   Eberly, P. E.; Kimberli.Cn; Miller, W. H.; Drushel, H. V. Coke Formation on Silica-Alumina Cracking Catalysts. *Ind. Eng. Chem. Proc. Des. Dev.* **1966,** *5*, 193-&.

(44)   Froment, G. F.; Bischoff, K. B. Non-steady Behavior of Fixed Bed Catalytic Reactors due to Catalyst Fouling. *Chem. Eng. Sci.* **1961,** *16*, 201.

(45)   Froment, G. F.; Bischoff, K. B. Kinetic Data and Product Distributions from Fixed Bed Catalytic Reactors Subject to Catalyst Fouling. *Chem. Eng. Sci.* **1962,** *17*, 105.

(46)   Dumez, F. J.; Froment, G. F. Dehydrogenation of 1-Butene into Butadiene - Kinetics, Catalyst Coking, and Reactor Design. *Ind. Eng. Chem. Proc. Des. Dev.* **1976,** *15*, 291-301.

(47)   Depauw, R. P.; Froment, G. F. Deactivation of a Platinum Reforming Catalyst in a Tubular Reactor. *Chem. Eng. Sci.* **1975,** *30*, 789-801.

(48)   Snoeck, J. W.; Froment, G. F.; Fowles, M. Steam/CO2 Reforming of Methane. Carbon Filament Formation by the Boudouard Reaction and Gasification by CO2, by H2, and by Steam: Kinetic Study. *Ind. Eng. Chem. Res.* **2002,** *41*, 4252-4265.

(49)   Snoeck, J. W.; Froment, G. F.; Fowles, M. Steam/CO2 Reforming of Methane. Carbon Formation and Gasification on Catalysts with Various Potassium Contents. *Ind. Eng. Chem. Res.* **2002,** *41*, 3548-3556.

(50)   Wauters, S.; Marin, G. B. Kinetic Modeling of Coke Formation during Steam Cracking. *Ind. Eng. Chem. Res.* **2002,** *41*, 2379.

(51)   Marin, G. B.; Beeckman, J. W.; Froment, G. F. Rigorous Kinetic-Models for Catalyst Deactivation by Coke Deposition - Application to Butene Dehydrogenation. *J. Catal.* **1986,** *97*, 416-426.

(52)   Devoldere, K. R.; Froment, G. F. Coke Formation and Gasification in the Catalytic Dehydrogenation of Ethylbenzene. *Ind. Eng. Chem. Res.* **1999,** *38*, 2626-2633.

(53)   Froment, G. F. A Rigorous Formulation of the Effect of Coke Formation on Catalyst Activity. In *Progress in Catalyst Deactivation. Proceedings of the NATO Advanced Study Institute on Catalyst Deactivation*; Figueiredo, J. L., Ed.: Martinus Nijhoff Publishers: The Hague, 1981; p. 103.

(54)   Froment, G. F. Modeling of Catalyst Deactivation. *Appl. Catal. A-Gen.* **2001,** *212*, 117-128.

(55)   De Pauw, R. P.; Froment, G. F. Deactivation of a Platinum Reforming Catalyst in a Tubular Reactor. *Chem. Eng. Sci.* **1975,** *30*, 789.

(56)   Wagner, E. S.; Froment, G. F. Steam Reforming Analyzed. *Hydrocarbon Process.* **1992,** *71*, 69.

(57)   Beirnaert, H. C.; Vermeulen, R.; Froment, G. F. A Recycle Electrobalance Reactor for the Study of Catalyst Deactivation by Coke Formation. *Catalyst Deactivation 1994* **1994,** *88*, 97-112.

(58)   Snoeck, J. W.; Froment, G. F.; Fowles, M. Filamentous Carbon Formation and Gasification: Thermodynamics, Driving Force, Nucleation, and Steady-state Growth. *J. Catal.* **1997,** *169*, 240-249.

(59)   Beeckman, J. W.; Froment, G. F. Catalyst Deactivation by Active-Site Coverage and Pore Blockage. *Ind. Eng. Chem. Fund.* **1979,** *18*, 245-256.

(60)   Beeckman, J. W.; Froment, G. F. Catalyst Deactivation by Site Coverage and Pore Blockage - Finite Rate of Growth of the Carbonaceous Deposit. *Chem. Eng. Sci.* **1980,** *35*, 805-815.

(61)   Beeckman, J. W.; Froment, G. F. Deactivation of Catalysts by Coke Formation in the Presence of Internal Diffusional Limitation. *Ind. Eng. Chem. Fund.* **1982,** *21*, 243-250.

(62)   Sahimi, M.; Tsotsis, T. T. A Percolation Model of Catalyst Deactivation by Site Coverage and Pore Blockage. *J. Catal.* **1985,** *96*, 552-562.

(63)   Beyne, A. O. E.; Froment, G. F. A Percolation Approach for the Modeling of Deactivation of Zeolite Catalysts by Coke Formation. *Chem. Eng. Sci.* **1990,** *45*, 2089-2096.

(64)   Beyne, A. O. E.; Froment, G. F. A Percolation Approach for the Modeling of Deactivation of Zeolite Catalysts by Coke Formation - Diffusional Limitations and Finite Rate of Coke Growth. *Chem. Eng. Sci.* **1993,** *48*, 503-511.

(65)   Beyne, A. O. E.; Froment, G. F. The Effect of Pore Blockage on the Diffusivity in ZSM5: A Percolation Approach. *Chem. Eng. J.* **2001,** *82*, 281-290.

(66)   Chen, D.; Rebo, H. P.; Holmen, A. Diffusion and Deactivation during Methanol Conversion over SAPO-34: A Percolation Approach. *Chem. Eng. Sci.* **1999,** *54*, 465.

(67)   Sahimi, M.; Gavalas, G. R.; Tsotsis, T. T. Statistical and Continuum Models of Fluid Solid Reactions in Porous-Media. *Chem. Eng. Sci.* **1990,** *45*, 1443-1502.

(68)   Connell, C.; Dumesic, J. A. Migration of Potassium on Iron and Alumina Surfaces as Studied by Auger-Electron Spectroscopy. *J. Catal.* **1985,** *82*, 17.

(69)   Mross, W. D. Alkali Doping in Heterogeneous Catalysis. *Catal. Rev.-Sci. Eng.* **1983,** *25*, 17.

(70)   Dellinger, P. W.; Moore, R. G.; Sherrod, F. A.; Smith, A. R. Process Using a Catalyst to Dehydrogenate an Alkyl Aromatic Compound. US Patent 5,510,552.

(71)   Rase, H. F. *Handbook of Commercial Catalysts: Heterogeneous Catalysts*; CRC Press: Boca Raton, FL., 2000.

(72)   Addiego, W. P.; Liu, W.; Boger, T. Iron Oxide-based Honeycomb Catalysts for the Dehydrogenation of Ethylbenzene to Styrene. *Catal. Today* **2001,** *69*, 25-31.

(73)   Kochloefl, K. Dehydrogenation of Ethylbenzene. In *Handbook of Heterogeneous Catalysis*; Ertl, G.,Knozinger, H.,Weitkamp, J., Eds.; VCH: Weinheim, 1997; Vol. 5, p. 2151.

(74)   Cavani, F.; Trifiro, F. Alternative Processes for the Production of Styrene. *Appl. Catal. A-Gen.* **1995,** *133*, 219.

(75)   Mitchell, J. E., Jr. The Dow Process for Styrene Production. *Trans. Am. Inst. Chem. Engrs.* **1946,** *42*, 293.

(76)   Lummus/UOP Classic SM Process. http://www.uop.com/objects/32%20Classic% 20SM.PDF (accessed October 2005).

(77)   *Annual Book of ASTM Standards, D5135-95*; American Society for Testing and Material: Philadelphia, PA, 2002; 06.04.

(78)   *CRC Handbook of Chemistry and Physics*, 77th ed.; CRC Press Inc.: Boca Raton, 1996.

(79)   *Annual Book of ASTM Standards, D2827-00*; American Society for Testing and Material: Philadelphia, PA, 2002; 06.04.

(80)   Froment, G. F.; Bischoff, K. B. *Chemical Reactor Analysis and Design*, 2nd ed.; John Wiley & Sons: New York, 1990; Chapter 7.

(81)   IUPAC-NIST Solubility Database, Version 1.0. http://srdata.nist.gov/solubility (accessed October 2005).

(82)   Lowell, S.; Shields, J. E. *Powder Surface Area and Porosity*, 2nd ed.; Chapman and Hall: London, 1984.

(83)   Barrett, E. P.; Joyner, L. G.; Halenda, P. P. The Determination of Pore Volume and Area Distributions in Porous Substances. I. Computations from Nitrogen Isotherms. *J. Am. Chem. Soc.* **1951,** *73*, 373.

(84)   Froment, G. F.; Bischoff, K. B. *Chemical Reactor Analysis and Design*, 2nd ed.; John Wiley & Sons: New York, 1990; Chapter 3.

(85)   Courty, P.; Le Page, J. F. In *Preparation of Catalysts II*; Delmon, B.,Grange, P.,Jacobs, P.,Poncelet, G., Eds.; Elsevier: Amsterdam, 1979; p. 293.

(86)   Rossetti, I.; Bencini, E.; Trentini, L.; Forni, L. Study of the Deactivation of a Commercial Catalyst for Ethylbenzene Dehydrogenation to Styrene. *Appl. Catal. A: Gen.* **2005,** *292*, 118.

(87)   Sing, K. S. W.; Everett, D. H.; Haul, R. A. W.; Moscou, L.; Pierotti, R. A.; Rouquerol, J.; Siemieniewska, T. Reporting Physisorption Data for Gas Solid Systems with Special Reference to the Determination of Surface-Area and Porosity (Recommendations 1984). *Pure Appl. Chem.* **1985,** *57*, 603-619.

(88) Brunauer, S.; Deming, L. S.; Deming, W. E.; Teller, E. On a Theory of the van der Waals Adsorption of Gases. *J. Am. Chem. Soc.* **1940,** *62*, 1723.

(89) Abdalla, B. K.; Elnashaie, S. S. E. H.; Alkhowaiter, S.; Elshishini, S. S. Intrinsic Kinetics and Industrial Reactors Modeling for the Dehydrogenation of Ethylbenzene to Styrene on Promoted Iron-Oxide Catalysts. *Appl. Catal. A-Gen.* **1994,** *113*, 89-102.

(90) Xu, J. G.; Froment, G. F. Methane Steam Reforming, Methanation and Water-Gas Shift .1. Intrinsic Kinetics. *AIChE J.* **1989,** *35*, 88-96.

(91) Bruinsma, O. S. L.; Geertsma, R. S.; Bank, P.; Moulijn, J. A. Gas Phase Pyrolysis of Coal-Related Aromatic Compounds in a Coiled Tube Flow Reactor 1. Benzene and Derivatives. *Fuel* **1988,** *67*, 27.

(92) Bruinsma, O. S. L.; Moulijn, J. A. The Pyrolytic Formation of Polycyclic Aromatic Hydrocarbons from Benzene, Toluene, Ethylbenzene, Styrene, Phenylacetylene and n-Decane in Relation to Fossil Fuels Utilization. *Fuel Process. Technol.* **1988,** *18*, 213.

(93) Hougen, O. A.; Watson, K. M. *Chemical Process Principles. Part Three*; John Wiley & Sons, Inc.: New York, 1947.

(94) Smith, J. M. Thirty-Five Years of Applied Catalytic Kinetics. *Ind. Eng. Chem. Fund.* **1982,** *21*, 327-332.

(95) Froment, G. F.; Bischoff, K. B. *Chemical Reactor Analysis and Design*, 2nd ed.; John Wiley & Sons: New York, 1990; Chapter 2.

(96) Djega-Mariadassou, G.; Boudart, M. *Kinetics of Heterogeneous Catalytic Reactions*; Princeton University Press: Princeton, N.J., 1984.

(97) Weller, S. W. Kinetic Models in Heterogeneous Catalysis. *Adv. Chem. Ser.* **1975,** *148*, 26-49.

(98) Boudart, M. Classical Catalytic Kinetics: A Placebo or the Real Thing? *Ind. Eng. Chem. Fund.* **1986,** *25*, 656.

(99) Froment, G. F. Model Discrimination and Parameter Estimation in Heterogeneous Catalysis. *AIChE J.* **1975,** *21*, 1041-1057.

(100) Boudart, M.; Mears, D. E.; Vannice, M. A. *Ind. Chim. Belge.* **1967,** *32*, 281.

(101) Vannice, M. A.; Hyun, S. H.; Kalpakci, B.; Liauh, W. C. Entropies of Adsorption in Heterogeneous Catalytic Reactions. *J. Catal.* **1979,** *56*, 358.

(102) Sundaram, K. M.; Froment, G. F. Modeling of Thermal-Cracking Kinetics .1. Thermal-Cracking of Ethane, Propane and Their Mixtures. *Chem. Eng. Sci.* **1977,** *32*, 601-608.

(103) Devoldere, K. R.; Froment, G. F., Artie McFerrin Department of Chemical Engineering, Texas A&M University, Personal Communication, June, 2002.

(104) Froment, G. F.; Bischoff, K. B. *Chemical Reactor Analysis and Design*, 2nd ed.; John Wiley & Sons: New York, 1990; Chapter 9.

(105) Constantinides, A.; Mostoufi, N. *Numerical Methods for Chemical Engineers with MATLAB Applications*; Prentice Hall Inc.: Upper Saddle River, N. J., 1999.

(106) Edgar, T. F.; Himmelblau, D. M. *Optimization of Chemical Processes*, 2nd ed.; McGraw-Hill: New York, 2001.

(107) Marquardt, D. W. An Algorithm for Least-Squares Estimation of Nonlinear Parameters. *J. Soc. Indust. Appl. Math.* **1963,** *11*, 431.

(108) Bard, Y.; Lapidus, L. Kinetics Analysis by Digital Parameter Estimation. *Catal. Rev.* **1968,** *2*, 7.

(109) Kittrell, J. R. Mathematical Modeling of Chemical Reactions. *Adv. Chem. Eng.* **1970,** *8*, 97.

(110) Gear, C. W. *Numerical Initial Value Problems in Ordinary Differential Equations*; Prentice-Hall: Englewood Cliff, N. J., 1971.

(111) Schule, A.; Shekhah, O.; Ranke, W.; Schlogl, R.; Kolios, G. Microkinetic Modelling of the Dehydrogenation of Ethylbenzene to Styrene over Unpromoted Iron Oxides. *J. Catal.* **2005,** *231*, 172-180.

(112) Ranke, W.; Joseph, Y. Determination of Adsorption Energies and Kinetic Parameters by Isosteric Methods. *Phys. Chem. Chem. Phys.* **2002,** *4*, 2483.

(113) Dulamita, N.; Maicaneanu, A.; Sayle, D. C.; Stanca, M.; Craciun, R.; Olea, M.; Afloroaei, C.; Fodor, A. Ethylbenzene Dehydrogenation on Fe_2O_3-Cr_2O_3-K_2CO_3 Catalysts Promoted with Transitional Metal Oxides. *Appl. Catal. A-Gen.* **2005,** *287*, 9.

(114) Raghavan, N. S.; Doraiswamy, L. K. On the Validity of Kinetic Modeling for Vapor Phase Catalytic Reactions: Isomerization of n-butene to Isobutene. *J. Catal.* **1977,** *48*, 21.

(115) Boudart, M. Two-Step Catalytic Reactions. *AIChE J.* **1972,** *18*, 465.

(116) Mears, D. E.; Boudart, M. The Dehydrogenation of Isopropanol on Catalysts Prepared by Sodium Borohydride Reduction. *AIChE J.* **1966,** *12*, 313.

(117) Van Trimpont, P. A.; Marin, G. B.; Froment, G. F. Kinetics of Methylcyclohexane Dehydrogenation on Sulfided Commercial Platinum Alumina and Platinum-Rhenium Alumina Catalysts. *Ind. Eng. Chem. Fund.* **1986,** *25*, 544-553.

(118) Stull, D. R.; Westrum, E. F., Jr.; Sinke, G. C. *The Chemical Thermodynamics of Organic Compounds*; John Wiley & Sons: New York, 1969.

(119) Everett, D. H. The Thermodynamics of Adsorptions Part II. Analysis and Discussion of Experimental Data. *Trans. Faraday Soc.* **1950,** *46*, 957.

(120) Froment, G. F.; Bischoff, K. B. *Chemical Reactor Analysis and Design*, 2nd ed.; John Wiley & Sons: New York, 1990; Chapter 11.

(121) Carberry, J. J.; Wendel, M. A Computer Model of the Fixed Bed Catalytic Reactor: The Adiabatic and Quasi-Adiabatic Cases. *AIChE J.* **1963,** *9*, 129.

(122) Young, L. C.; Finlayson, B. A. Axial Dispersion in Nonisothermal Packed Bed Chemical Reactors. *Ind. Eng. Chem. Fund.* **1973,** *12*, 412.

(123) Hlavacek, V.; Kubicek, M. Modeling of Chemical Reactors-XXV. Cylindrical and Spherical Reactor with Radial Flow. *Chem. Eng. Sci.* **1972,** *27*, 177.

(124) Reid, R. C.; Prausnitz, J. M.; Poling, B. E. *The Properties of Gases and Liquids*, 4th ed.; McGraw-Hill, Inc.: New York, 1987.

(125) Ergun, S. Fluid Flow through Packed Columns. *Chem. Eng. Prog.* **1952,** *48*, 89.

(126) Handley, D.; Heggs, P. J. Momentum and Heat Transfer Mechanisms in Regular Shaped Packings. *Trans. Inst. Chem. Eng.* **1968,** *46*, T251.

(127) Hicks, R. E. Pressure Drop in Packed Beds of Spheres. *Ind. Eng. Chem. Fund.* **1970,** *9*, 500.

(128) Smith, J. M.; Van Ness, H. C. *Introduction to Chemical Engineering Thermodynamics*, 4th ed.; McGraw-Hill: New York, 1987.

(129) Reid, R. C.; Prausnitz, J. M.; Sherwood, T. K. *The Properties of Gases and Liquids*, 3rd ed.; McGraw-Hill: New York, 1977.

(130) Froment, G. F., Artie McFerrin Department of Chemical Engineering, Texas A&M University, Personal Communication, July, 2005.

(131) Lim, H.; Kang, M.; Park, S.; Lee, J. Modeling and Optimization of a Styrene Monomer Reactor System Using a Hybrid Neural Network Model. *Ind. Eng. Chem. Res.* **2004,** *43*, 6441.

(132) Thiele, E. W. Relation between Catalytic Activity and Size of Particle. *Ind. Eng. Chem.* **1939,** *31*, 916.

(133) Damkohler, G. The Influence of Diffusion, Flow, and Heat Transport on Yield in Chemical Reactors. *Der Chemie-Ingenieur* **1937,** *3*, 430.

(134) Wheeler, A. Reaction Rates and Selectivity in Catalyst Pores. In *Catalysis*; Emmett, P. H., Ed.: Rheinhold Publishers: New York, 1955; Vol. II,

(135) Weisz, P. B.; Prater, C. D. *Advances in Catalysis*; Academic Press: New York, 1954; VI, p 143.

(136) Wicke, E. Über die Stationären Zustande Exothermer Gasreaktionen an Porösen Katalysatoren. *Chem.-Ing.-Tech.* **1957,** *29*, 305.

(137) Aris, R. *The Mathematical Theory of Diffusion and Reaction in Permeable Catalysts*; Clarendon Press: Oxford, 1975; Chapter 3-5.

(138) Bischoff, K. B. Effectiveness Factors for General Reaction Rate Forms. *AIChE J.* **1965,** *11*, 351.

(139) Satterfield, C. N. *Mass Transfer in Heterogeneous Catalysis*; MIT Press: Cambridge, MA, 1970.

(140) Bird, R. B.; Steward, W. E.; Lightfoot, E. N. *Transport Phenomena*; Wiley: New York, 1960.

(141) Hsu, H. W.; Bird, R. B. Multicomponent Diffusion Problems. *AIChE J.* **1960,** *6*, 516.

(142) Fuller, E. N.; Schettler, P. D.; Giddings, J. C. A New Method for Prediction of Binary Gas-Phase Diffusion Coefficients. *Ind. Eng. Chem.* **1966,** *58*, 19.

(143) Satterfield, C. N. *Heterogeneous Catalysis in Industrial Practice*, 2nd ed.; McGraw-Hill: New York, 1991.

(144) Wang, C. T.; Smith, J. M. Tortuosity Factors for Diffusion in Catalyst Pellet. *AIChE J.* **1983,** *29*, 132.

(145) Bosanquet, C. H. *British TA Report BR-507*; September 27, 1944.

(146) Evans, R. B.; Watson, G. M.; Mason, E. A. Gaseous Diffusion in Porous Media at Uniform Pressure. *J. Chem. Phys.* **1961,** *35*, 2076.

(147) Johnson, M. F. L.; Stewart, W. E. Pore Structure and Gaseous Diffusion in Solid Catalyst. *J. Catal.* **1965,** *4*, 248.

(148) Feng, C.; Stewart, W. E. Practical Models for Isothermal Diffusion and Flow of Gases in Porous Solids. *Ind. Eng. Chem. Fund.* **1973,** *12*, 143-147.

(149) Wakao, N.; Smith, J. M. Diffusion in Catalyst Pellet. *Chem. Eng. Sci.* **1962,** *17*, 825.

(150) Satterfield, C. N.; Cadle, P. J. Diffusion in Commercially Manufactured Pelleted Catalysts. *Ind. Eng. Chem. Proc. Des. Dev.* **1968,** *7*, 256.

(151) Patel, P. V.; Butt, J. B. Multicomponent Diffusion in Porous Catalysts. *Ind. Eng. Chem. Proc. Des. Dev.* **1975,** *14*, 298-304.

(152) Dumez, F. J.; Froment, G. F. Problem of Intraparticle Mass-Transfer Limitations in Reactor Design - Simplified Approach. *Chem. Eng. Sci.* **1977,** *32*, 974-977.

(153) De Deken, J. C.; Devos, E. F.; Froment, G. F. Steam Reforming of Natural-Gas - Intrinsic Kinetics, Diffusional Influences, and Reactor Design. *ACS Symp. Ser.* **1982,** *196*, 181-197.

(154) Sharma, R. K.; Cresswell, D. L.; Newson, E. J. Effective Diffusion Coefficients and Tortuosity Factors for Commercial Catalysts. *Ind. Eng. Chem. Res.* **1991,** *30*, 1428.

(155) Mason, E. A.; Malinauskas, A. P.; Evans, R. B. Flow and Diffusion of Gases in Porous Media. *J. Chem. Phys.* **1967,** *46*, 3199.

(156) Coppens, M. O.; Froment, G. F. Fractal Aspects in the Catalytic Reforming of Naphtha. *Chem. Eng. Sci.* **1996,** *51*, 2283-2292.

(157) Wong, R. L.; Denny, V. E. Diffusion, Flow, and Heterogeneous Reaction of Ternary Mixtures in Porous Catalytic Media. *Chem. Eng. Sci.* **1975,** *30*, 709-716.

(158) Salmi, T.; Warna, J. Modeling of Catalytic Packed-Bed Reactors Comparison of Different Diffusion-Models. *Comput. Chem. Eng.* **1991,** *15*, 715-727.

(159) Graaf, G. H.; Scholtens, H.; Stamhuis, E. J.; Beenackers, A. A. C. M. Intraparticle Diffusion Limitations in Low-Pressure Methanol Synthesis. *Chem. Eng. Sci.* **1990,** *45*, 773-783.

(160) Xu, J. G.; Froment, G. F. Methane Steam Reforming. 2. Diffusional Limitations and Reactor Simulation. *AIChE J.* **1989,** *35*, 97-103.

(161) Villadsen, J. V.; Stewart, W. E. Solution of Boundary-Value Problems by Orthogonal Collocation. *Chem. Eng. Sci.* **1967,** *22*, 1483.

(162) Kaza, K. R.; Jackson, R. Diffusion and Reaction of Multicomponent Gas-Mixtures in Isothermal Porous Catalysts. *Chem. Eng. Sci.* **1980,** *35*, 1179-1187.

(163) Goyal, S. K.; Esmail, M. N.; Bakhshi, N. N. Application of Orthogonal Collocations to Some Transport Phenomena Problems in Coaxial Cylinders and Spheres. *Can. J. Chem. Eng.* **1987,** *65*, 833-844.

(164) Villadsen, J. *Selected Approximation Methods for Chemical Engineering Problems*; Instituttet for Kemiteknik, Danmarks Tekniske Hojskole: Lyngby, Denmark, 1970.

(165) Villadsen, J.; Michelsen, M. L. *Solution of Differential Equation Models by Polynomial Approximation*; Prentice-Hall: Englewood Cliffs, NJ, 1978.

(166) Finlayson, B. A. *Nonlinear Analysis in Chemical Engineering*; Ravenna Park Publishing Inc.: Seattle, WA, 2003.

(167) Abashar, M. E. E.; Elnashaie, S. S. E. H. Mathematical Modeling of Diffusion-Reaction, and Solution Algorithm for Complex Reaction Networks in Porous Catalyst Pellet-Steam Reforming of Natural Gas. *Math. Comput. Model.* **1993,** *18*, 85.

(168) Wang, J. Modeling, Parametric Sensitivity Analysis and Parameter Estimation for Methanol Synthesis in Trickle Bed Reactors. Ph.D. dissertation, Texas A&M University, College Station, 1994.

(169) Rice, R. G.; Do, D. D. *Applied Mathematics and Modeling for Chemical Engineers*; John Wiley & Sons: New York, 1995.

(170) Herzog, B. D.; Rase, H. F. In situ Catalyst Reactivation - Used Ethylbenzene Dehydrogenation Catalyst with Agglomerated Potassium Promoter. *Ind. Eng. Chem. Prod. Res. Dev.* **1984,** *23*, 187-196.

(171) Menon, P. G. Diagnosis of Industrial Catalyst Deactivation by Surface Characterization Techniques. *Chem. Rev.* **1994,** *94*, 1021.

(172) Mims, C. A.; Chludzinski, J. J.; Pabst, J. K.; Baker, R. T. K. Potassium-Catalyzed Gasification of Graphite in Oxygen and Steam. *J. Catal.* **1984,** *88*, 97-106.

(173) Froment, G. F.; Bischoff, K. B. *Chemical Reactor Analysis and Design*, 2nd ed.; John Wiley & Sons: New York, 1990; Chapter 5.

(174) Nam, I. S.; Froment, G. F. Catalyst Deactivation by Site Coverage through Multi-Site Reaction-Mechanisms. *J. Catal.* **1987,** *108*, 271-282.

(175) Ergun, S. Kinetics of the Reactions of Carbon Dioxide and Steam with Coke. *U.S. Bur. Mines Bull.* **1962,** *598*, 38.

(176) Giberson, R.; Walker, P. Reaction of Nuclear Graphite with Water Vapor Part1. Effect of Hydrogen and Water Vapor Partial Pressures. *Carbon* **1966,** *3*, 521.

(177) Andrigo, P.; Bagatin, R.; Pagani, G. Fixed Bed Reactors. *Catal. Today* **1999,** *52*, 197.

(178) Ponzi, P. R.; Kaye, L. A. Effect of Flow Maldistribution on Conversion and Selectivity in Radial Flow Fixed-bed Reactors. *AIChE J.* **1979,** *25*, 100.

(179) Fogler, H. S. *Elements of Chemical Reaction Engineering*, 2nd ed.; Prentice-Hall: Englewood Cliffs, NJ, 1992; Chapter 4.

(180) Zardi, U., Review These Developments in Ammonia and Methanol Reactors. *Hydrocarbon Process.,* 1982, p. 129.

(181) Moates, F. C.; McMinn, T. E.; Richardson, J. T. Radial Reactor for Trichloroethylene Steam Reforming. *AIChE J.* **1999,** *45*, 2411.

(182) Lyubovsky, M.; Roychoudhury, S. Novel Catalytic Reactor for Oxidative Reforming of Methanol. *Appl. Catal. B: Environmental* **2004,** *54*, 203.

(183) Mu, Z.; Wang, J.; Wang, T.; Jin, Y. Optimum Design of Radial Flow Moving-bed Reactors Based on a Mathematical Hydrodynamic Model. *Chem. Eng. Process.* **2003,** *42*, 409.

(184) Yoo, C.-S.; Dixon, A. G. Modeling and Simulation of a Mixed-flow Reactor for Ammonia and Methanol Synthesis. *Chem. Eng. Sci.* **1988,** *43*, 2859.

(185) Liu, W.; Addiego, W. P.; Sorensen, C. M.; Boger, T. Monolith Reactor for the Dehydrogenation of Ethylbenzene to Styrene. *Ind. Eng. Chem. Res.* **2002,** *41*, 3131-3138.

(186) Zardi, F.; Bonvin, D. Modeling, Simulation and Model Validation for an Axial-radial Ammonia Synthesis Reactor. *Chem. Eng. Sci.* **1992,** *47*, 2523.

(187) Panahandeh, M. R.; Fathikaljahi, J.; Taheri, M. Steady-state Modeling and Simulation of an Axial-Radial Ammonia Synthesis Reactor. *Chem. Eng. Technol.* **2003,** *26*, 666.

APPENDIX A

STANDARD TEST METHOD FOR ANALYSIS OF

STYRENE BY CAPILLARY GAS CHROMATOGRAPHY

(DESIGNATION: D5135-95)

A.1 Summary of Test Method

In this test method, the chromatogram peak area for each impurity is compared to the peak area of the internal standard (*n*-heptane or other suitable known) which is added to the sample. From the response factors of these impurities relative to that of the internal standard and the amount of internal standard added, the concentration of the impurities is calculated. The styrene content is obtained by subtracting the total amount of all impurities from 100.00.

A.2 Significance and Use

This test method is designed to obtain styrene purity on the basis of impurities normally present in styrene and may be used for final product inspections and process control.

This test method will detect the following impurities: non-aromatic hydrocarbons containing ten carbons or less, ethylbenzene, *p*- and *m*-xylene, cumene, *n*-propylbenzne, *m*- and *p*- ethyltoluene, alpha-methylstyrene, *o*-xylene, *m*- and *p*-vinyltoluene and others where specific impurity standard are available. Absolute purity cannot be determined if unknown impurities are present.

A.3 Apparatus

Any gas chromatography having a flame ionization detector and a splitter injector suitable for use with a fused silica capillary column may be used, provided the system has sufficient sensitivity to obtain a minimum peak height response of 0.1 mV for 0.010% internal standard when operated at the stated conditions. Background noise at these conditions is not to exceed 3μV.

Capillary columns have been found to be satisfactory for the quantitative analysis. For example, 60 m of 0.32 mm inside diameter polar-fused silica capillary internally coated to a 0.5 μm thickness with a cross-linked polyethylene glycol can be used (See Table A.1 for parameters). Other columns may be used after it has been established that such a column is capable of separating all major impurities and the internal standard from the styrene under operating conditions appropriate for the column.

A.4. Procedure

1. Prepare a calibration mixture containing approximately 99.5 weight% styrene and the expected significant impurities at their expected concentration. Weigh all comonents to the accuracy required to calculate the concentration of each to the near est 0.001%.

2. With a microsyringe, add 50μL of internal standard to a 100 mL volumetric flask about three-fourths full of the calibration mixture. Mix well. Add calibration mixture to mark and again mix well. If *n*-heptane is used as the internal standard, using a density of 0.684 for *n*-heptane and 0.906 for styrene, this solution will

contain 0.0377 weight % *n*-heptane.

3. Also prepare a sample of the styrene used for the calibration blend with and without n- heptane to determine the concentration of existing impurities and interfering compounds with internal standard. If impurities in the styrene emerge with the chosen internal standard, an alternate internal standard must be used.

4. Inject an appropriate amount sample into the GC and obtain a chromatogram.

5. Measure the areas of all peaks, including the internal standard, except the styrene peak.

6. Calculate the response factors for each impurity relative to the internal standard as follows:

$$RF_i = \frac{C_i}{C_s\left(\dfrac{A_i}{A_{si}} - \dfrac{A_b}{A_{sb}}\right)}$$

(A.1)

where:

RF_i = response factor relative to the internal standard,

A_{si} = area of internal standard in calibration mixture,

A_i = area of impurity peak in calibration mixture,

A_{sb} = area of internal standard in styrene used in making calibration mixture,

A_b = area of impurity in styrene used to make calibration mixture,

C_s = weight percent internal standard in calibration mixture, and

C_i = weight percent impurity in calibration mixture.

Table A.1 Typical instrument parameters

Carrier gas	helium
Carrier gas flow rate at 110°C, ml/min	1.2
Detector	flame ionization
Detector temperature, ^{o}C	240
Injection port temperature, ^{o}C	230
Hydrogen flow rate, mL/min	30
Air flow rate, mL/min	275
Make up gas	nitrogen
Make up gas flow rate, mL/min	23
Split flow, mL/min	150
Column	60m×0.32mm ID×0.5μm bonded polyethylene glycol-fused silica capillary
Column temperature, ^{o}C	110
Sample size, μL	0.6

APPENDIX B

GC DETECTOR MAINTENANCE

The problem frequently encountered in the GC analysis could be attributed to the possible deposition and/or adsorption of high molecular weight aromatics onto the detectors, both FID and TCD. Here presented were the remedy procedures for this problem and the results of experiments on the reproducibility of GC calibration curves.

B.1   Procedure of FID Cleaning

First, the detector and the gases to detector must be turned off. It is required to wait for the detector zone to cool down. One can open the top cover and remove the FID collector assembly by pulling it straight up. And then, one need to look inside the detector base and check if there is any loose material, *viz.* carbonaceous deposits or white silica from column bleed. Black soot is sometimes found inside the collector, and should be blown out using compressed N_2. Next, the jet should be removed from the detector base and washed with 1:1 (v/v) solution of methanol and acetone. Finally, the jet and detector cover need to be reinstalled. More detailed cleaning procedure is described in the *HP 5890A GC reference manual*, volume 1, p 12-18.

B.2   Procedure of TCD Conditioning

Fused silica tube column with no liquid phase is recommended for the ease of operation. When a normal column is connected, one should not connect it to the detector and the

detector inlet is to be covered with graphite ferrule and split nut. The temperature should be set to a value higher than that for analysis by approximately 30°C. Keep in mind that the maximum operating temperature of the TCD is 400°C. The flow rates of carrier gas and make-up gas is set to the same values as those for analysis. For more information, refer to *User's manual for Shimadzu thermal conductivity detector (TCD-17),* Ver. 2, p 8-4.

APPENDIX C

EXPERIMENTAL DATA

	Space time, gcat. hr/mol EB	Temp., K	y^0_{EB}	y^0_{ST}	$y^0_{H_2}$	X_{H_2}	X_{BZ}	X_{TO}	X_{EB}
1	15.00	913.15	0.0489	0	0	0.514	0.0161	0.0094	0.551
2	24.00	913.15	0.0489	0	0	0.653	0.0195	0.0153	0.692
3	29.00	913.15	0.0489	0	0	0.672	0.0214	0.0229	0.733
4	31.00	913.15	0.0489	0	0	0.681	0.0213	0.0236	0.741
5	37.00	913.15	0.0489	0	0	0.715	0.0221	0.0295	0.812
6	50.00	913.15	0.0489	0	0	0.730	0.0243	0.0428	0.843
7	61.00	913.15	0.0489	0	0	0.745	0.0265	0.0513	0.871
8	22.00	913.15	0.0477	0.0143	0	0.513	0.0155	0.0114	0.560
9	34.00	913.15	0.0477	0.0143	0	0.612	0.0197	0.0213	0.6701
10	45.00	913.15	0.0477	0.0143	0	0.678	0.0212	0.0302	0.742
11	58.00	913.15	0.0477	0.0143	0	0.699	0.0241	0.0414	0.812
12	25.00	913.15	0.0481	0.0096	0	0.573	0.0175	0.0147	0.634
13	42.00	913.15	0.0481	0.0096	0	0.675	0.0221	0.0295	0.758
14	57.00	913.15	0.0481	0.0096	0	0.712	0.0243	0.0432	0.831
15	22.00	913.15	0.0458	0	0.0367	0.541	0.0175	0.0351	0.634
16	30.00	913.15	0.0458	0	0.0367	0.585	0.0211	0.0545	0.715
17	43.00	913.15	0.0458	0	0.0367	0.626	0.0235	0.0787	0.780
18	54.00	913.15	0.0458	0	0.0367	0.629	0.0255	0.0901	0.836
19	26.00	913.15	0.0470	0	0.0221	0.600	0.0197	0.0342	0.672
20	42.00	913.15	0.0470	0	0.0221	0.671	0.0230	0.0563	0.800
21	58.00	913.15	0.0470	0	0.0221	0.678	0.0261	0.0747	0.853
22	25.00	913.15	0.0733	0	0	0.621	0.0232	0.0251	0.712
23	51.60	913.15	0.0733	0	0	0.694	0.0255	0.0620	0.842
24	60.00	913.15	0.0733	0	0	0.713	0.0266	0.0700	0.851
25	18.08	893.15	0.0489	0	0	0.466	0.0094	0.0052	0.472
26	29.70	893.15	0.0489	0	0	0.571	0.0122	0.0117	0.616
27	30.96	893.15	0.0489	0	0	0.581	0.0127	0.0113	0.621
28	36.28	893.15	0.0489	0	0	0.625	0.0130	0.0135	0.651
29	36.28	893.15	0.0489	0	0	0.613	0.0132	0.0141	0.663
30	41.89	893.15	0.0489	0	0	0.631	0.0138	0.0174	0.681
31	46.77	893.15	0.0489	0	0	0.651	0.0143	0.0298	0.724
32	55.56	893.15	0.0489	0	0	0.679	0.0152	0.0262	0.747
33	57.53	893.15	0.0489	0	0	0.683	0.0154	0.0275	0.753
34	59.80	893.15	0.0489	0	0	0.690	0.0156	0.0289	0.764
35	6.50	893.15	0.0489	0	0	0.251	0.0050	0.00068	0.269

* y^0_j = Feed mole fraction of component j; X_j = fractional conversion into component j

	Space time, gcat. hr/mol EB	Temp., K	y^0_{EB}	y^0_{ST}	$y^0_{H_2}$	X_{H_2}	X_{BZ}	X_{TO}	X_{EB}
36	22.02	893.15	0.0485	0.0048	0	0.460	0.0095	0.0063	0.493
37	30.13	893.15	0.0485	0.0048	0	0.535	0.0115	0.0113	0.567
38	40.05	893.15	0.0485	0.0048	0	0.582	0.0125	0.0154	0.647
39	50.23	893.15	0.0485	0.0048	0	0.641	0.0147	0.0212	0.698
40	32.43	893.15	0.0481	0.0096	0	0.511	0.0105	0.0116	0.530
41	42.45	893.15	0.0481	0.0096	0	0.565	0.0122	0.0151	0.612
42	52.12	893.15	0.0481	0.0096	0	0.600	0.0135	0.0213	0.664
43	33.28	893.15	0.0477	0.0143	0	0.470	0.0188	0.0102	0.501
44	42.19	893.15	0.0477	0.0143	0	0.521	0.0113	0.0133	0.563
45	64.3	893.15	0.0477	0.0143	0	0.624	0.0149	0.0251	0.683
46	64.3	893.15	0.0477	0.0143	0	0.618	0.0143	0.0254	0.691
47	26.82	893.15	0.0467	0	0.0266	0.521	0.0112	0.0243	0.547
48	36.27	893.15	0.0467	0	0.0266	0.550	0.0127	0.0287	0.626
49	47.11	893.15	0.0467	0	0.0266	0.589	0.0143	0.0395	0.675
50	53.21	893.15	0.0467	0	0.0266	0.611	0.0147	0.0452	0.712
51	30.12	893.15	0.0733	0	0	0.552	0.0117	0.0168	0.601
52	44.05	893.15	0.0733	0	0	0.626	0.0141	0.0255	0.682
53	58.06	893.15	0.0733	0	0	0.649	0.0153	0.0361	0.749
54	11.30	873.15	0.0489	0	0	0.268	0.0034	0.0014	0.250
55	20.00	873.15	0.0489	0	0	0.362	0.0057	0.0021	0.370
56	27.00	873.15	0.0489	0	0	0.420	0.0059	0.0037	0.443
57	35.00	873.15	0.0489	0	0	0.486	0.0069	0.0061	0.498
58	37.00	873.15	0.0489	0	0	0.494	0.007	0.0066	0.511
59	41.00	873.15	0.0489	0	0	0.522	0.0074	0.0082	0.543
60	45.14	873.15	0.0489	0	0	0.533	0.0078	0.0092	0.562
61	64.00	873.15	0.0489	0	0	0.613	0.0091	0.0158	0.648
62	20.00	873.15	0.0477	0.0143	0	0.234	0.0034	0.0015	0.250
63	30.00	873.15	0.0477	0.0143	0	0.321	0.0045	0.0029	0.321
64	39.43	873.15	0.0477	0.0143	0	0.371	0.0053	0.0047	0.393
65	50.01	873.15	0.0477	0.0143	0	0.433	0.0063	0.0078	0.454
66	62.00	873.15	0.0477	0.0143	0	0.471	0.0073	0.0105	0.493
67	23.00	873.15	0.0481	0.0096	0	0.356	0.0043	0.0022	0.321
68	34.00	873.15	0.0481	0.0096	0	0.388	0.0055	0.0046	0.412
69	45.00	873.15	0.0481	0.0096	0	0.449	0.0065	0.0073	0.463
70	55.00	873.15	0.0481	0.0096	0	0.482	0.0072	0.0113	0.516

* y^0_j = Feed mole fraction of component j; X_j = fractional conversion into component j

	Space time, gcat. hr/mol EB	Temp., K	y^0_{EB}	y^0_{ST}	$y^0_{H_2}$	X_{H_2}	X_{BZ}	X_{TO}	X_{EB}
71	22.00	873.15	0.0458	0	0.0367	0.323	0.0048	0.0094	0.345
72	30.00	873.15	0.0458	0	0.0367	0.381	0.0058	0.0143	0.416
73	36.00	873.15	0.0458	0	0.0367	0.410	0.0064	0.0186	0.458
74	45.31	873.15	0.0458	0	0.0367	0.452	0.0072	0.0233	0.527
75	53.47	873.15	0.0458	0	0.0367	0.481	0.0081	0.0286	0.541
76	19.00	873.15	0.0470	0	0.0221	0.321	0.0046	0.0061	0.322
77	30.00	873.15	0.0470	0	0.0221	0.414	0.0062	0.0114	0.430
78	40.00	873.15	0.0470	0	0.0221	0.465	0.0072	0.0157	0.501
79	60.00	873.15	0.0470	0	0.0221	0.539	0.0087	0.0254	0.593
80	25.00	873.15	0.0733	0	0	0.380	0.0058	0.0046	0.414
81	51.60	873.15	0.0733	0	0	0.521	0.0084	0.0142	0.562
82	68.30	873.15	0.0733	0	0	0.571	0.0091	0.0213	0.621

* y^0_j = Feed mole fraction of component j; X_j = fractional conversion into component j

VITA

Won Jae Lee was born in Uijongbu, Korea on January 8, 1970, the son of Kangson Lee and Jeongja Ryoo. He entered SungKyunKwan University in 1989 and completed the military service in Republic of Korea Army in 1993. He continued his study and received the degree of Bachelor of Science in 1996. He began the graduate study at Pohang University of Science and Technology in Korea and earned the Master of Science degree in 1998. The title of the thesis is "Hydrodesulfurization of Benzothiophene over Mo_2N supported on SiC-coated Alumina Catalyst". From 1998 to 2000 he worked as a research engineer for LG Institute of Environment, Safety, and Health in Korea. He enrolled in the graduate program in the Department of Chemical Engineering at Texas A&M University in August 2000. He is married to Sohyun Park. His permanent address is: Shinil UtovillPlus Apt. 101-1301, Howon-Dong, Uijongbu, Kyungki, Korea 480-021. His email address is iwjlee@yahoo.com.